



TECHNISCHE UNIVERSITÄT MÜNCHEN

TUM School of Life Sciences

**Profiling of organic matter in olivine
mineral and meteorites with high
resolution mass spectrometry and the
role of metalorganic compounds**

Marco Matzka

Vollständiger Abdruck der von der TUM School of Life Sciences der
Technischen Universität München zur Erlangung des akademischen Grades eines

Doktors der Naturwissenschaften

genehmigten Dissertation.

Vorsitzender: Prof. Dr. Erwin Grill

Prüfer der Dissertation:

1. apl. Prof. Dr. Philippe Schmitt-Kopplin
2. Prof. Dr. Job Boekhoven

Die Dissertation wurde am 04.05.2022 bei der Technischen Universität
München eingereicht und durch die TUM School of Life Sciences am
04.10.2022 angenommen.

This page intentionally left blank

Table of contents

Summary	v
Zusammenfassung	vii
Acknowledgments	x
List of abbreviations	xi
Glossary	xiii
Chapter 1 - Introduction and Materials and Methods	1
1.1 General Introduction	1
1.1.1 Organic Molecules in Geological Samples	1
1.1.2 Research Questions	1
1.1.3 Applied Methods	3
1.1.4 Aim of this Work	4
1.2 Organics in Meteorites	5
1.2.1 Origin of Meteorites	5
1.2.2 Organic Compounds in Meteorites	7
1.2.3 Analysis of Meteorites and Implications	10
1.3 Olivine Mineral	11
1.3.1 Olivine Mineral on Earth	14
1.3.2 Extraterrestrial Olivine	15
1.3.3 Serpentinization	15
1.3.4 Carbon in Olivine	17
1.3.5 Deep Carbon	17
1.4 Synthesis of Organic Compounds in Geological Samples	18
1.5 State of the Art with FT-ICR-MS	23
1.6 State of the Art with NMR	25
1.7 State of the Art of LC-MS in NOM Analysis	26
1.8 Materials and Methods	28
1.8.1 FT-ICR Mass Spectrometry	28

1.8.2	Basics of FT-ICR-MS	29
1.8.3	High Resolving Power and Mass Accuracy	29
1.8.4	Ionization Techniques	30
1.9	Nuclear Resonance Spectroscopy	32
1.10	Liquid Chromatography Mass Spectrometry	35
1.11	Representation and Data Treatment	37
1.12	Python	40
 Chapter 2 - Thermal History of Asteroid Parent Bodies is Re-		
flected in Their Metalorganic Chemistry		48
2.1	Introduction	49
2.2	Results and Discussion	50
2.2.1	Description of the CHOSMg Space	50
2.2.2	Chemical Structure of CHOSMg Compounds	52
2.2.3	Temperature-induced Formation and Stability of CHOSMg	55
2.2.4	CHOSMg Compounds as a Surrogate Parameter for Temperature Incidents	60
2.2.5	Conclusion and Outlook	61
 Chapter 3 - Diversity of Organic Molecules in Olivine Mineral		
Detected with High Resultion Mass Spectrometry		64
3.1	Introduction	65
3.2	FT-ICR-MS Analysis	66
3.2.1	Materials and Methods	66
3.2.2	Organic Compounds in Olivine	67
3.2.3	Comparison of Ionization Modes	68
3.2.4	ESI Analysis of Unheated Åheim Olivine	74
3.2.5	Heated Åheim Olivine and CHOSMg Compounds	88
3.3	LC-MS Analysis	93
3.3.1	Metabolite Method Results	93
3.3.2	Lipid Method Results	98

3.3.3	Discussion of the LC-MS Results	101
3.4	NMR Analysis	103
3.4.1	NMR Spectrum of Åheim Olivine	103
3.4.2	NMR Spectra of Heated Olivine	107
3.4.3	Discussion of the NMR Results	109
3.5	Discussion and Conclusion	111
Chapter 4 - Conclusion and outlook		112
4.1	Implications for the Emergence of Life	112
4.2	Further Research on Metalorganic Compounds	116
4.3	High Content Screening	118
4.4	Research Questions	120
Appendix		122
A.1	Material and Methods to Chapter 2	122
A.2	Figures and Tables to Chapter 2	126
B.1	Material and Methods to Chapter 3	137
B.1.1	Material and Methods - FT-ICR-MS	137
B.1.2	Material and Methods - LC-MS	138
B.1.3	Material and Methods - NMR	140
References		141
List of tables		158
List of figures		160
List of listings		161
Curriculum Vitae		162
List of scientific communications		164
Eidesstattliche Erklärung		166

Summary

A newly discovered chemical space of CHOSMg compounds was discovered in olivine mineral as well as in meteorites. They are theorized to be an intermediate form between the CHO and CHOMg compounds, as they are similar in points of chemical structure. The newly discovered compounds represent a thermal stable class of organic molecules, which is readily formed by heat, but also further transform to CHOMg compounds as a most stable form of organo metallic compounds. The presence of these compounds and their stability can have implications towards stability of organic compounds in harsh conditions such as the extraterrestrial environment or the properties of the Hadean times. CHOSMg and CHOMg compounds might fuel and catalyze prebiotic metabolism, and ultimately represent an important factor for the emergence and sustainment of life on Earth.

Non-targeted high-resolution analytical techniques such as Fourier Transform Ion Cyclotron Resonance Mass Spectrometry is a suitable method to analyse organic compounds in olivine mineral and in meteorites. As the presence of organic compounds in olivine mineral was up to this date barely investigated, the organic cargo of olivine was analyzed by multiple analytical techniques to complementarily describe the organic compounds found in olivine. Applied techniques are Fourier Transform Ion Cyclotron Resonance Mass Spectrometry, liquid chromatography quadrupole time-of-flight mass spectrometry, and nuclear magnetic resonance spectroscopy. To evaluate the stability of these organic compounds in olivine, heating experiments were conducted. Organic molecules in olivine are stable to 600°C and above and especially CHOSMg compounds reflect thermal alteration within their specific organic signature.

CHOSMg compounds were consequently found to be present in a large set of meteorites, which were specifically analyzed for the CHOSMg compound class. Organosulfur magnesium compounds were present in higher abundances in fusion crust compared to the inner matrix of the same meteorite. The systematic analysis revealed that sulfur-magnesium organic compounds allow

a differentiation of hydrothermal background without short-duration heating meteorites, meteorites with moderate short-duration heating, meteorites with intense short-duration heating and meteorites with long duration heating. The data allows furthermore to predict unknown samples and classify them to one of the four groups by comparing their CHOSMg signature. Moreover, the chemical structure and properties were analyzed by MS/MS fragmentation experiments and computational calculations to reinforce the assumptions on how CHOSMg compounds could be made up.

Zusammenfassung

Eine neu entdeckte chemische Verbindungsklasse von CHOSMg-Verbindungen wurde sowohl im Olivin-Mineral als auch in Meteoriten entdeckt. Es wird vermutet, dass sie eine Zwischenform zwischen den CHO- und CHOMg-Verbindungen sind, da sie in Aspekten der chemischen Struktur ähnlich sind. Die neu entdeckten Verbindungen stellen eine thermisch stabile Klasse organischer Moleküle dar, die leicht durch Hitze gebildet werden, sich aber auch weiter zu CHOMg-Verbindungen als stabilste Form von metallorganischen Verbindungen umwandeln. Das Vorhandensein dieser Verbindungen und ihre Stabilität kann Auswirkungen auf die Stabilität organischer Verbindungen unter extremen Bedingungen, wie z.B. in der extraterrestrischen Umgebung oder den Eigenschaften der Hadean-Zeit, haben. CHOSMg- und CHOMg-Verbindungen könnten den präbiotischen Stoffwechsel antreiben und katalysieren und letztlich einen wichtigen Faktor für die Entstehung und Erhaltung des Lebens auf der Erde darstellen.

Nicht zielgerichtete hochauflösende Analysetechniken wie die Fourier-Transform-Ionen-Zyklotron-Resonanz-Massenspektrometrie sind geeignete Methoden, um organische Verbindungen in Olivinmineralen und in Meteoriten zu analysieren. Da das Vorhandensein von organischen Verbindungen im Olivinmineral bisher kaum untersucht wurde, wurde die organischen Moleküle von Olivin mit mehreren analytischen Techniken untersucht, um die im Olivin gefundenen organischen Verbindungen komplementär zu beschreiben. Die angewandten Techniken sind Fourier-Transform-Ionen-Zyklotron-Resonanz-Massenspektrometrie, Flüssigchromatographie-Quadrupol-Flugzeit-Massenspektrometrie und Kernspinresonanz-Spektroskopie. Um die Stabilität dieser organischen Verbindungen in Olivin zu betrachten, wurden Erhitzungsexperimente durchgeführt. Organische Moleküle in Olivin sind bis 600°C und darüber stabil und insbesondere CHOSMg-Verbindungen spiegeln thermische Veränderungen innerhalb ihrer spezifischen organischen Signatur wider.

CHOSMg-Verbindungen wurden folglich in einem großen Satz von Meteoriten gefunden, die spezifisch auf die CHOSMg-Verbindungsklasse ana-

lysiert wurden. Schwefelorganische Magnesiumverbindungen waren in der Schmelzkruste in höheren Abundanzen vorhanden als in der inneren Matrix desselben Meteoriten. Die systematische Analyse ergab, dass die schwefelmagnesiumorganischen Verbindungen eine Unterscheidung von Meteoriten mit hydrothermaletem Hintergrund ohne Kurzzeiterhitzung, Meteoriten mit moderater Kurzzeiterhitzung, Meteoriten mit intensiver Kurzzeiterhitzung und Meteoriten mit Langzeiterhitzung erlauben. Die Daten ermöglichen es außerdem, die Gruppe unbekannter Proben vorherzusagen und sie durch den Vergleich ihrer CHOSMg-Signatur einer der vier Gruppen zuzuordnen. Darüber hinaus wurden die chemische Struktur und die Eigenschaften durch MS/MS-Fragmentierungsexperimente und chemischen Berechnungen analysiert, um die Annahmen zu untermauern, wie CHOSMg-Verbindungen aufgebaut sein könnten.

Acknowledgements

This work has been prepared at the Helmholtz Zentrum München, Ingolstädter Landstraße 1, 85764 München, in the research unit Analytical BioGeoChemistry (BGC) of Prof. Dr. Philippe Schmitt-Kopplin. The work was funded by the Deutsche Forschungsgemeinschaft (DFG, German Research Foundation) under Germany's Excellence Strategy - EXC-2094 - 390783311.

First of all, I would like to thank my supervisor Prof. Dr. Philippe Schmitt-Kopplin. You allowed me to pursue my dreams to become a PhD and you helped me a lot in troubling times and I will never forget that. Thank you very much for always having an open ear and an open door for my topics. And thank you for all the trust you put in me and that I could do this work in such an interesting field.

I want to thank Prof. Dr. Erwin Grill and Prof. Dr. Job Boekhoven who joined on my thesis defense. I really appreciate the time and effort you invested into my work.

Many thanks the research group Analytical BioGeoChemistry of the Helmholtz Zentrum München. All of you made this experience important to me, scientifically and personally. The friendly and cooperative social climate is probably the most important factor, which allowed me to work independently and freely in science. I will never forget how you helped me in many aspects, and I will surely miss my loved friends at the BGC.

I also want to thank you colleagues for their support during my time at the BGC. Many thanks to Michelle Marara Berger, who supported this work mentally, but also physically when B2 was drawing air again. With all of your memes and comments, you really made my time at the BGC very entertaining and special. And many thanks to Philippe Diederich, who worked with me in the CRC group and shared the office with me. With your humor, you always brightened the day. I am going to miss our fruitful discussion about our work. 映飞- 你是我最好的中国朋友。我很高兴认识你。谢谢你教我汉语。我会很想你的。 Special thanks go to Jenny Uhl, Dr. Marianna Lucio and Dr. Jasmine Hertzog who not only gave outstanding scientific advices, but also

helped me through the pandemic via countless zoom meetings aka the Food for Life Meetings. There will be always food for you at my place. Very many thanks to Astrid Bösl, Tina Daubmeier, and Brigitte Look. You not only helped with a lot organization and bureaucracy, but you also became close friends during the morning coffee session.

Also many thanks go to Dr. Alesia Walker, Dr. Daniel Hemmler, Dr. Franco Moritz, Dr. Norbert Hertkorn, Dr. Constanze Müller, Dr. Silke Heinzmann and Dr. Mourad Harir. You always had an open ear for my problems and always helped me when needed. You are the backbone of the BGC and without all of you, it just wouldn't work. Furthermore I want to thank all of my fellow PhD students Eva-Maria Harrieder, Kristina Hauslauer, Siyu Li, Stefan Pieczonka, Liesa Salzer and Leopold Weidner. We are all in the same boat and we are not capsized (yet).

Also I want to thank some special people in my life. First of all I want to thank Linda Vöhringer and Ilona Weber, for being by my side since day one of the university. I want to thank Lisa Kreutzer and Katharina Huber, for always having supported me, also when our way parted and still up to this day. Furthermore, I want to thank Svenja Körner and, who cheer me up in the pharmacy and make the nine hours on Saturdays worth the time. I want to thank Jonas and Elisa Wörlein for their endless support and their large collection of gin. And thanks go to Verena Munzert and Sebastian Mattheis for the best supportive BBQs one ever can have. I want to thank Julia Miller, Anna Grothe, Jana Schlosser, Anika Schmidt and Theresa Hilber for still being my friends and always being by my side after fifteen years (or more?). Many thanks go to Viktoria Bondarets who supported me in my new role as QA Officer and helped me calm down in stressful times. And thanks to Daniela Artelsmair, Judith Brehmer and the whole bookclub for our vivid discussions on everything. Bedankt Daphne De Lange och tack Louise Kihlberg for your support, all this time, every day. But wait, there are more: Thank you very much to Vanessa and Jonas Gebauer who supported me with food, laughter and good advice.

I especially want to thank my parents Elisabeth and Helmut Matzka and my brother Thomas together with Johann, for the support since day one on this Earth. I gave me all the tools and abilities to master my life up to this point and I couldn't be prouder. All of this is only possible because you always supported me. Thank you so much.

And to Edeltraud and Edgar Riedel, who also stood by my side all the time. I can always trust in you and I want to thank you for that today, for all the time you were there for me.

And lastly, thanks to Simon, who had to endure all of my moods during this time and always cheered me up no matter what. Your infinite support (and amazing cooking skills) gave me the strength to finish this project. And your question "Phd machi?" can finally be answered with "Ja, heute".

Acknowledgements for chapters

Chapter 2.2: I want to thank Michelle Berger and Dr. Alesia Walker for their scientific support and help with the LC-MS measurements.

Chapter 2.4: Thanks to Philippe Diederich and Dr. Norbert Hertkorn for their help performing the NMR experiments and for the excellent quality of the spectra.

Chapter 1.1: I want to thank Dr. Basem Kanawati for performing the computations for the CHOSMg compounds and his expertise in this field.

Chapter 1.3: Thanks to Dr. Marianna Lucio who helped me a lot performing the PCA and PLS-DA analysis and furthermore helped me with the interpretation of the data.

List of Abbreviations

2D NMR	two dimensional nuclear resonance spectroscopy
AI	aromaticity index
APCI	atmospheric pressure chemical ionization
APPI	atmospheric pressure photoionization
CI	chemical ionization
Cos	carbon oxidation state
COSY	correlation spectroscopy
DBE	double bond equivalent
DESI	desorption electrospray ionization
DOM	dissolved organic matter
EI	electron ionization
ESI	electrospray ionization
FAB	fast atom bombardment
FFT	fast fourier transform
FID	free induction decay
FT	Fischer Tropsch
FT-ICR	fourier transform ion cyclotron resonance
FT-ICR-MS	fourier transform ion cyclotron resonance mass spectrometry
FWHM	full width half maximum
HCS	high content screening
HPLC	high performance liquid chromatography
HSQC	heteronuclear single quantum coherence
ICR	ion cyclotron resonance

IOM	insoluble organic matter
JRES	J-resolved Spectroscopy
LC	liquid chromatography
LC-MS	liquid chromatography - mass spectrometry
MALDI	matrix-assisted laser desorption/ionization
MS/MS	tandem mass spectrometry
MS	mass spectrometry
NMR	nuclear resonance spectroscopy
NOM	natural organic matter
NP-HPLC	normal phase high performance liquid chromatography
PAH	polyaromatic hydrocarbons
PCA	principal component analysis
PLS	partial least squares regression
PLS-DA	partial least squares regression discriminant analysis
ppm	parts per million
RF	radio frequency
RP-HPLC	reversed phase high performance liquid chromatography
S/N	signal-to-noise
SEM	scanning electron microscopy
SOM	soluble organic matter
TOCSY	total correlated spectroscopy
TOF	time of flight
TOF-MS	time of flight mass spectrometry
Xc	aromaticity equivalent

Glossary

CHO	Compounds which contain carbon, hydrogen, and oxygen
CHNO	Compounds which contain carbon, hydrogen, oxygen, and nitrogen
CHOS	Compounds which contain carbon, hydrogen, oxygen, and sulfur
CHNOS	Compounds which contain carbon, hydrogen, oxygen, nitrogen, and sulfur
CHOMg	Compounds which contain carbon, hydrogen, oxygen, and magnesium (organo magnesium compounds)
CHOSMg	Compounds which contain carbon, hydrogen, oxygen, sulfur, and magnesium (organo sulfur magnesium compounds)
CHNOMg	Compounds which contain carbon, hydrogen, oxygen, nitrogen, and magnesium
CHNOSMg	Compounds which contain carbon, hydrogen, oxygen, nitrogen, sulfur, and magnesium
H/C	Describes the calculated ratio of the number of hydrogen vs the number of carbon
O/C	Describes the calculated ratio of the number of oxygen vs the number of carbon
<i>m/z</i>	Describes the mass per charge ratio of a molecule as measured in mass spectrometry
Olivine	A magnesium iron mineral, which is usually found in mafic rocks, but also in meteorites
Meteorite	A solid rocky piece from outer Space, which survived the atmospheric entry

Chapter 1 - Introduction and Materials and Methods

1.1 General Introduction

1.1.1 Organic Molecules in Geological Samples

For most of the time, geological samples were regarded as abiotic stony structures consisting of various minerals and elements. The largest proportion of the conducted research is solely focused on these mineral features, their evaluation, their transformation under certain conditions of their physical and chemical properties. For many people, the fact that geological samples do only contain and consist of inorganic molecules is irrevocable. However, over the last decades, research showed the existence of a large variety of organic compounds within many geological samples of different origins. At first, elemental carbon and simple carbon containing compounds were evidenced within rocky samples by analyzing the elemental bulk composition. Later, more refined research was conducted to investigate chemical structures and oxidation states of the carbon within the samples. Today it is more and more acknowledged that geological not only consist of inorganic molecules, but also contain a large variety of organic compounds. Nevertheless, the organic molecules inside of geological samples are barely investigated. They make up only a small part of the total volume of compounds and thus were overlooked for most of the passed time so far.

1.1.2 Research Questions

This work was written in the context of the emergence and sustainment of life on Earth. The research of this field focuses on possible ways how life in our universe can start and how it could have evolved over time until today. Three major topics are looked at in this field, namely early synthesis, replication and translations, and early metabolism and cells. Replication and translation research focuses on DNA and RNA formation and their replication as well

as peptides and proteins with catalytic functions. Early metabolism and cell research is focused on amplification, self-replication, and physical and chemical conditions, which were present at early Earth and how they could have promoted life. The research field where this work contributes to is the early synthesis. The topic focuses on the stability of compounds and how early synthesis could have worked in the primordial soup. The theories of this research field either represent the hypothesis that early Earth provided enough small molecules to start and fuel chemical reactions, or state that small and medium sized molecules already emerged in space and were brought to Earth by carriers. This work presents a combination from both of these theories, that larger molecules were built on Earth, but also that they came from outer Space. The first question to answer is **"Do geological samples contain the suitable compounds to fuel and sustain the emergence of life on Earth?"**.

Moreover, the question of stability of organic compounds within the mineral matrix of geological samples arises. Organic compounds are known to decompose in high-energy situations such as high temperature, impact, and high pressure incidents. Nevertheless, minerals and rocks and many times face these situations either in outer space during their appearance and evolution, but also inside of our Earth in the mantle and in magma chambers. It is thus unlikely to find organic compounds in geological samples and their presence could be seen as counter-intuitive regarding all information which is up to this date available regarding geological samples. Against all odds, organic compounds can survive these harsh situations within the mineral matrix. A second question is consequently **"Do organic compound survive harsh conditions and how are these conditions influencing the molecules within the geological samples?"**

Furthermore, the questions of the localization of the organic molecules and the properties of the geological samples arose. It can likely be assumed that organic compounds are not evenly distributed within samples and moreover that not all geological samples contain similar amounts of carbon containing

compounds. Consequently a question to be answered is **"Where are organic compounds located within geological samples?"** Ultimately, a differentiation between geological samples from extraterrestrial origin and terrestrial origin can be analyzed to see if processes are similar in both regimes, so a last question to be looked at would be **"Are organic compounds in geological samples more dependent on their origin or are there others factors which have to be considered?"**

1.1.3 Applied Methods

One of the reasons that organic compounds within geological samples are largely uninvestigated is that their abundance is low compared to inorganic molecules. Science had to develop a certain level of sensitivity and accuracy to detect these compounds in the first place and hereafter investigate their chemical structure. Nowadays, instrumental analysis has come far enough to be able to firstly detect these compounds and secondly analyze them to a certain level of confidence. One of the most applied techniques to unknown compounds in samples is fourier transform ion cyclotron resonance mass spectrometry (FT-ICR-MS). Due to high mass resolution and sensitivity, even smallest amounts of organic compounds can be detected with this technique. The accuracy and resolution of this technique is high enough to even assign precise chemical compositions to detected mass signals. Similarly precise is the technique of nuclear resonance spectroscopy (NMR) spectroscopy, which allows to make statements about chemical connectivity. Ultimately, this technique allows to investigate the abundance of chemical bonds of the organic compounds in geological samples. Moreover liquid chromatography - mass spectrometry (LC-MS) can be applied as a method to not only separate organic compounds in a chromatographic run, but also provides fragmentation spectra, which allow the chemical identification of chemical compounds. These techniques together with data analysis and computational methods were applied to investigate organic compounds in geological samples.

1.1.4 Aim of this Work

Organic molecules within geological samples are widely investigated. Less is known about their chemical properties as well as about their life cycle. In this work, approaches to analyze organic compounds in mineral samples will be shown. The implications of organic compounds in geological samples will be outlined and the applications of organic analysis will be discussed.

The **first chapter** of this work will cover introducing information regarding the general topic, the materials and methods applied in this research field and a small recapitulation of the state of the art.

In the **second chapter** of this work, the organic compounds of a large sample set of meteorites was investigated in a comparative manner. During this process, a up to this point investigated compound class of CHOSMg compounds was found and further analyzed. These molecules reflect differences in the thermal history of the samples.

During further analysis it was shown that especially olivine mineral contains a large amount of diverse organic compounds compared to other compartments of geological samples. Olivine is a magnesium-iron silicate mineral that is abundantly present in the Earth's upper mantle, [1] but also in many chondritic meteorites [2]. In **chapter three**, olivine mineral was further investigated. Also the influence of temperature on organic compounds of olivine mineral was investigated. Furthermore, the comparison of three different analytical techniques to investigate organic compounds in olivine is presented.

An outlook will further evaluate possibilities and research gaps which are up to date not investigated. The here presented results can be further looked at and can be refined as the discovery of organic compounds in mineral samples is a very young field of research. The existence of organic compounds implies an in depth analysis of these compounds and ultimately a deeper understanding of the formation and implication of these organic compounds as found in olivine and meteorites.

1.2 Organics in Meteorites

For a long time, interstellar medium, molecular clouds, comets, and meteorites were thought to be void of organic compounds. The rough extraterrestrial conditions were assumed to be too hostile for organic compounds. However, astronomical spectroscopy enabled the detection of first organic compounds in the 1970s and until now, a large number of detected extraterrestrial compounds followed [3, 4]. Optical spectroscopy, radio spectroscopy, and X-ray spectroscopy were successfully used to unravel the broad variety of large compounds and simple molecules, which are omnipresent in our universe [5, 6]. Consequently the assumption that meteorites also bear organic compounds was quickly made and many times proven correct [7]. In contrast to the targets of astronomical spectroscopy however, some samples, e.g. meteorites, can be found on earth and thus enable the investigation of extraterrestrial organic matter with all available methods on our planet. These samples from outer Space consequently allow an in-depth analysis of organic molecules, which was successfully performed by a manifold of groups with a broad variety of scientific techniques (see Material and Methods part of this work).

1.2.1 Origin of Meteorites

A meteorite is defined as a solid body coming from an interstellar object such as comets and asteroid, which survives the atmospheric entry to earth and can be sampled on the surface. Meteorites are theorized to have formed from the solar nebula and are consequently approximately 4.5 billion years old [8]. As carriers of organic compounds, meteorites can give insights into the chemical speciation of carbon and the chemical development of our solar system. Meteorites are classified in different categories by geological and mineral grouping [9]. As more than 200 different mineral types have been found in meteorites so far, an exact identification is difficult. However, meteorites were classified in three major classes. Firstly, iron meteorites, which are composed of mostly an iron-nickel matrix, secondly, stony meteorites, which are composed of silicates of rocks, and thirdly, stony-iron meteorites, which

represent a combination of various degree of the first two classes.

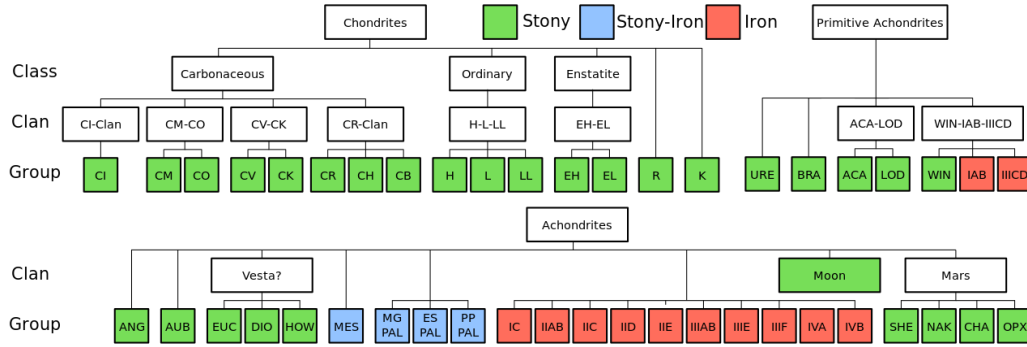


Figure 1: Schematic classification of meteorites, adapted from Weisberg, McCoy, and Krot 2006 [9] and taken from [10].

Especially in the group of chondrites, the carbonaceous chondrites are of interest as they contain the largest amount of carbon of all meteorites [11]. They consist of approximately 3% carbon in various oxidation states and versatile molecules. Carbonaceous chondrites are grouped again into different types depending on their composition and their degree of hydration. For example CI chondrites (Ivuna type) do not contain chondrules (round grains), but have a high degree of hydration. CM chondrites (Mighei type) contain small chondrules, a fine grained matrix and abundant hydrated minerals. CV chondrites (Vigarano type) contain large chondrules and abundant matrix [12]. Another interesting group for the research of organic compounds are ordinary chondrites, which are divided into three groups regarding their metal content. H chondrites are high in iron and metal content, L chondrites are intermediate between H chondrites and LL chondrites, which have low total iron and low metal. Moreover, a special group of achondrites are the pallasites, which are solely composed of a iron-nickel matrix together with olivine mineral inclusions [12].

1.2.2 Organic Compounds in Meteorites

When speaking about organic molecules in meteorites, most literature refers to the organic compounds of carbonaceous chondrites as this class of meteorites contains the most carbon [13–15]. A broad variety of meteorites has been investigated with various different methods so far. All of these studies concluded that meteorites contain organic compounds in two different forms, namely soluble organic matter (SOM) and insoluble organic matter (IOM). Analyzing these two different forms of organic compounds has to be conducted in different ways due to their different chemical properties.

The IOM is a large macromolecular polyaromatic construct of organic structures, which are interconnected, but insoluble in solvents due to chemical size and polarity. Most studies conclude that the IOM represents the largest proportion of the organic compounds in meteorites [16]. IOM has been investigated since the 1980s with spectroscopic methods and with degradative methods [17]. Degradative methods try to demineralize and extract the organic matter with repeated use of hydrofluoric and/or hydrochloric acid [16, 18]. Besides polyaromatic macromolecular structures, also heteroatoms such as oxygen, nitrogen, and sulfur were detected in the IOM. Spectroscopic methods can be used on the extracted and cleaved IOM, but also can be applied on the intact meteorite. Examples of these methods are ^1H and ^{13}C NMR, transmission electron microscopy, electron energy-loss spectroscopy, Raman-spectroscopy, infrared spectroscopy, or X-ray absorption near edge structure spectroscopy [19–21]. A possible chemical structure of the IOM of Murchison meteorite was published and can be seen in Fig. 2 [22].

The proposed structure contains high amount of (poly)aromatic structures, which are cross-linked by aliphatic hydrocarbon chains with incorporation of hetero-atoms. IOM is also highly susceptible to temperature alteration and reflects the temperature history of meteorites. This enables an improved classification of heat history and allows an allocation of samples to geological groups, even where geology does not provide enough information [23, 24].

In contrast to the IOM, the SOM, also called free organic compounds,

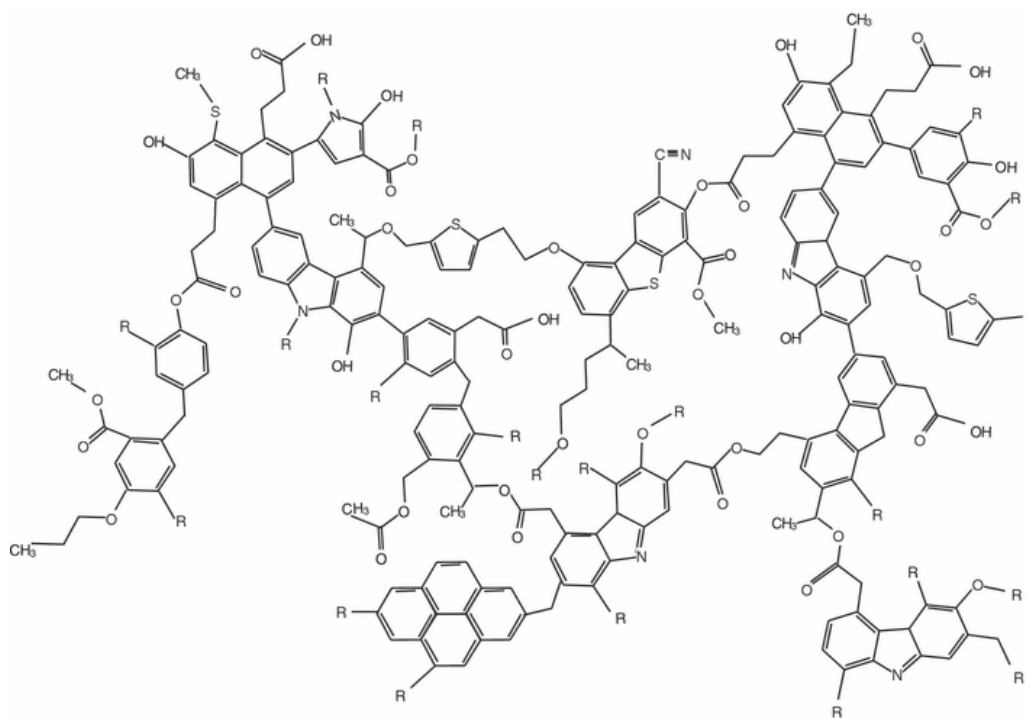


Figure 2: Theoretical chemical structure of IOM as proposed to be found in meteorites as stated by Derenne et al. [22]. Polyaromatic structures are cross linked by aliphatic chains with hetero atom contribution.

can be more easily accessed for analysis and investigation [25]. Until today, a manifold of organic compounds has been detected in meteorites, of which many are also important for the sustainment of life and consequently could also be essential for the emergence of life. Already in 1983, amino acids were detected and analyzed in meteorites [26]. As building blocks of proteins, amino acids are essential for life. Many of the proteinogenic amino acids were found in different meteorites [19, 26–28]. Interestingly, also many amino acids, which are not part of proteins were found in meteorites. More than 150 different amino acids were discovered in the SOM of meteorites [29]. Also nucleobases, which are the buildings blocks of RNA and DNA, were found in meteorites [30–32]. Differently substituted purine and pyrimidine molecules were detected in varying amounts in multiple meteorites [31]. In

combination to this, sugar and sugar-like compounds were identified in many meteorites [33, 34]. Thus all compounds to generate DNA and RNA are provided within these extraterrestrial samples. Furthermore, carboxylic fatty acids were detected also in meteorites in large amounts [35–37]. These compounds are essential building blocks for cellular membranes and for prebiotic metabolism. To sum up, the SOM found in various meteorites provides the necessary building blocks to sustain life and even might augment chances that life emerged on Earth, as all necessary compounds for life could have been brought by meteorites. The investigation of organic compounds enables to have a glance at the chemistry of outer Space a few billion years ago, and also give indications of how our biological chemistry and metabolism evolved from simple molecules (see Figure 3).

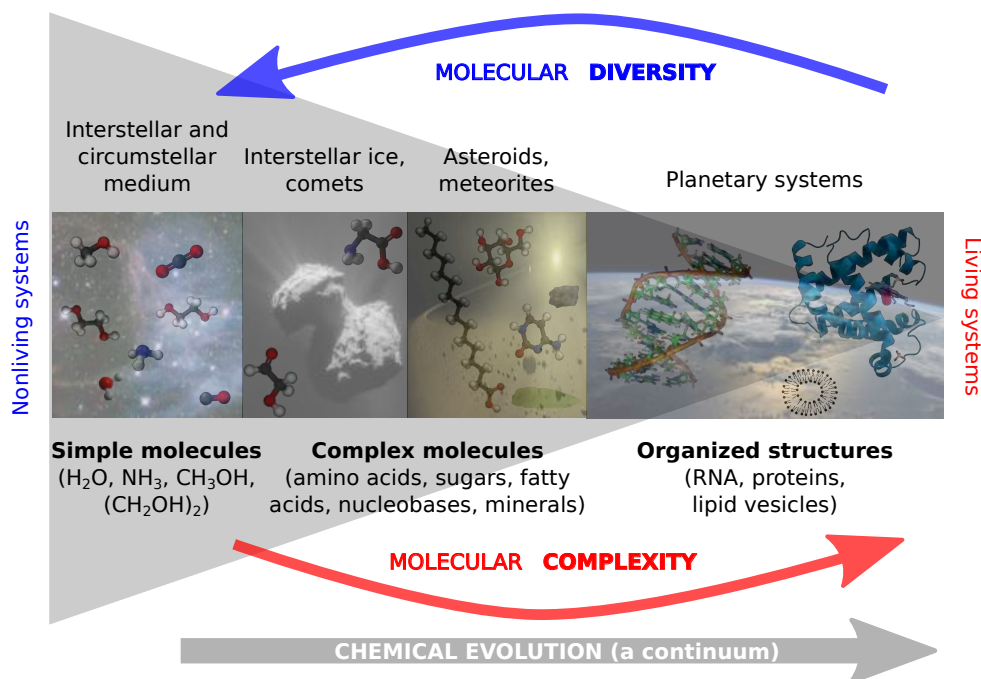


Figure 3: Sketching chemical evolution in terms of molecular diversity and molecular complexity. Molecular transformation within time and space is illustrated. Simple molecules within interstellar and circumstellar media evolve to highly-oriented, organized, complex macromolecules on planetary systems, enabling the potential of living systems. Originally published by Ruf *et al* in Life Journal - MDPI Open Access. [38]

1.2.3 Analysis of Meteorites and Implications

The analysis of organic compounds in meteorites and extraterrestrial material not only helps us to understand extraterrestrial chemistry and the beginnings of our Solar System, but is also of utmost importance when it comes to the preparation for upcoming and already launched return missions. Meteorites were for a long time the only extraterrestrial samples, which were accessible for the analysis of physical and chemical properties of space. Their analysis improved our understanding of the universe and helps to set the right focus on the research questions and analytical procedures for the returned samples, which are pristine and unchanged as found on the interstellar object. A famous already finished return mission is the Hayabusa 2 mission [39], an ongoing mission is the Osiris Rex mission [40]. From both missions, we can expect a pristine extraterrestrial probe containing organic compounds from the beginning of the solar system which ultimately shed more light on the physical and chemical properties of our universe. Meteorite analysis and the understanding of the formation of organic compounds enables a in-depths analysis and interpretation of return mission samples to a up until today unreached level of profoundness.

1.3 Olivine Mineral

Olivine ($(\text{Mg,Fe})_2\text{SiO}_4$) is a neo- or orthosilicate mineral which belongs to a group of magnesium iron silicate minerals. The name derives from its green colour, but depending on elemental composition and oxidation state, yellow and brown colors are also seen [41]. While olivine, which contains more magnesium displays a green/gray to white color, iron containing olivines show brownish color. Olivine consists of isolated silicon tetrahedra with magnesium and iron cations at the octahedral positions. From a coordination point of view, olivine mineral can be seen as an array of isolated SiO_4^{4-} tetrahedra with Me^{2+} ions in octahedral holes [42] (see Figure 4). The mineral mostly contains a mixture of magnesium and iron cations but also the pure magnesium and pure iron forms can be found in nature. The magnesium endmember (Mg_2SiO_4) is called Forsterite, the iron endmember (Fe_2SiO_4) is called Fayalite. Forsterite has a high melting temperatures of 1900°C while the Fayalite has a melting temperature of about 1200°C . The melting temperature of olivine decreases with increasing iron content. Besides oxygen, silicon, magnesium, and iron, the mineral also can contain nickel, calcium, aluminum, chromium, manganese, and other cations, but far fewer in amount. Also part of the olivine group are Tephroite (Mn_2SiO_4), Liebenbergite (Ni_2SiO_4), Monticellite (CaMgSiO_4), Kirschsteinite (CaFeSiO_4), and Glaucocroite (CaMnSiO_4) [43, 44]. A concise description of the mineralogy of the olivine group has been published by Smyth et al. (2000) [44].

Many studies to investigate the chemical and physical properties of olivine have been performed, investigating abiotic features and mineral characteristics. Recently, olivine gained new attention due to its ability to abiotically generate methane and elemental hydrogen, and within this topic, the connection to small organic molecules was drawn. Besides the methane production, olivine is also discussed to fuel the formation of organic compounds by aqueous alteration on parent bodies [45, 46]. The presence of olivine could be decisive factor when it comes to abiotic synthesis of organic compounds in terrestrial samples as well as in meteorites [47]. This discovery has opened many questions as well

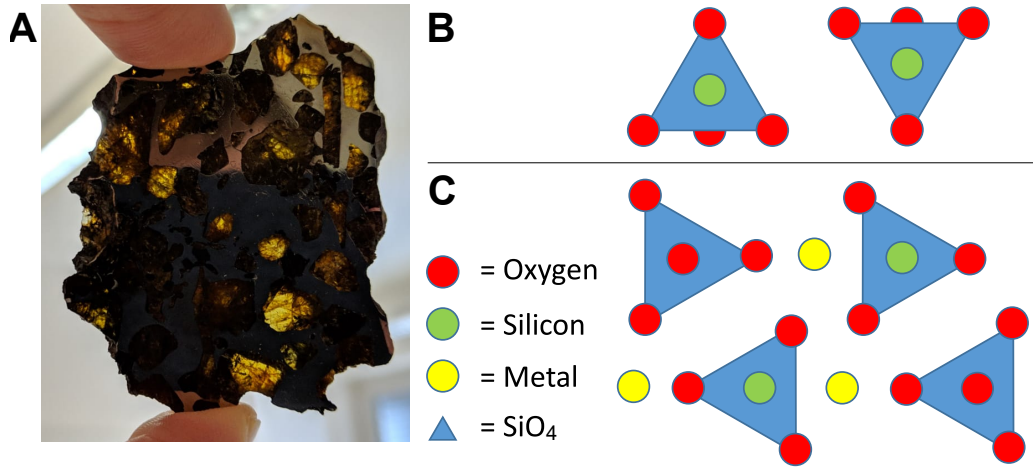


Figure 4: **A** Olivine (green-yellow and shine-through) inside iron-nickel matrix of a pallasite. **B** Side view of olivine crystal structures. **C** Top view of olivine crystal structure

as allows different possible implications for multiple research fields.

Firstly, olivine might be a contributor to the emergence and sustainment of life on earth. The abiotic formation of methane and other small organic compounds can play an important role to provide prebiotic molecules, more precisely essential compounds to form early organisms or to generate molecules fueling prebiotic reactions. Olivine has been present on Hadean Earth and is up to today still present on Earth and in extraterrestrial systems. Its ubiquitous presence implies its contribution to the nowadays present organic matter as it can be found in nature.

Secondly, an important field for olivine research is the sequestration of carbon dioxide in regards to the greenhouse effect and the climate change. Olivine undergoes serpentinization (see chapter 1.3.3 and 1.4) reaction when in contact with water, for example on seafloors, in the mantle with disperse groundwater reservoirs, or at olivine beaches. During this reaction, carbon dioxide is transformed to either methane or carbonates, which are considered as educts for subsequently evolving organic compounds. Magnesium carbonates serve as nourishment for coral reefs or are subject to subduction transporting

carbon back into the Earth's mantle. By weathering on tropical beaches, olivine minerals could compensate for the yearly carbon dioxide emission of humanity. Consequently olivine mineral plays a vital role in the terrestrial carbon cycle.

Thirdly, another research topic on olivine is the abiotic formation of methane in order to use it as fuel to replace crude oil. Several studies investigated ideal reaction conditions to increase the yield of methane or other biofuels generated by the reaction of olivine with water and carbon dioxide. Critical parameters in this process are grain size, pH conditions, abrasion, temperatures, and time.

Fourthly, olivine might be an important factor of the synthesis and preservation of organic compounds in meteorites. As olivine represents a frequently encountered mineral in many meteorites, the mineral could be a critical factor for the carbon speciation in extraterrestrial geological samples. Preliminary experiments showed that olivine contains a richer and broader diversity of organic compounds in meteorites compared to fusion crust, melts, or inner matrix of the same meteorite (data not shown). It can consequently be assumed that olivine plays an important role in the formation of organic compounds inside of meteorites.

Besides all of these research fields however, the hitherto unknown broad variety of diverse and complex organic compounds in olivine mineral, which is the crucial basis for the mentioned research fields, remains uninvestigated to this date. Besides methane, also a broad variety of organic compounds are formed in and on olivine. These small organic molecules show specific characteristics depending on the conditions under which the olivine has been formed, but also reflect environmental influences such as heating incidents. Analyzing the organic molecules of olivine not only enables to more precisely describe geological conditions during formation, which is especially essential for extraterrestrial samples, but also enables the comparison of samples with unknown origin, namely abundant meteorites which have been found on earth.

1.3.1 Olivine Mineral on Earth

Olivine is the most abundant mineral in the Earth's upper mantle, followed by orthopyroxene, clinopyroxene, and garnet [1,48]. It usually occurs in mafic and ultramafic rocks, for example basalt or dunite, as well as in metamorphic rocks. Consequently olivine can mostly be found in former or recent active volcanic sites such as La Réunion, the Azores, Hawai'i, or Iceland. Olivine can also be found in Ophiolites, but quickly weathers when coming into contact with water. The mineral is thus scarce on the Earth's surface and only exists if close to its source [49]. With increasing pressure in the Earth's mantle, olivine undergoes transitions. At 300 km of depth, the formation of wadsleyite is observed, followed by spinel, perovskite, and magnesiowüstite with increasing depth [48]. Olivine from the mantle can be brought back to the Earth's surface by active volcanism. The mineral phase mixes with the magma down in the magma chamber. Thereby, it experiences intense heat and pressure before eruption. The olivines from Shiveluch volcano, Kamchatka, for example, encountered temperatures of approximately 1260°C and pressure of approximately 6 kbar [50]. These conditions can last from several days up to several years depending on timepoint of eruption.

A famous example of olivine on Earth is the green sand beach on the Big Island of Hawai'i. Its green colored sand is coming from volcanic olivine from the tuff ring south of Mauna Loa by washout. Other examples of green sand beaches are in Guam, Floreana Island, and Norway. Furthermore, one of the largest industrial used olivine deposits can be found in Norway, for example near Åheim.

Despite the countless amounts of possible olivines to analyze, the most famous terrestrial sample of investigated olivine is called "San Carlos" from Arizona [51]. Due to its large availability, the olivine has been used by many groups as a standard olivine to conduct research on the mineral. A detailed description of the San Carlos olivine has already been published [52]. San Carlos olivine has been classified as a Fo90, meaning that 90% of the olivine are forsterite. Trace amounts of calcium and manganese have been found [53].

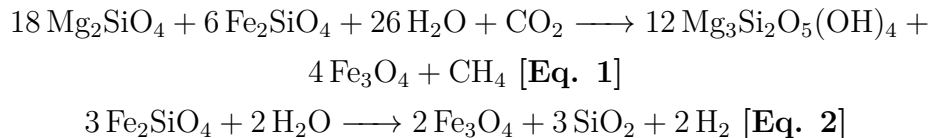
1.3.2 Extraterrestrial Olivine

Similar to the Earth's mantle, olivine is also the most abundant mineral in many chondritic meteorites, which are the biggest class of meteorites [2]. Olivine is the first magnesium mineral to crystalize from the cooling solar nebula [54]. This can be explained due to its high melting temperatures. The mineral has been so far found in meteorites [55, 56], on asteroids [57, 58], on Mars [59, 60], and on the moon [61, 62]. Especially pallasites are of interest for olivine research since they mostly consist of metal and olivine mineral. These stony-iron meteorites are possibly coming from core-mantle boundaries of planetesimals or now disrupted asteroids [63–66]. Olivine derived from pallasites have been shown to display chemical gradients of elements from diffusion during slow cooling at temperatures above 800°C [65, 67–71]. Over many different pallasites, the found olivines show differences in their chemical composition even though the cooling temperature with 0.5° to 2.0° C per million years is a lot slower than on Earth [64]. Consequently the history of the organic matter in these olivines should be different from each other, but especially different to terrestrial olivine's temperature history. The most famous pallasite is Krasnojarsk, which was found 1749 in Siberia. Other famous samples are Brahin, found 1807 in Belarus, and Esquel, found 1951 in Argentina [72]. Up to this date, more than 120 different pallasite samples have been classified and most of them were found in Antarctica and in North West Africa [12]. Organic matter in olivines from extra-terrestrial samples are important in an astrobiological context and may contribute to the emergence and sustainment of life. Furthermore, the history of these pallasites shed light on carbon speciation in space. Organic compounds could consequently not have emerged on Earth but were brought to our planet from outer Space.

1.3.3 Serpentinization

Olivine, which comes in contact with water under 500°C undergoes serpentinization reaction, thereby forming serpentinite minerals [73]. This is a hydration reaction, during which olivine ($(\text{Mg,Fe})_2\text{SiO}_4$) is hydrated to ser-

pentinite $((\text{Mg,Fe})_3\text{Si}_2\text{O}_5(\text{OH})_4)$ (see Eq. 1). Furthermore, Fe^{2+} in the olivine is oxidized to Fe^{3+} leading to the abiotic generation of molecular hydrogen [74]. Especially this process of iron oxidation is the cause for the abiotic production of hydrogen, which is able to promote further reactions (see Eq. 2).



As one of the first building blocks of life, H_2 is able to fuel reactions that lead to a diverse and complex organic matter [73,75–78]. H_2 , a strong reducing agent, is able to react with CO_2 dissolved in water and from the atmosphere to form methane, ethane, propane, and many other organic compounds [73]. This reaction has been widely researched regarding the methane production as well as corresponding reaction parameters. Abiotic methane production has been observed in terrestrial as well as in extra-terrestrial context. A famous spot for serpentinization and abiotic methane production is the hydrothermal field of lost city [79–81]. In this area, alkaline hydrothermal vents produce simple molecules such as methane and hydrogen, which consequently represents a famous research side for prebiotic compound synthesis. Olivine is exposed to seawater at the mid-atlantic ridge with high pressure and temperature as well as alkaline conditions. The conditions are ideal for serpentinization of olivine. Consequently Lost City has been discussed as an exemplary site for a possible emergence of life.

Furthermore, serpentinization reactions have also been observed on celestial bodies [76,82]. In theory, many extra-terrestrial environments feature suitable conditions for abiotic methane formation by serpentinization. A methane cloud detected on Mars for example is assumed to derive from the serpentinization reaction [82]. In contrast to the abiotic production of methane, the diverse and complex amorphous organic phase created by serpentinization has been so far less investigated, but occurs besides methane aswell.

1.3.4 Carbon in Olivine

Carbon incorporation in the olivine is controversially discussed in the literature. Carbon could be a direct substitute of silicon in the tetrahedral structure of the olivine [83, 84] or it could be later dissolved in the structure, found as carbonaceous phases, graphite, silicon carbide, and other compounds as well as in sub-microscopic bubbles or cracks [85, 86]. Freund et al. suggested, that H_2O and CO_2 are, to a certain extent, soluble in upper mantle olivine. These elements can further be converted to form H_2 and reduced carbon to then cause the formation of C-H entities. These organic molecules either exist in the form of carboxylic acids, dicarboxylic acids, and medium chain fatty acids or are directly attached to the Mg-silicate matrix by bonding to two O^- moieties [87]. Similar organomagnesium molecules were also evidenced in carbonaceous chondrites such as CM2 Murchison meteorite [88]. The carbon concentration in olivine has been investigated by different groups and methods. Depending on the used analytical technique, the amount of carbon is approximately between 10 ppm and 30 ppm in San Carlos olivine [85, 86, 89–91]. A more recent approach reports a carbon solubility in olivine of 0.1 ppm to 1 ppm [92].

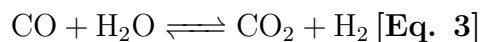
1.3.5 Deep Carbon

Olivine plays an important role in the storage of carbon in the Earth's mantle in the context of deep carbon. In this context of deep carbon, olivine is accountable for mass and energy transfer, tectonic deformation, mineral deposit formation, carbon sequestration, and rheological changes in the lithosphere. By comparing the numbers of amounts of carbon in, estimates predicted that more than 99.99% of all carbon on Earth is in the mantle and crust, excluding the core [93, 94]. These deep carbon sources, also called endogen carbon, are in equilibrium with exogen carbon, the carbon found on the Earth's Surface [94]. By degassing events, for example volcanic eruptions, carbon is transferred from deep carbon sources to the surface. At subduction zones, carbon in the form of for example precipitated carbonates is transferred back into the Earth's mantle [95]. Both processes are slow and equilibrated

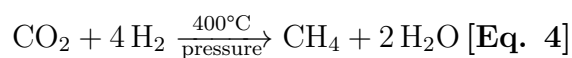
depending on the depth of the endogen carbon within a range of million years. Nevertheless, this process functions as Earth's thermostat. During glacial periods, the amount of greenhouses gases such as methane and CO₂ were significantly lower compared to warmer periods. While this process nowadays is quite slow, the exchange of carbon used to be a lot faster during Hadean Earth [96]. Because of this process, olivine contains many molecules derived from biological sources, but also molecules which were created inside the olivine. The organic cargo of terrestrial olivine is different compared to olivines from extra-terrestrial sources due to the contribution of life derived compounds. Furthermore, the organic molecules in olivine also serve as a source of energy for the deep biospheres [97,98]. Especially anaerobic bacteria, which have been found at depths as deep as the Earth's mantle profit from organic molecules in olivine as a source of local energy sources. Consequently, the storage of carbon in olivine plays an important role regarding climate effects and thus is of utmost importance for the terrestrial carbon cycle [93].

1.4 Synthesis of Organic Compounds in Geological Samples

Up to this date, the processes which allow the formation of organic compounds in geological samples is not elucidated. However, basic and well described chemical pathways have been investigated, which present plausible scenarios for the organic synthesis in meteorites and olivine. As seen before, olivine and the serpentinization reaction cause the generation of elemental hydrogen, methane, and magnetite. These together with water and carbon dioxide, which is readily found in meteorites as well as in olivine, are vital edcuts for the subsequent synthesis of organic compounds. Both water and carbon dioxide are furthermore provided by the Hadean environment, which could also have promoted the synthesis of organic compounds. It is important to know that carbon monoxide, carbon dioxide, water, and hydrogen are in equilibrium to a certain extent (see Eq. 3).

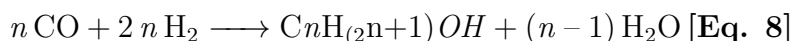


One of the reactions enabling the formation of methane is the Sabatier reaction [99,100]. The Sabatier process allows the formation of methane from carbon dioxide and hydrogen under high temperature and pressure conditions (see Eq. 4). Both carbon dioxide and carbon monoxide can be educts for this reactions (see Eq. 5).



CO₂ or CO and H₂ together can abiotically form methane which has been many times observed in olivine. As CO₂ and CO are present in olivine mineral from inclusion or from the atmosphere and H₂ is created by oxidation of iron in olivine, the Sabatier process is a possible reaction pathway to describe the generation of organic compounds in olivine and meteorites.

Moreover, the Fischer Tropsch (FT) synthesis is also a plausible chemical way to abiotically generate alkanes, alkenes, and alcohols in mineral samples [101, 102]. FT reactions require catalytic reaction surfaces such as metal oxides in combinations with metal catalysis as known from nickel and iron.



Similar to the Sabatier process, CO and H₂ are consumed to produce small organic compounds (see Eq. 6-8). FT reactions can results in alkanes, alkenes, and alcohols which then again are educts for subsequent reactions. The setting of this reactions in a catalytic environment within the olivine or meteorites can cause further reductions by elemental hydrogen, but also incorporation of hetero atoms or addition reactions towards double bonds are plausible. The Sabatier process and the FT are two chemical reactions schemes which allow the generation of a broad variety of organic compounds

within the mineral environment of olivine and meteorite. All components contribute to a diverse reaction pattern and are ultimately the educts for the complex organic matter which can be observed within the mineral of olivine mineral and meteorites.

The question of stability of organic compounds within the mineral matrix of olivine arises. Generally, olivine is found in mafic rocks on earth and in pallasites within extraterrestrial samples. Mafic rocks show characteristics of high temperature alteration. Olivine are in contact with magma of above 1000°C in temperature. Within this temperature range, organic compounds are unlikely to be stable and quickly decompose to small compounds, to volatile gases, or completely to their elements such as black carbon. Also, pallasites could be generally considered as hostile environments for organic compounds due to intense heat in the parent body. Furthermore, they witness cosmic radiation and space weathering which terminate at atmospheric entry, a high temperature incident. A similar harsh treatment of organic matter can be theoretically observed in meteorites and other extraterrestrial samples. It is thus unlikely to find organic compounds in olivine and meteorites and their presence could be seen as counter-intuitive regarding all information which is up to this date available regarding geological samples.

Even though organic molecules in olivine and in meteorites experience harsh conditions, they are not destroyed completely while inside the mineral matrix. In contrast to the assumption that organic compounds cannot survive such temperatures or conditions, olivine and meteorites provide a suitable matrix to protect organic compounds from external conditions and shelters them from hostile environments. Due to this fact, organic compounds can not only survive in olivine and meteorites, but also change within the protective matrix. Even though organic compounds are not destroyed by external influences, they are also not unaffected by environmental changes.

Organic compounds, which are detectable by the introduced analysis methods belong to the so called SOM. This SOM is soluble in polar protic solvents such a methanol and consequently can be detected in for example

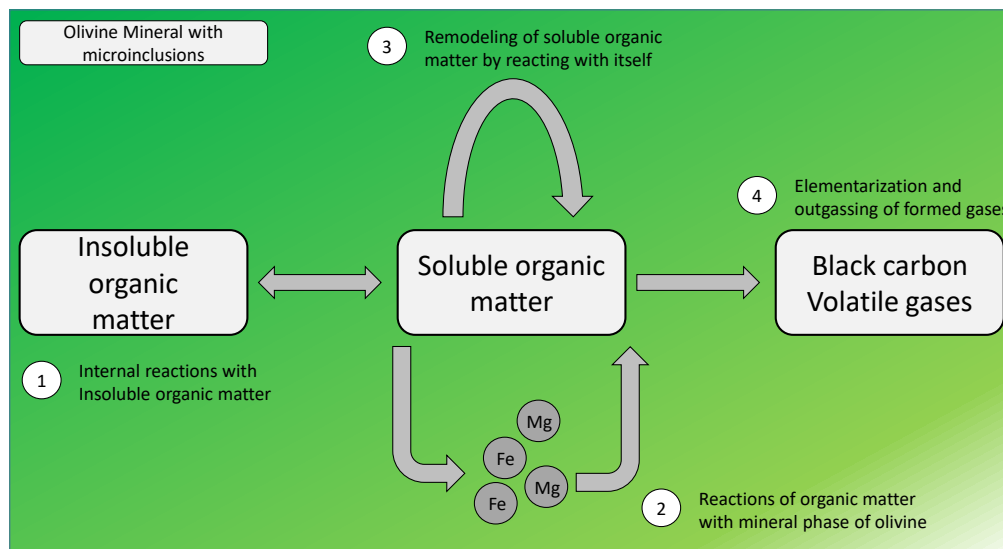


Figure 5: Schematic figure of soluble organic matter in olivine. Possible reaction pathways are shown when under temperature influence.

FT-ICR-MS. This part of the organic compounds are detectable to the used methods and thus can be the basis for further evaluation of the data. Temperature incidents can change the composition of the organic compounds, especially the SOM, in olivine. Fig. 5 shows possible pathways how organic compounds can change with temperature in the olivine. As in the introduction part discussed, the organic matter is trapped within the olivine in so called micro-inclusions. This represents a closed system where organic matter mainly reacts with itself. In some cases, reaction products, which are small enough, for example molecular hydrogen, can escape the closed system, but also can return in matters of time.

First of all, organic matter can react with itself. The SOM is assumed to be nonreactive until temperature increases to supply the necessary energy for reactions. This means, on the one hand, that organic matter in an olivine is preserved for a long period of time, but on the other hand, that organic compounds also reflect the temperature history of the olivine or the meteorites. By increasing temperature, fragile bonds, for example such as in hydroxy-

groups or amines, can easily break under the formation of gaseous water or ammonia. New carbon-carbon bonds can be formed due to high temperature and high pressure chemistry. The formation of more temperature stable organic structures is favored compared to less stable ones. The whole organic matter within in the micro-inclusion undergoes a wide variety of reactions which are vastly unpredictable due to the high temperature and pressure environment.

The SOM can also undergo reactions which render the molecules insoluble in methanol. This can arise for example due to increase in size from newly formed carbon-carbon bonds, but also because of reduced polarity when loss of polar groups occurred. Ultimately this means that strong temperature can change organic compounds in such kind of ways to make them undetectable for the applied methods. For carbonaceous chondrites, the SOM represents only 30% of all organic matter in the chondrites while the IOM represents around 70% of all organic compounds [25]. In contrast, heat can also influence the IOM to produce SOM which wasn't detectable before heat. Consequently, heat incident can completely change the composition of the SOM and then IOM in olivine.

Moreover, the SOM can undergo reactions at the catalytic iron and magnesium mineral matrix of the olivine. Magnesium and iron itself have catalytic properties accelerating reactions of the organic compounds inside the olivine. Furthermore, these metal can react with the organic compounds themselves creating organo-metallic compounds. These compounds have been predicted and their existence has been proven [88, 103, 104]. The unique environment of organic compounds trapped within a catalytic matrix enables the formation of hitherto unknown compounds, which will be further discussed within this work.

Lastly, the energy provided by temperature increase can cause destruction and elementarisation of organic compounds. Carbon is not infinite stable at high temperatures and consequently transforms into elemental carbon, also known as black carbon. During these reactions, atoms can also form small

gases such as NH_3 , CO_2 , H_2 , SH_2 , and many more, which are small enough to escape the micro-inclusions through the mineral matrix. However while such gases can escape the closed system, they also can return within certain time frames. It was shown that heated olivine shows reduced amount of molecular hydrogen, which returns to the system after equilibrium time at atmospheric conditions [87].

1.5 State of the Art with FT-ICR-MS

A large amount of research has been conducted on carbon-based compounds which are omnipresent on our earth. Natural organic matter (NOM) is a description of all organic matter which can be found in natural or engineered environments. It is a product of biological tissue decay together with metabolism products from life [105]. A subgroup of NOM is the so called dissolved organic matter (DOM), which refers to carbon compounds dissolved in an environment of choice [106]. DOM is mostly investigated in aquatic samples (either freshwater or seawater) as well as in soil samples [106–108]. Since most of the NOM molecules exist only in trace amounts, high-resolution techniques are needed to detect and characterize these compounds. Many studies are thus conducted with FT-ICR-MS mass spectrometry in an untargeted approach to describe the complexity and diversity of NOM and DOM. Untargeted FT-ICR-MS is an ideal method for NOM and DOM research. Primarily, fourier transform ion cyclotron resonance (FT-ICR) provides the necessary resolution and sensitivity to detect thousands of compounds found in NOM and DOM samples. This is especially important due to the high diversity and complexity of the compounds in these samples. A targeted approach, in comparison, might be blind for certain structural modifications of compounds when they are out of the analytical windows. Thus a comprehensive analysis of all compounds is favored [109].

FT-ICR-MS was many times used to detect DOM in freshwater and seawater samples. Within these samples, the method is able to detect pollutants of different origins. Of special interest are disinfection byproduct from wastew-

ater treatment facilities and pollution of drinking water. Here, FT-ICR-MS can detect traces of unwanted chemical compounds which reduce water quality. This ultimately gives insights into water safety which is important for human health [110–128]. The same approach was used to detect organic compounds and pollutants in soil and to determine their impact. Soil organic matter is important for understanding how soils form, how they evolve and how they are influenced by external stimuli [129]. The organic compounds in soil contribute to the global carbon cycle. Furthermore they mirror soil quality in questions of agriculture and are investigated regarding the climate change and global warming [129–138].

FT-ICR-MS also proved its application to numerous extraterrestrial geological samples to determine their organic compounds. Organic matter in extraterrestrial samples was witnessed in comets [139], interstellar/pre-cometary ice analogues [140] and in many meteorites [141–147]. One of the most investigated meteorite is carbonaceous chondrite Murchison. It fell 1969 in Australia and a total of approximately 100 kg of the meteorite were found. FT-ICR-MS analysis revealed 14197 unique soluble chemical compositions within the meteorite in the CHNOS chemical space with CHO, CHNO, CHOS, CHNOS, and CHOMg molecular series [141]. Furthermore the extraction solvent was investigated in this study. Methanol was shown to extract the most amount of chemical compounds and is thus further used in follow-up studies. The results from FT-ICR-MS were later corroborated with high-resolution nuclear magnetic resonance spectrometry [148]. A recent study of Murchison meteorite illustrates the influence of different ionization techniques in FT-ICR-MS. In the study, atmospheric pressure photoionization (APPI) (+), electrospray ionization (ESI) (+), and ESI (-) measurements were compared and their contribution to the soluble organic matter was elucidated [147]. Another meteorite very similar to Murchison is Maribo. Also here, FT-ICR-MS was able to detect 15600 unique signals belong to organic matter [142]. In contrast to Murchison and Maribo, the Diepenveen meteorite was also analyzed with FT-ICR-MS with the same parameters. It only contained 945

assignable mass peaks [149]. This indicates that organic matter in geological samples is strongly influenced by temperature and shock events of respective samples. Many other meteorites were analyzed and organic molecules are omnipresent in all of these extraterrestrial samples [139, 143–145, 150–154].

1.6 State of the Art with NMR

The ability to scan a broad range of aliphatic and aromatic chemical environments of organic matter makes NMR an ideal method to use it for NOM and DOM research [155]. Similar to FT-ICR-MS, NMR was broadly applied to NOM research. Mostly water samples, for example freshwater or marine water, soil samples, and geological samples of terrestrial and extra-terrestrial origin were analysed with NMR. Of interest are besides ^1H NMR also ^{13}C and ^{15}N NMR analysis. The technique allows the observations of chemical environments and also allows the comparison between samples [156]. Especially two dimensional nuclear resonance spectroscopy (2D NMR) provides information regarding connectivity of nuclei and contribution of mayor aliphatic and aromatic groups. NMR independently, but also in combination with other high-resolution techniques, enables a broader and more comprehensive view on NOM and DOM in samples [148]. NMR was broadly used to analyse DOM in freshwater and marine aquatic samples. The technique allowed a comparison of NOM in water resources which ultimately implications for water treatment regarding NOM removal in drinking water [157]. NMR has also been used for groundwater analysis [158], and marine DOM analysis, which revealed differential changes in the amount of DOM for different sampling depth. The research on the field shows the wide diversity and complexity of marine DOM and helps to understand biogeochemical processes in our seas as well as biodiversity in marine environments [156]. NMR was also proven to be a valuable tool for NOM and DOM research in soil geochemistry. The method is used to characterize soil samples as well as humification processes in soil [159]. Also here ^{13}C and ^{15}N NMR analysis are important for the analysis of soil and its humin, humic acid, and fulvic acid fractions [160]. For the diverse and complex

organic matter in soil, NMR is an ideal analysis tool [161–164]. Organic matter in terrestrial and extra-terrestrial geological samples potentially records a succession of chemical histories. For extra-terrestrial samples this could have started with reactions in the interstellar medium, followed by evolution of the early solar nebula as well as hydrothermal alteration in the meteorite parent bodies [165]. Similarly organic matter of terrestrial geological samples can reflect their respective temperature and pressure experience as well as water alteration and repeated subduction in the Earth’s mantle. NMR was used already very early to detect organic compounds in carbonaceous chondrite Murchison [16, 166]. The detection of a broad structural heterogeneity in the sample was postulated. Most detected signals belonged to alkane structures, either linear or branched. This was also confirmed by another study comparing insoluble organic matter of the meteorites Murchison, Tagish Lake, EET92042, and Orgueil. The most striking differences were observed in the presence of sp³-hybridized carbon atoms [165]. Tagish Lake meteorite was also analysed with ¹³C NMR. Besides aliphatic structures, signals were also assigned to aromatic carbon atoms [167]. A recent study of Murchison meteorite with high resolution NMR and high-resolution FT-ICR-MS corroborate the previously found results. The organic matter found in the extra-terrestrial sample showed a diversity of aliphatic and aromatic signals in the methanolic extract of the meteorite. Also 2D NMR was performed for the sample to show the interconnectivity of the nuclei in Murchison organic matter [148]. Natural organic matter, either in terrestrial or extra-terrestrial samples, is omnipresent. High-resolution NMR facilitates the analysis of hundreds of different chemical structures within the NOM in the various samples.

1.7 State of the Art of LC-MS in NOM Analysis

The benefits of LC-MS analysis for a variety of compounds and samples has been shown by various groups. The method is valuable for the detection and separation of similar compound classes. It showed its advantages in many scientific fields including analytical chemistry, life sciences, food chemistry as

well as in NOM research [168]. LC-MS was used for the NOM analysis of water samples investigating pollution and by-products. NOM which reacted with chlorine or ozone during water treatment can be cause possible health risks. Systematic investigation of water samples with LC-MS enabled the detection disinfection byproducts in drinking water [169]. More than ever, pharmaceutical drugs found their ways in freshwater and drinking water sources. Their large structural differences render their separation and simultaneous analysis difficult. The LC-MS was successfully used to track and quantify the pharmaceutical compounds in water samples. The research help to better understand contamination of water samples in order to develop better water treatment procedures [170,171]. In the research of NOM in soil, LC-MS was also used to detect and characterize contamination. Especially in regards to drugs residuals in soil, which can negatively influence soil microorganisms, LC-MS provided valuable insights [172]. Other soil contaminations were also analyzed by LC-MS. Poly-and perfluoroalkyl substances are known substances to have severe influences on human health. These compounds are not eliminated by water treatment facilities and thus can cause potential health risks to humans. LC-MS was able to detect and describe the extent of this soil pollution [173].

Also extra-terrestrial geological samples were analyzed with LC-MS. In the context of the emergence of life, building blocks of life in meteorites were of special interest for LC-MS analysis. Several carbonaceous chondrites from Antarctica were scanned for their amino acid content. Besides the known 20 amino acids, several other amino acids were also detected in the samples [174]. A similar study also analyzed amino acids, but in CR meteorites [175]. Furthermore some compounds of a possible prebiotic pyruvate reaction were witnessed in meteorites [176].

1.8 Materials and Methods

1.8.1 FT-ICR Mass Spectrometry

The measurements were carried out with a 12 T FT-ICR mass spectrometer Solarix (Bruker Daltonics) and the parameters were optimized via software FTMS-Control V2.2.0 (Bruker Daltonics).

FT-ICR-MS is high a resolution mass spectrometry technique. It emerged through the combination of two separate discoveries. First, the ion cyclotron and the second, the Fourier transformation. The ion cyclotron was invented by Earnest Orlando Lawrence in 1929. It is able to accelerate small charged particles to high kinetic energies within a small volume [177, 178]. In 1963 the ion cyclotron was improved with the introduction of the ion cyclotron resonance (ICR) experiment. The keys idea is detection based on electric field interaction of ions instead of using impact techniques which was state of the art at that time [179–181]. This leads to the development of a clearly defined “cell” which is the basis for nowadays technological approaches. Only two years later, Cooley and Tukey applied to the fast fourier transform (FFT) algorithm to ICR experiments. This is considered as the most important event in the development of FT-ICR-MS [181–184]. The application of the FT-ICR technology allowed the reduction of time from several minutes to one second for a single run because all excited m/z species were measured simultaneously. Furthermore, the resolving power increased strongly compared to impact detection. Ultimately, the resolution of the method is either limited by magnetic field strength and magnetic field homogeneity, or trapping voltage of the ions. Nowadays, strong magnets for FT-ICR are a question of price, but significantly increase the resolution power, dynamic range, and mass range of the mass spectrometry technique for a great extant. Depending on field strength of the magnet and the respective analyzed sample, resolution is now more precise than the mass of a single electron [181, 185].

1.8.2 Basics of FT-ICR-MS

The fundamental basis of FT-ICR-MS is the physical behavior of charged particles in a homogenous magnetic field. In the case of FT-ICR-MS, the charged particles are the ionized compounds of samples which are subject to measurement. The charged ions in the ICR move in circles while being exposed to the homogenous magnetic field. While charged particles move inwards under such conditions, the centrifugal force partly compensates that effect and pushes the ions on a certain radius. To achieve a stable circulation of the ions, the frequency must match the cyclotron frequency. The cyclotron frequency is described by the following formula:

$$f = \frac{qB}{2\pi m} \quad (1)$$

B is the magnetic field strength, q is the charge of the particle and m the relativistic mass of the ion. Consequently, the frequency of the ions is only dependable on magnetic field strength, charge, and mass of the ion. This facilitates physical calculations to encrypt the signals obtained by FT-ICR-MS. To keep the ions rotating, oscillating dipolar electric fields are applied. These also can be used to enlarge the radius of the circulation for proximity of ions to the detecting electrodes, allowing for a longer transient time of ions at the detector electrodes, but also create coherent motion of same m/z species. An image current is created and recorded as sinusoidal patterns, the free induction decay (FID). Amplitude and periodic information are indicative for abundance and cyclotron frequency of the ions. The FID is then, with consideration to the time domain, converted to a mass spectrum with the FFT algorithm [186–188].

1.8.3 High Resolving Power and Mass Accuracy

High-resolution is one of the most important benefits of FT-ICR-MS compared to other mass spectrometrical approaches [189]. The resolving power is defined as the ability to separate two peaks from each other. The resolution

is defined as the ratio of the peak position (m/z value) to its full width half maximum (FWHM) of the respective peak. The resolution is ultimately dependent on magnetic fields strength and can be influenced by transient duration. Recently as resolution greater than 2700000 at m/z 400 was reported with a 21 Tesla FT-ICR-MS device [185]. Ultimately, mass accuracy depends on mass spectral signal-to-noise (S/N) ratio and digital resolution [190]. High mass accuracy and high mass resolution enable the differentiation of the manifold of masses behind one nominal mass as seen in Figure 6. Consequently high resolution and high mass accuracy is of utmost importance for the investigation of complex organic matter such as NOM, petroleum, meteorite organic matter, and DOM samples [191].

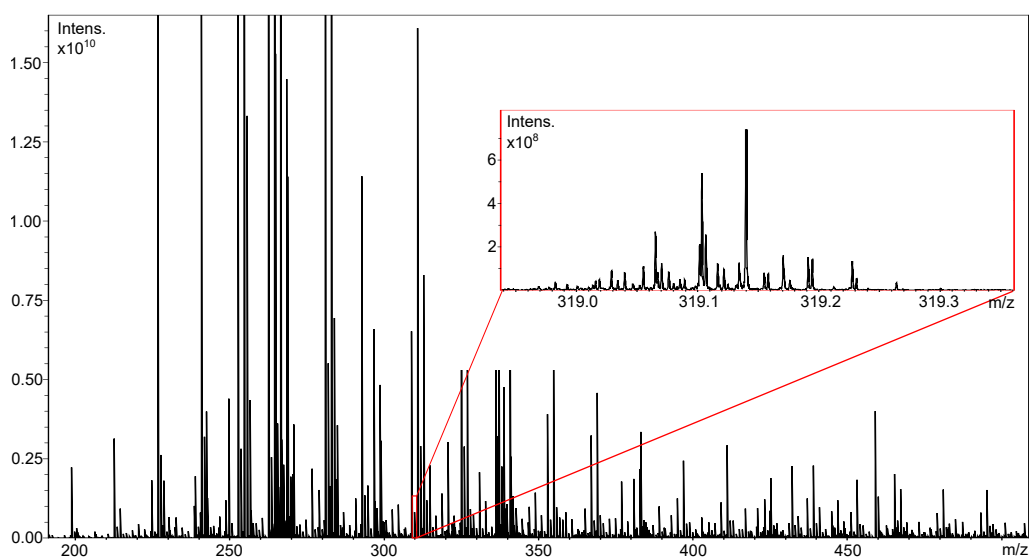


Figure 6: Fourier transform ion cyclotron resonance mass spectrometry spectrum depicting thousands of different masses. Red box shows zoomed-in spectrum of m/z 319 with several exact masses at one nominal mass.

1.8.4 Ionization Techniques

To generate charged ions for mass spectrometry, multiple methods have been developed over the years, all with certain advantages and disadvantages. The

ionization techniques can be divided into soft and hard ionization techniques. Soft techniques are ionizing molecules without breaking their chemical bonds and structures. Typical fragmentation reactions induced by soft ionization are rarely observed. Examples for soft ionization include ESI, APPI, fast atom bombardment (FAB), chemical ionization (CI), atmospheric pressure chemical ionization (APCI), desorption electrospray ionization (DESI), and matrix-assisted laser desorption/ionization (MALDI) [192, 193]. An example for a hard ionization technique, which usually causes chemical bonds to break, is electron ionization (EI) [188]. Figure 7 shows important ionization techniques and their ionization capabilities [194–196]. During this thesis, the used ionization techniques include ESI and APPI. They will be further elaborated.

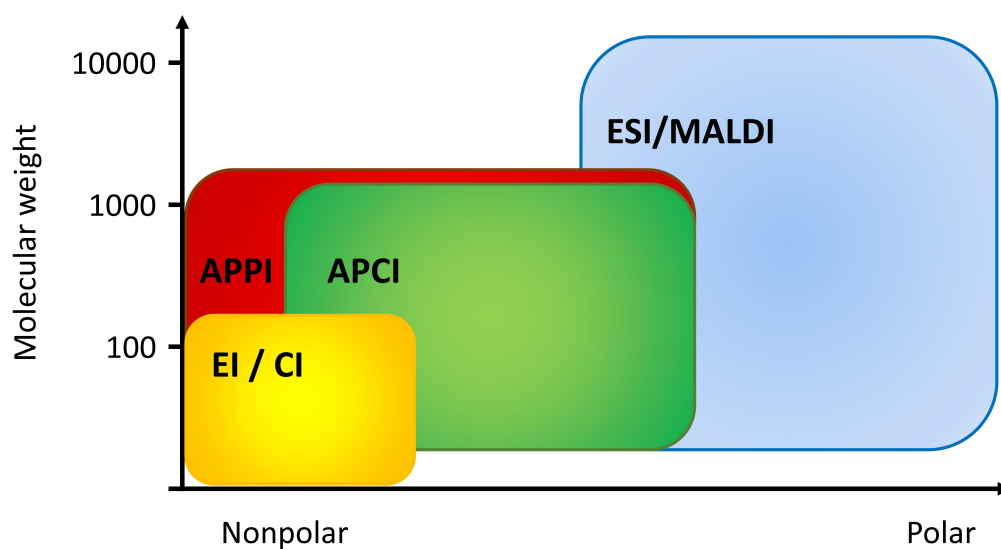


Figure 7: Common ionization techniques and their respective ionization capabilities for polarity and molecular weight

ESI is one of the most applied ionization techniques in mass spectrometry [197]. The sample has to be in liquid form or dissolved in a solvent of choice. In a first step, the sample is continuously flushed into the ESI-needle. Within the needle, high voltage is present. At the end of the needle, the sample is

sprayed into fine droplets with the help of a nebulizing gas, mostly nitrogen. The nebulizing gas together with increased temperature and a Taylor cone helps to generate a mono-disperse aerosol to easily evaporate the solvent of the sample. This leads to an increase of surface charge density of the droplets and a decrease of the droplet radius. A droplet of a certain size can only contain a certain amount of similar charges according to the Rayleigh limit. By reducing the volume and thus the surface, droplets are more and more unstable with reduced size. Ultimately the droplets fall apart and emit ionized molecules into the gas phase (Coulomb-Explosion). Positively or negatively charged ions in the sample, depending if the positive or negative acquisition mode, are then further analyzed. The ions are then transported into the mass spectrometer by a sampling skimmer cone. The exact details of the method are extensively described in literature [197,198]. ESI is especially useful for polar ions and shows ideal soft ionization properties for this group of compounds [199,200].

APPI is a modification of APCI. Similar to ESI, the sample has to be liquid or dissolved in a solvent of choice. The continuous flow of liquid sample is, with an inlet, directly dispersed into a nebulizing gas current. The gas passes a heating unit which enables evaporation of residual solvent, releasing the sample into the gas phase. The sample in the gas phase then bypasses vacuum ultraviolet radiation which causes ionization. Similar to ESI, the ions then pass a sampling skimmer cone with subsequent transportation to the mass spectrometry (MS) system [201]. In contrast to ESI, APPI mostly ionizes nonpolar species and thus represents a complementary ionization technique to ESI to fully cover polar as well as nonpolar species in the analyzed sample with both techniques combined [110,202].

1.9 Nuclear Resonance Spectroscopy

The physical phenomenon of NMR was discovered by Block and Purcell in 1946 [154,203,204]. In the beginning, it was mostly used for analytical chemistry and chemical structure elucidation. Starting at the end of 1970, its

importance for the investigation of biochemical processes grew. It also found its way into clinical practice as a diagnostic tool due to its ability to observe morphological changes in tissues, namely magnetic resonance imaging. [204]. The technique allows to observe magnetic fields around atomic nuclei. In early years, the analysis of substances was difficult because NMR required a large amount of sample to receive enough signal during the measurement. The development of stronger magnets as well as more sensitive receivers enabled the analysis of trace amounts reducing the needed amount of sample significantly. Furthermore, the increasing resolution of NMR also enabled the analysis of NOM and DOM samples, where several hundreds of molecules are overlaying each other [161]. The development of special pulse programs lead to the development of the so called 2D NMR spectrometry. 2D NMR allows to see the coupling of nuclei to each other within a molecule to better investigated chemical connections between the signals. Famous 2D NMR experiments are correlation spectroscopy (COSY), total correlated spectroscopy (TOCSY), and heteronuclear single quantum coherence (HSQC). [205–207].

The sample is, in a first step, dissolved in solvent of choice. Also the direct measurements of liquid samples is possible. Deuterated solvents are used in proton NMR to suppress the signals coming from these solvents. Solid state NMR Spectroscopy is also feasible, but not further discussed in this work. The sample is stored in a NMR glass tube and, for measurements, placed inside the magnet of the NMR. Similar to FT-ICR-MS, a strong homogenous magnetic field is also needed for NMR analysis. The homogeneity of the magnetic field is of utmost importance for correct NMR measurement. To avoid small local disruptions of the magnetic field, so called shims are used. They correct the magnetic field in a small scale to homogenize it within the sample. Furthermore a lock is used on the deuterated solvent to further compensate for inhomogeneities in the magnetic field. Besides the magnet, there are also radio frequency emitter coils and signal detection coils inside the NMR. To excite the nuclei in the samples, a radio frequency (RF) pulse is emitted. The frequency of the RF pulse has to perfectly match the nuclei

of the sample, otherwise the energy is not absorbed and no resonance can be observed. Most NMR emit several frequencies to cover a wide range of nuclei. When nuclei absorb the RF pulse, they get into a so called excited state. Nuclei excited by this pulse take a certain time to relax back to their normal state. This relaxation can be measured by the signal detection coils. If the RF pulses are repeated several times, the average spectrum will have a better signal to noise ratio. The received signal is measured as the frequency over time of relaxation, the so called FID. Fourier transformation is applied to the FID, similarly to FT-ICR-MS. The received spectrum then shows the chemical shift, a unit to compare nuclei with each other. The higher the chemical shift (unit: parts per million (ppm)), the more “shielded” is the nucleus (see Figure 8). Unshielded protons are for example methyl-group protons, while more shielded protons are for example aromatic protons [203, 205, 208–213].

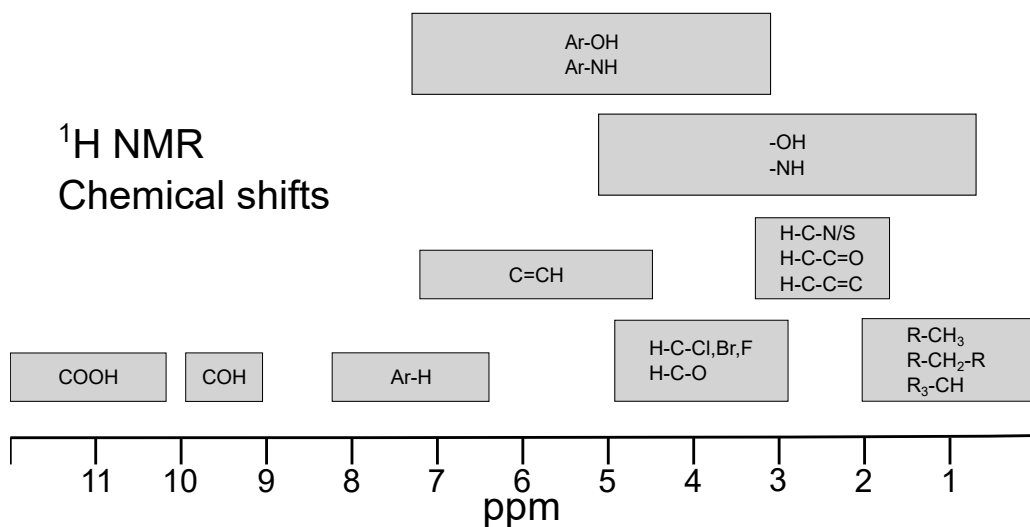


Figure 8: Chemical proton shifts of common functional groups in ¹H NMR spectrum.

1.10 Liquid Chromatography Mass Spectrometry

LC-MS analysis was performed using a maXis instrument (time of flight mass spectrometry (TOF-MS)), (Bruker Daltonics, Bremen, Germany) in combination with an UHPLC system (Acquity, Waters, Eschborn, Germany) equipped with a photodiode array detector.

Liquid chromatography (LC) is a technique in analytical chemistry to separate and identify components of a mixture. Chromatography itself is a very old technique and maybe was first described in 1855 by Runge who described the separation of dye on paper [214]. The phenomenon was further investigated and used under the term “paper chromatography”. Liquid chromatography was first introduced in 1941 [215]. In the late 1960’s, the first reports of high performance liquid chromatography (HPLC) were published [216–218]. In the following years, the method was further improved, better detectors were introduced, and HPLC became a worldwide used method for the separation and analysis of chemical mixtures [219].

Nowadays HPLC and its further improvements like UPLC are the gold standard to chromatographically separate molecules in samples. Under high pressure, the liquid or dissolved sample is flushed through the chromatography column. The most important factors here are the stationary phase (in the column) and the mobile phase (a solvent flushing the sample through the column). Both have significant influence on the separation of the compounds in the sample [220]. The compounds of the samples are separated and retained by interactions with the stationary phase and the mobile phase which causes the segregation of different chemical compounds [168].

In normal phase high performance liquid chromatography (NP-HPLC) the stationary phase is silica gel. The surface mostly consists of hydroxyl groups, so called silanol groups, causing polar interactions with the analytes. For more specified purposes, the silanol groups can be bounded with usually amino, diol, nitro, or cyano group for different polar interactions. In NP-HPLC, the mobile phase consists of mostly apolar solvents. Frequently used solvents are n-hexane, n-heptane, dichloromethane, dichloroethane, diethyl ether, methyl

acetate, ethyl acetate, acetone, isopropanol, ethanol, or methanol as well as mixtures of the mentioned solvents [221]. NP-HPLC is mostly used to separate polar compounds and quickly elutes apolar compounds. Reverse phase high performance liquid chromatography (RP-HPLC) is the most important and most widely applied version of LC [221]. Here, the stationary phase is apolar made by covalently attaching octadecyl silica chains to the free hydroxyl groups. This is known as C18 phase [221]. Contrary to NP-HPLC, the solvents for RP-HPLC are mostly polar solvents such as water, acetonitrile, ethanol, and acetone or mixtures from those. RP methods are mostly used to separate apolar compounds while polar compounds show a quick elution with the polar solvents. Both NP-HPLC and RP-HPLC were refined over the years and more and more elaborated methods were developed. Besides stationary and mobile phase, also flow rate of the sample, additional chemicals in the mobile phase, pressure, column temperature, pH of the mobile phase, and many more factors are influencing the chromatographic runs. For new compounds and mixtures, method development takes a significant amount of time to improve separation methods. However, the HPLC technique is indispensable for modern research.

1.11 Representation and Data Treatment

For untargeted FT-ICR-MS analysis, the organic matter is prepared with a method of choice (e.g. solvent extraction, solid phase extraction etc.) and then measured. Due to the development of increasing field strengths of magnets, the resolution of measured peaks increases and error margins of elemental assignments shrink. Up to date, mass precision is better than the mass of an electron (< 200 ppb) [88,141,185]. For better mass accuracy, the FT-ICR-MS is externally calibrated with a medium choice. After acquisition, the data is processed with a software, in the case of this work with Data Analysis 5.0 from Bruker. The signal to noise ratio for peak detection is applied and an internal calibration with known compounds can be applied to the spectrum. Afterwards, the exported spectrum is further cleaned by certain filters such as a mass defect filter, an isotope filter, and a wiggle filter to remove satellite peaks. The cleaned spectrum is then subject to a formulae assignment mechanism. High mass accuracy allows the precise assignment of elemental compositions to respective signals in the mass spectrum. This can be done by calculating elemental compositions which fit the detected masses in a certain error range. For better annotation results, rules regarding chemical compositions have to be applied [222]. Another method to assign masses is mass differences networks [191,223–225] in regards to sought reactions. This approach is particularly interesting in metabolomics to evidence the metabolic pathways. Both methods have advantages and disadvantages, but both yield chemical formulae which were to m/z values assigned in a certain mass error range. With the chemical formulae assignments, general information about the analyzed organic matter can be given. Usually, molecules are grouped in specific compound classes according to their chemical composition, mostly CHO, CHNO, CHOS, CHNOS, and CHOMg. Furthermore, ratios of certain elements can be calculated. Most prominent are the O/C and H/C ratio. The H/C ratio gives information regarding the saturation of the molecules. Values around $H/C = 2$ are mostly saturated structures, for example saturated long chain fatty acids, long chain alcohols, or long chain hydrocarbons. Lower

values around $H/C = 1$ resemble aromatic structures, for example benzene or polyaromatic hydrocarbons (PAH). The O/C value shows oxygenation of molecules. Low O/C values are typical for fatty acid like structures as well as condensed hydrocarbons. Higher values up to $O/C = 1$ belong to sugar-like compounds or polyphenolic compounds such as tannins. Both O/C and H/C value can be plotted in the so called Van Krevelen diagram [226]. In this diagram the position of the molecules allow approximations about their biochemical class: carbohydrates, lipids, phenolics, black carbon, and many more. Also, homologous chemical structures in the CHO space are seen as lines in the graphs. Usually the intensity of assigned formulae of m/z values are represented as dot size in the diagram [227]. Figure 4 shows an exemplary Van Krevelen diagram from carbonaceous chondrite Murchison as well as explanatory features. Furthermore, more descriptive ratios have been developed to describe the natural organic matter. A first approximation of the aromaticity and the presence of double bonds of organic matter is the calculation of double bond equivalent (DBE) [228].

$$DBE = C - 0.5 * H + 0.5 * N + 1 \quad (2)$$

Certain ratios of elements are used to approximate the number of double bonds a structure has. This was further developed to the aromaticity index (AI) value to give more precise information. The AI was developed [229], giving more precise values of aromaticity by better including heteroatoms in the chemical formulae. The aromaticity index was calculated by the following formula:

$$AI = \frac{1 + C - O - S - 1/2H}{C - O - S - N - P} \quad (3)$$

The aromaticity equivalent (X_c) is a value which allows precise differentiation of aromatic compounds [230]. It describes especially aromatic compounds more precisely than the aromaticity index or DBE. The aromaticity equivalent

was calculated by the following formula:

$$X_c = \frac{2C + N - H - 2mO}{DBE - mO} \quad (4)$$

The values of m in this formula can vary and usually are either 0, 0.5 or 1 depending on the class of compounds. For untargeted compounds in the CH and CHO spaces, $m=0$ was chosen as a value in this work.

Regarding the oxidation of molecules, the carbon oxidation state (Cos) can be calculated [231]. It is especially useful to determine the oxidation of CH and CHO compounds, but can be challenging for heteroatom containing molecules. The following formula was used to calculate the Cos. This is an approximation which only works for CH and CHO compounds.

$$Cos = 2\frac{O}{C} - \frac{H}{C} \quad (5)$$

The calculation needs respective oxidation state of heteroatoms which is hardly feasible for NOM samples. All of these ratios allow the comparison and description of NOM samples and their respective classes. Furthermore, supervised and unsupervised methods such as principal component analysis (PCA), partial least squares regression (PLS), partial least squares regression discriminant analysis (PLS-DA), heat map analysis, and many more are viable techniques for data evaluation [232, 233].

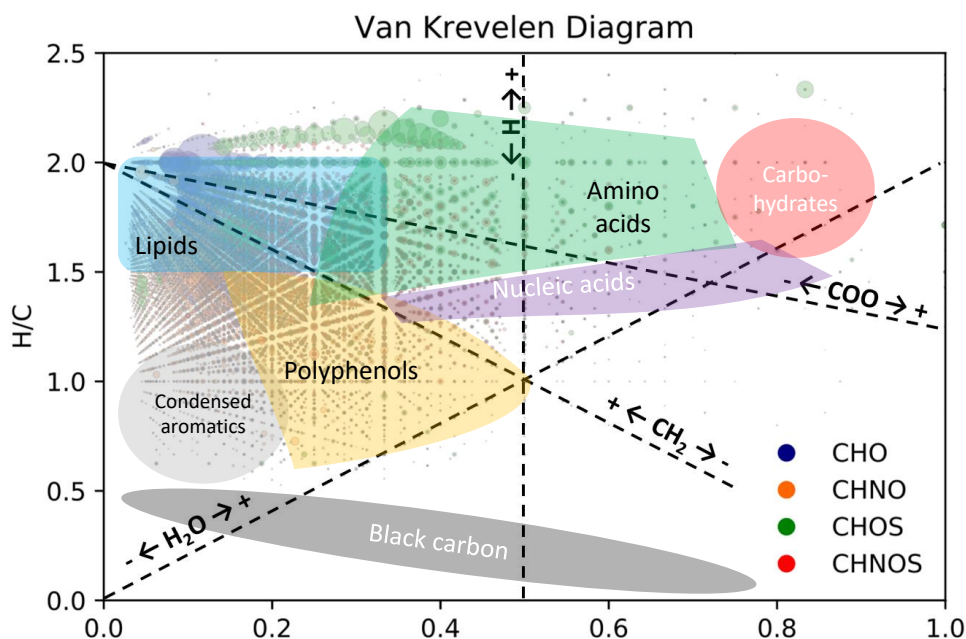


Figure 9: Exemplary Van Krevelen Diagram. O/C vs. H/C is plotted. Data taken from carbonaceous chondrite Murchison – methanolic fraction analysed with FT-ICR-MS in ESI(-) mode. Dot color represents chemical spaces – CHO (blue), CHNO (orange), CHOS (green) and CHNOS (red). Dot size represents intensity in the spectrum. Characteristic lines and areas are marked in the diagram.

1.12 Python

To facilitate the data evaluation, some computational calculations and figure designs were automated via several Python scripts. The used input files for Python are the generated output files from NetCalc 2017 [223]. Calculations and figures were performed in Python 3.8.5 within the Jupyter Notebook environment of Anaconda (Version 1.9.7).

Loaded packages include Pandas, Math, and Numpy for dataframe management and computations. Seaborn and Matplotlib were used for visual design of figures. Imported files include the annotation file and the loaded spectrum for NetCalc. Both files are used to create a dataframe on which all further calculations are running. Edge and node files were also imported and expanded with additional information like chemical space. Both files

ultimately can be used to create mass difference networks.

Since the NetCalc 2017 output only contains calculated amounts of each of the elements, Python was used to facilitate and accelerate the data evaluation. The function "assign_class" is used to assign each chemical composition a respective chemical space (see Listing 1).

Listing 1: Function to assign chemical spaces

```
1 # Creates a function to assign the different chemical spaces
2 def assign_class(Frame):
3     if Frame.H > 0 and Frame.C > 0 and Frame.O > 0 and Frame.N ==
4         0 and Frame.S == 0 and Frame.P == 0 and Frame.Mg == 0 and
5         Frame.Br == 0:
6             return "CHO"
7     elif Frame.H > 0 and Frame.C > 0 and Frame.O == 0 and Frame.N
8         == 0 and Frame.S == 0 and Frame.P == 0 and Frame.Mg == 0 and
9         Frame.Br == 0:
10            return "CH"
11    elif Frame.H > 0 and Frame.C > 0 and Frame.O == 0 and Frame.N
12        > 0 and Frame.S == 0 and Frame.P == 0 and Frame.Mg == 0 and
13        Frame.Br == 0:
14            return "CHN"
15    elif Frame.H > 0 and Frame.C > 0 and Frame.O == 0 and Frame.N
16        == 0 and Frame.S > 0 and Frame.P == 0 and Frame.Mg == 0 and
17        Frame.Br == 0:
18            return "CHS"
19    elif Frame.H > 0 and Frame.C > 0 and Frame.O > 0 and Frame.N
20        > 0 and Frame.S == 0 and Frame.P == 0 and Frame.Mg == 0 and
21        Frame.Br == 0:
22            return "CHNO"
23    elif Frame.H > 0 and Frame.C > 0 and Frame.O > 0 and Frame.N
24        == 0 and Frame.S > 0 and Frame.P == 0 and Frame.Mg == 0 and
25        Frame.Br == 0:
26            return "CHOS"
27    elif Frame.H > 0 and Frame.C > 0 and Frame.O > 0 and Frame.N
28        > 0 and Frame.S > 0 and Frame.P == 0 and Frame.Mg == 0 and
29        Frame.Br == 0:
30            return "CHNOS"
31    elif Frame.H > 0 and Frame.C > 0 and Frame.O >= 3 and Frame.N
32        == 0 and Frame.S == 0 and Frame.P == 0 and Frame.Mg == 1 and
33        Frame.Br == 0:
34            return "CHOMg"
35    elif Frame.H > 0 and Frame.C > 0 and Frame.O >= 3 and Frame.N
36        == 0 and Frame.S == 0 and Frame.P == 0 and Frame.Mg == 2 and
37        Frame.Br == 0:
38            return "CHOMg"
39    elif Frame.H > 0 and Frame.C > 0 and Frame.O >= 3 and Frame.N
```

```

22     == 0 and Frame.S > 0 and Frame.P == 0 and Frame.Mg == 1 and
Frame.Br == 0:
23         return "CHOSMg"
24     elif Frame.H >0 and Frame.C > 0 and Frame.O >= 3 and Frame.N
> 0 and Frame.S == 0 and Frame.P == 0 and Frame.Mg == 1 and
Frame.Br == 0:
25         return "CHNOMg"
26     elif Frame.H >0 and Frame.C > 0 and Frame.O >=3 and Frame.N
> 0 and Frame.S > 0 and Frame.P == 0 and Frame.Mg == 1 and
Frame.Br == 0:
27         return "CHNOSMg"
28     elif Frame.H >0 and Frame.C > 0 and Frame.O >=3 and Frame.N
== 0 and Frame.S == 0 and Frame.P == 0 and Frame.Br > 0 and
Frame.Mg == 1:
29         return "CHOBrMg"
30     elif Frame.iCl > 1:
31         return "Not useful"
else: return "Not useful"

```

By simply comparing if numbers of certain elements are higher than or equal to zero, the function assigns all of the needed chemical spaces. If a composition has no valid chemical composition, for example only H and Mg are larger than zero, these mass peaks are assigned to the chemical space "Not useful". Those chemical composition which are not useful are removed from the table in a later step. Also the function already detects if a chlorine adduct would be possible for a structure, which is only possible in negative mode. Depending on the desired compounds, the families to assign can be adjusted. For biological samples, also phosphorus can be included in this function. Also possible is a in-depth analysis of all compounds, where already the amounts of hetero atoms are specified, for example CHOS₁, CHOS₂ and so on.

Similar to the assignment of the chemical composition, another function was written to calculate the chemical composition in a sum formula kind of way. The function reads out every chemical space as defined before and calculates the chemical sum formula. The result of this function would be C₆H₁₂O₆ for the CHO compounds glucose. These sum formulae are especially useful to compare measured compounds between different measurements, especially when negative and positive ionization mode were used. By adding

a proton to $[M-H]^-$ species from negative ionization mode and by subtracting a proton from $[M+H]^+$ from positive ionization mode, both sum formulae are in the neutral form and are thus similar for the same compounds. In this function, also the possibility to differentiate between adducts is given. $[M-H]^-$ adducts and $[M+Cl]^-$ adducts could be considered as different chemical formulae regarding their atoms. The subtraction of chlorine for $[M+Cl]^-$ adducts is possible which renders both adducts to the same chemical formula. Thus similar molecular structures are not considered as different compounds in the analysis. The underlying code for this function can be seen in Listing 2.

Listing 2: Function to assign chemical composition

```
1 # Creates a function to calculate the compositional formulae
2 def assign_Composition(Frame):
3     if Frame.Family == "CHO":
4         return ("C" + str(Frame.C) + "H" + str(Frame.H) + "O" +
5 str(Frame.O))
6     elif Frame.Family == "CHNO":
7         return ("C" + str(Frame.C) + "H" + str(Frame.H) + "O" +
8 str(Frame.O) + "N" + str(Frame.N))
9     elif Frame.Family == "CH":
10        return ("C" + str(Frame.C) + "H" + str(Frame.H))
11    elif Frame.Family == "CHN":
12        return ("C" + str(Frame.C) + "H" + str(Frame.H) + "N" +
13 str(Frame.N))
14    elif Frame.Family == "CHS":
15        return ("C" + str(Frame.C) + "H" + str(Frame.H) + "S" +
16 str(Frame.S))
17    elif Frame.Family == "CHOS":
18        return ("C" + str(Frame.C) + "H" + str(Frame.H) + "O" +
19 str(Frame.O) + "S" + str(Frame.S))
20    elif Frame.Family == "CHNOS":
21        return ("C" + str(Frame.C) + "H" + str(Frame.H) + "O" +
22 str(Frame.O) + "N" + str(Frame.N) + "S" + str(Frame.S))
23    elif Frame.Family == "CHOMg":
24        return ("C" + str(Frame.C) + "H" + str(Frame.H) + "O" +
25 str(Frame.O) + "Mg" + str(Frame.Mg))
26    elif Frame.Family == "CHOSMg":
27        return ("C" + str(Frame.C) + "H" + str(Frame.H) + "O" +
28 str(Frame.O) + "S" + str(Frame.S) + "Mg" + str(Frame.Mg))
29    elif Frame.Family == "CHNOMg":
30        return ("C" + str(Frame.C) + "H" + str(Frame.H) + "O" +
31 str(Frame.O) + "N" + str(Frame.N) + "Mg" + str(Frame.Mg))
```

```

23     elif Frame.Family == "CHNOSMg":
24         return ("C" + str(Frame.C) + "H" + str(Frame.H) + "O" +
str(Frame.O) + "N" + str(Frame.N) + "S" + str(Frame.S) + "Mg"
+ str(Frame.Mg))
25     elif Frame.Family == "CHOBrMg":
26         return ("C" + str(Frame.C) + "H" + str(Frame.H) + "O" +
str(Frame.O) + "Br" + str(Frame.Br) + "Mg" + str(Frame.Mg))
27     else:
28         return "Not Possible"

```

Both functions are readily applied on the dataframe and new columns are added with the additional information. Also the "not useful" rows are deleted from the data which is a first cleaning step in data analysis.

Furthermore, basic calculations can be performed to add descriptive numbers to the data frame. The algorithm can easily perform calculations to get H/C and O/C ratios as well as the AI. For plots to visualize Kendrick mass defects, calculations are performed to receive the Kendrick mass, the nominal mass, and lastly the Kendrick of all compounds. Further calculative numbers which are computed here are DBE, DBE per carbon, Xc with different values of O, and some weighted averages of values. The exact calculations of all of these values can be found in the Materials and Methods part of this work. Easier calculations such as the ratios between carbon and hydrogen or oxygen and carbon are also calculated via script (not shown in code). The weighted averages have to be summed and divided but the sum of all intensities to receive valuable information. The code for all the calculations can be seen in Listing 3.

Listing 3: Calculation of descriptive values

```

1 H_C = (df.H/df.C)
2
3 O_C = (df.O/df.C)
4
5 # According to Koch 2006
6 AI1 = 1 + df.C - df.O - df.S - 0.5*df.H
7 AI2 = df.C - df.O - df.N - df.S
8 A_I = AI1/AI2
9
10 DBE = (df.C) - (df.H * 0.5) + (df.N * 0.5) + 1
11
12 DBE/C = df.DBE / df.C

```

```

13
14 Xc(m=0) = (((df.C*2) + (df.N) - df.H - (df.O *2 *0)) / ((df.DBE)
      - (df.O *0))) + 1

```

Furthermore, Python allows the automatic scaling of data, which can be necessary in mass spectrometry data. Since intensities of many peaks can differ by large amounts (sometimes up to 10^6), a scaling of the intensities yields better data evaluation and visualization results. Intensities are scaled by calculating the n-th root of the original intensities or by using logarithmic transformation. Depending on the data set, the n-th root has to be set to different values of n. Intensities are afterwards more uniform, show smaller ranges in between, but still reflect important differences in intensities. Another possibility is to cut high intensities to a certain value. This method however neglects the ratio between the intensities of different peaks.

Listing 4: Van Krevelen Diagram

```

1 Van_Krevelen_scatter = sns.scatterplot(data = data_Van_Krevelen ,
2     x="OC",y="HC" ,
3     size = data_Van_Krevelen.Intensity ,
4     sizes = (0.01,500) ,
5     legend = False ,
6     alpha = 0.5 ,
7     edgecolor = "black" ,
8     linewidth = 0.1 ,
9     hue = "Family" ,
10    palette=dict(CHO="#000080" , CHNO="#FF6600" , CHOS=
      "#008000" , CHNOS = "#FF0000"))
11
12 Van_Krevelen_scatter.set(xlim =(0,1),ylim = (0,2.5))
13 Van_Krevelen_scatter.set_xlabel("O/C",fontsize = 14)
14 Van_Krevelen_scatter.set_ylabel("H/C",fontsize = 14)
15 Van_Krevelen_scatter.set_title("Van Krevelen Diagram")
16 Van_Krevelen_scatter.xaxis.set_tick_params(labelsize=14)
17 Van_Krevelen_scatter.yaxis.set_tick_params(labelsize=14)

```

Listing 5: Mass-edited H/C Diagram

```

1 MZ_edited_scatter = sns.scatterplot(data =
      data_MZ_edited_scatter ,
2     x="mz_value_x",y="OC" ,
3     size = data_MZ_edited_scatter.Intensity ,
4     sizes = (0.01,500) ,
5     legend = False ,

```

```

6         alpha = 0.5,
7         edgecolor = "black",
8         linewidth = 0.1,
9         hue = "Family",
10        palette=dict(CHO="#000080", CHNO="#FF6600", CHOS=
        "#008000", CHNOS="#FF0000"))
11
12 MZ_edited_scatter.set(xlim=(100,750),ylim=(0,0.5))
13 MZ_edited_scatter.set_xlabel("m/z value",fontsize=14)
14 MZ_edited_scatter.set_ylabel("O/C",fontsize=14)
15 MZ_edited_scatter.set_title("O/C Diagram")
16 MZ_edited_scatter.xaxis.set_tick_params(labelsize=14)
17 MZ_edited_scatter.yaxis.set_tick_params(labelsize=14)

```

As one of the most preferred figures for visualization, mass-edited H/C diagrams and Van Krevelen diagrams are used in NOM and DOM research. An explanation of these diagrams can be found in the materials and methods part of this work. Both diagrams can be readily computed and visualized in Python. By scaling the x-axis and y-axis to certain ranges, using color codes for different chemical spaces and applying an alpha-value to make bubbles in the diagrams see-through, the understanding and interpretation of the diagrams is facilitated. The code which was used to generate mass-edited H/C diagrams is shown in listing 5 and Van Krevelen diagrams is shown in listing 4. This code can be adapted to specific chemical spaces and further adapted for enhanced visualization of data. To show relationships of the relative and absolute amounts of different compound classes, pie charts and bar plots can be applied in a comparative way. While pie charts show the relative amount of compounds compared to the total amount, bar charts can easily visualize absolute amounts of counts of compounds. To compare the amounts of different elements in different chemical spaces, a comparative bar chart can be the solution. Either chemical spaces as well as the analyzed element can be changed readily. This comparison is also possible with relative amounts of compounds which ultimately facilitates comparison of samples with a large difference in absolute amounts of compound classes. This is especially valuable to compare amounts of sulfur and nitrogen in compounds which do and do not contain magnesium.

All shown code is exemplary for the used code to conduct this work. Scripts were adapted to different tasks and output figures were enhanced for better understanding of the underlying message and information. Python is a highly diverse programming language also enabling statistical approaches for example multivariate analysis. Automated scripts facilitate and accelerate data evaluation, data treatment, and figure design to a great extent compared to older techniques. Most of the underlying calculations and the data analysis during this work was performed with these kinds of scripts. Programming with languages like Python is influenced highly by day to day developments. By the time this work is published, the stated code might already be outdated. Nevertheless, Python served as a useful analytic tool during this work.

Chapter 2

Thermal History of Asteroid Parent Bodies is Reflected in Their Metalorganic Chemistry

Matzka, M., Lucio, M., Kanawati, B., Quirico, E., Bonal, L., Loehle, S., and Schmitt-Kopplin, P. (2021). Thermal History of Asteroid Parent Bodies Is Reflected in Their Metalorganic Chemistry. *The Astrophysical Journal Letters*, 915(1), L7.

Organo-magnesium compounds were shown to contribute significantly to the soluble carbon molecular complexity and diversity of meteorites, and their analysis increases our knowledge on carbon stabilization/sequestration processes in the asteroidal parent body. Here we present a new group of sulfur-magnesium-carboxylates detected using ultra-high-resolution mass spectrometry in a variety of meteorites. These novel compounds show increased abundance correlated with the thermal history of the asteroid parent bodies. By comparing the soluble organic extracts of 44 meteorites having experienced variable post-accretion history, we describe distinct organic compound patterns of sulfur-magnesium-carboxylates in relation to their long- and short-duration thermal history. It is shown that the exceptional stability of these molecules enables survival of carbon under harsh thermal extraterrestrial conditions, even in the vitrified fusion crust formed during entry into the Earth's atmosphere. Sulfur-magnesium-carboxylates augment our understanding of parent body proceedings with regard to carbon sequestration and speciation in space.

Reprint permitted under the Creative Commons Attribution 4.0 International License (<http://creativecommons.org/licenses/by/4.0/>).

Contribution: M.M. designed and performed research, analyzed the data and built models. M.M. wrote the paper.

Impact factor 2020: 7.413

2.1 Introduction

Meteorites not only consist of mineral and inorganic metal phases but also embody an immense diversity of carbon-based chemistry. These organic compounds were reported in many extraterrestrial samples, including various carbonaceous, ordinary chondrites, as well as achondrites, such as HED (howardite-eucrite-diogenite) meteorites [86, 234–236]. Various life-relevant organic compounds such as the high variety of amino acids [28, 237], nucleobases [32, 238], carbohydrates [239], fatty acids [36], and inorganic gases [240] have generally been detected and analyzed in meteorites. The CM2 meteorite Murchison, a carbonaceous chondrite breccia from the Mighei type with alteration by water-rich fluids on its parent body, is still being intensively investigated since its fall in 1969 and considered as a well-known extraterrestrial sample for abiotic organic complexity [156, 241]. Recently, nontargeted organic spectroscopy involving ultra-high-resolution methods in mass spectrometry and nuclear magnetic resonance spectroscopy expanded the structure description of the soluble organic matter of such valuable meteorites [27, 242]. The access to high-resolution analytical information using these novel technologies enables fundamentally new ways to identify and characterize the organic variety in extraterrestrial samples, containing not only carbon (C), hydrogen (H), and oxygen (O) but also a continuum of heteroatoms such as nitrogen (N) and sulfur (S) and metal ions [141, 147, 148].

Over the past decade, metal-containing organic molecules have been proven to be important in meteorites. These molecules are, for example, an iron-cyanide compound with similarity to the active side of hydrogenases [103, 104] and a new class of dihydroxymagnesium carboxylate compounds, found in relation to strong metamorphic events in meteorites [88]. Light elements such as nitrogen (N) or sulfur (S) were detected in extraterrestrial meteoritic samples in different quantities and qualities in the form of gas to more complex molecular compounds [14]. Sulfur is especially known to be available in relatively high amounts as minerals such as pyrrhotite and pentlandite, as metal sulfides, and as organic molecules in various meteorites

[141, 243, 244]. This element was found under different oxidation states, as well as in different compound classes such as sulfides (e.g., H_2S), mono- and disulfides, heterocycles, sulfoxides, sulfites, sulfones, sulfonates, and sulfates [245]. Water alteration can mobilize sulfur from the mineral phases and from metal sulfides, which then can be subject for subsequent reactions [141]. Furthermore, heating and shock can also release sulfur-containing structures from the insoluble organic matter. Under high pressure and temperature conditions, sulfur in its various oxidation states can interact with metals and carbonaceous phases to form thermodynamically stable compounds, which will be thermodynamically stable and survive the harsh extraterrestrial conditions. Discussed reactions to geosynthesize organic compounds in meteorites are Fischer–Tropsch-type (FTT) reactions [102] or Sabatier processes [99, 100], which use CO and H_2 in which can undergo further reactions.

In this study, we demonstrate the existence of a yet unrecognized and novel organic compound class bearing the elements carbon, hydrogen, oxygen, sulfur, and magnesium—CHOSMg compounds. CHOSMg compounds are molecules with the general formula $\text{C}_x\text{H}_y\text{Mg}_{1-2}\text{O}_z$ with $x, y, z \in \mathbb{N}$. In the first part, we present structural and chemical properties of these CHOSMg compounds. We show that their formation is strongly dependent on the heating history of the fragment. This result is derived from the comparison of the inner matrix with crust material of the same meteorite. Finally, we show a correlation of CHOSMg compounds and the asteroid parent body temperature histories within a larger set of meteorite samples.

2.2 Results and Discussion

2.2.1 Description of the CHOSMg Space

We analyzed the methanol soluble fraction from 44 meteorites from different classes using direct injection electrospray ionization Fourier transform ion cyclotron resonance mass spectrometry (ESI-FT-ICR-MS). Besides the known

compositional organic content of the chemical families CHO, CHNO, CHOS, CHNOS, and CHOMg as described previously in meteoritic organic material [141], many signals were not covered by these compositional assignments. Using a combination of the elements C, H, O, S, and Mg enables the assignment of these signals to a new chemical family never described to date, CHOSMg. These CHOSMg compounds, together with their isotopic signature, ESI-FT-ICR-MS, and mass spectra of four representative meteorites, are illustrated in Figure 10 an ordinary chondrite (LL5, Chelyabinsk; [144]), a magnesian mafic silicates-rich ungrouped achondrite (NWA 7325; [88]), a heated anomalous CM2 chondrite (CM2-an, Diepenveen; [149]), and a moderately altered CM2 (CM2, Aguas Zarcas; [35]; see also Figure A.1 in the Appendix).

NWA 7325 (achondrite-ungrouped) presents 12% CHOSMg compounds in the SOM (Figure 1(A)). In Chelyabinsk (LL5), which experienced a heating history, CHOSMg compounds account for 15% of all assigned mass signals. Also, Diepenveen meteorite (CM2-an), which experienced extensive heating as seen from its petrology and organic molecules [149], constitutes 17% CHOSMg peak. In Diepenveen, the most intensive signals in the spectra could be assigned to CHOSMg compounds. Even though Diepenveen shows a similar profile of organic compounds to thermal stressed Y793321 (CM2; [149]), the amounts of CHOSMg compounds in Y793321 are only 4.6%. Aguas Zarcas (CM2, which fell in 2019) saw only low temperatures, similar to CM2 Murchison [35, 246]. Even though Aguas Zarcas contains an above-average amount of sulfur compared to other CM2 meteorites, with a diverse and complex CHOS chemical space (data not shown), only 1% of all annotations are CHOSMg compound.

To unambiguously assign CHOSMg elemental compositions from exact mass values, ultrahigh mass resolution techniques like FT-ICR-MS were needed. The combined resolving power of $R > 400,000$ at m/z 400 and a mass precision of < 200 ppb allow for an unambiguous chemical formula assignment owing to high mass accuracy, which can distinguish compounds by the precision of half a milli-atomic mass unit (mass of an electron; [141, 185]).

Furthermore, this high mass accuracy enables the detection of isotopologues of compounds if the natural abundance of the monoisotopic signal is sufficient. The isotope patterns as seen in the mass spectra are used to qualitatively confirm the assigned chemical composition by comparing the experimental results to a theoretical isotope pattern (Figures 10(C) and (D)). Mass peak m/z 375.16969 with the assignment $C_{16}H_{32}MgO_6S$ shows characteristic ^{25}Mg and ^{26}Mg isotope signatures and ^{34}S , ^{13}C , and ^{18}O peaks, as well as signals of their combinations with the intensity representative of their natural abundance.

2.2.2 Chemical Structure of CHOSMg Compounds

The profiles of CHOSMg compounds in the ungrouped achondrite NWA 7325 were further visualized in adapted van Krevelen diagrams (Figure 11). The complex and ordered chemical space of CHOSMg compounds covers a wide mass range between 200 and 700 m/z with H/C values between 2.5 and 1 (Figure 11(A)). Most of the CHOSMg compounds contain one sulfur atom and show mostly complete methylene-based homologous CH_2 -series. Intensities are fairly similarly distributed over even and uneven carbon numbers, which validates an abiotic origin [247, 248]. Figure 11(B) displays a zoomed-in area from panel (A). Most of the CHOSMg compounds belong to series that elongate by CH_2 units and differ by the amounts of oxygen, hydrogen, and sulfur. The theoretical pathway to obtain CHOSMg compounds thus involves a step either to formally add MgO_4S to CHO compounds or to formally add SO_2 with loss of H_2 to CHOMg compounds. By comparing the fatty acid chains of CHO, CHOMg, and CHOSMg compounds in NWA 7325, it can be seen that more than half of the CHOSMg compounds share their fatty acid chains with either CHO compounds, CHOMg compounds, or both (Figure 11(C)). CHOSMg compounds are closely related in their chemical structure to CHO and CHOMg compounds and may represent either an endpoint or an intermediate product in the chemical evolution and stabilization of carbon in asteroid parent bodies. Most detected CHOSMg molecules contain six oxygen atoms as seen in Figure 11(D), two oxygens more than the CHOMg

previously described by Ruf et al. (2017) They account for more than 1/3 of all CHOSMg compounds and are closely followed by CHOSMg molecules with five or seven oxygen atoms. As also seen in CHOMg compounds, principal chemical structures that exist in larger numbers than the others are probably the most stable ones [88]. Thus, it is to be expected that CHOSMg compounds with six oxygen atoms have characteristics that lead to the highest stability.

The CHOSMg compounds seem closely related in composition to CHO and CHOMg compounds and need some form of sulfur and magnesium to be generated. Sulfur is ubiquitous in its various oxidation states and is readily available in meteorites in mineral, (poly)sulfates/(poly)sulfides, and organic sulfurized molecules [245]. Magnesium ions from the magnesium silicates matrices have been hypothesized to be involved in CHOMg compounds in interaction with existing carboxylic aliphatic acids [88]. Equally likely is the formation of coordination complexes with liberated sulfur from sulfate minerals attached to magnesium ions before or after the complexation with the carboxylate group of CHO compounds. Oxidation reactions to form an $\text{H}_2\text{MgO}_6\text{S}$ head group from lower oxidized sulfur species are plausible.

Both the emergence of CHOSMg compounds from CHO and CHOMg compounds are chemically achievable. A mass difference network analysis (see Figures 12(A) and (B)) shows a close connectivity between the CHO, CHOMg, and CHOSMg compounds, as they are systematically linked to each other with the same mass transitions. CHOMg compounds and CHOSMg are proposed to have structural similarities (see Figures 12(C) and (D)) because they share similar chemical stability to that in fragmentations by tandem mass spectrometry experiments, as well as in their rapid degradation at low pH. The common moiety of all organosulfur magnesium fragments detected in tandem mass spectrometry was found to be MgO_6S as a head group after various aliphatic chain fragmentation (see Figure A.2 in the Appendix). The investigated peak of m/z 263.04448 shows decreasing intensities with increasing fragmentation energy. Detected fragments contain the stable sulfur-magnesium head group and a shortened carbon backbone. Ultimately, the

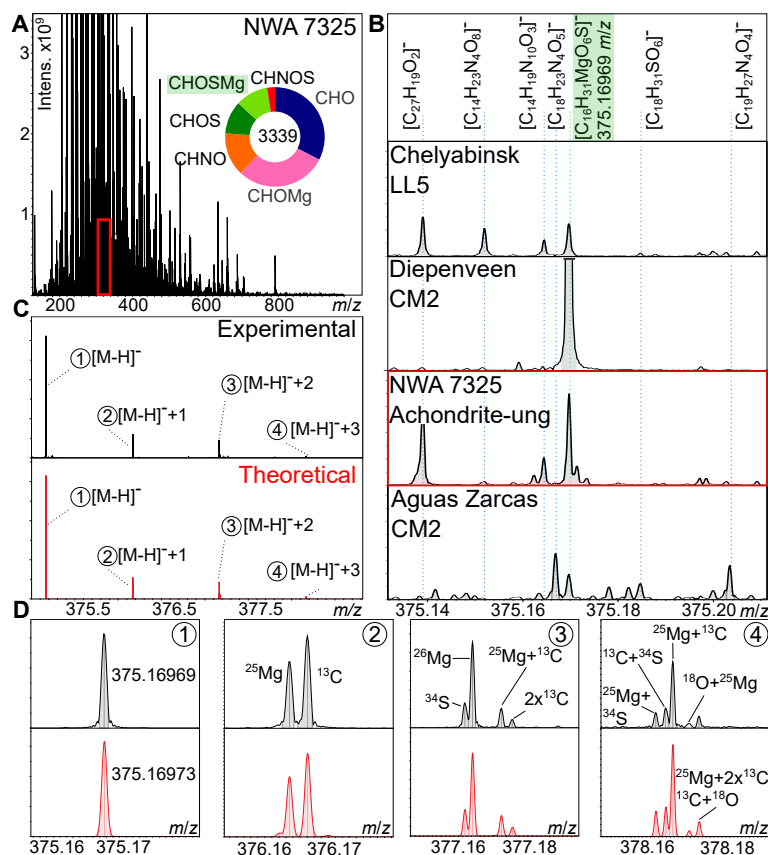


Figure 10: Detection of the CHOSMg compounds. (A) Negative electrospray ionization (ESI) Fourier transform ion cyclotron resonance mass spectrometry (FT-ICR-MS) mass spectrum of ungrouped achondrite NWA 7325 is shown. The donut plot shows the distribution over all chemical spaces, including the newly detected CHOSMg compounds in light green. The red box is enlarged in panel (B) under the name NWA 7325. (B) Comparison of the mass peak m/z 375.16969 assigned to monoisotopic formula $[C_{16}H_{31}MgO_6S]^-$ in ordinary chondrite Chelyabinsk (LL5), in ungrouped achondrite NWA 7325, and in carbonaceous chondrites Diepenveen (CM2-an) and Aguas Zarcas (CM2). Green color represents a chosen CHOSMg peak. The red box is the enlarged region from panel (A). (C) Comparison between the experimental and theoretical isotope pattern of m/z 375.16969 from panel (B) as the monoisotopic peak (^{12}C , ^{25}Mg , ^{32}S , ^{16}O , 1H). The given m/z value is from the respective highest isotope peak of each nominal mass. (D) Zoomed-in view of panel (C). Experimental and theoretical masses of isotope peaks are given. Isotope composition is specified in the experimental (upper) section of panel (D). Intensity scaling of spectra with shared x-axis is similar and thus allows comparison.

shortest possible fragment of solely the sulfur-magnesium head group without hydrocarbon chain attached was also detected through the fragmentation

experiments. To confirm the proposed structural formula, the stability of CHMgO_6S was calculated on the B3LYP/6-31+G(d,p) level of theory and given in Hartrees as seen in the Appendix (Figure A.3). Harmonic frequency analysis calculations performed on two anionic optimized structures confirm that both shown anions represent energy minimums. The proposed structure from Figure 12(D) represents the more likely isomer and also shows similar geometrical features to those observed in CHOMg compounds. Due to its noticeable stability, it is not possible to observe MgO_2 , SO_2 , SO_4 , or MgSO_4 losses in fragmentation experiments (see Figure A.2).

2.2.3 Temperature-induced Formation and Stability of CHOSMg

In contrast to many thermally altered meteorites, Murchison (CM2) barely contains compounds belonging to the CHOSMg class. By heating Murchison under secondary vacuum (10^{-5} mbar) to elevated temperatures for several hours, an increase of CHOSMg and CHOMg compounds was observed. At lower temperatures (lower 250°C), Murchison developed a large and complex chemistry regarding CHOSMg and CHOMg compounds. The CHOSMg compounds show a wider variation regarding aromaticity and oxygenation. Consequently, they are more easily generated and show higher abundance than CHOMg compounds (see Figure A.4(C)). At high temperatures (600°C and above), the CHOSMg compounds reduced in number and complexity compared to lower 250°C samples, whereas CHOMg compounds stay fairly similar. Numbers of CHO, CHOS, CHOMg, and CHOSMg compounds (see Figure A.5) show that short-time heating, e.g., triggered by impacts, reduces the amount of CHOS compounds that goes along with a liberation of, e.g., sulfates. These sulfates, as well as those from sulfur-containing minerals, allow the formation of CHOSMg compounds. However, at high temperatures, the sulfur from CHOSMg compounds is not stable enough to withstand the temperatures, but the more stable CHOMg compounds remain in the system. This can also be observed by the ratios of these compound families as seen in Figures A.6 and A.7. In a first step at 250°C , CHOSMg compounds are

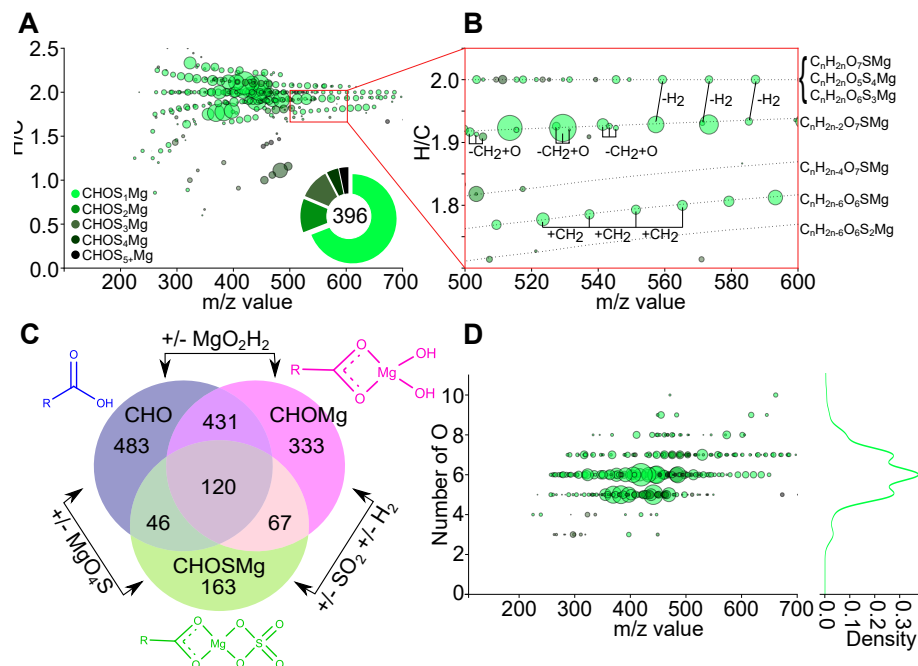


Figure 11: Characteristics of CHOSMg compounds of ungrouped achondrite NWA 7325 soluble organic matter analyzed with (-)ESI-FT-ICR-MS. (A) Mass-edited—H/C ratio diagram of CHOSMg compounds. Bubble size represents the intensity in the mass spectrum; color represents the amount of sulfur per CHOSMg compound according to the legend. The donut plot shows the total amount of CHOSMg compounds and shares of each of the five colored groups according to the legend. (B) Zoomed-in area from panel (A) with annotated homologous series and mass differences between the compounds. Methylene-based mass differences are marked by dotted lines. Examples for other mass differences than methylene-based ones are shown. Suggested chemical assignments of homologous series are depicted next to panel (B). (C) Venn diagram comparing the composition of fatty acid chain groups ("R") of CHO (blue), CHOMg (magenta), and CHOSMg (green) compounds. Numbers in the Venn diagram are counts of fatty acid chains with unique composition ($C_xH_yO_z$ with $x, y, z \in \mathbb{N}$). The chemical structure of head groups of CHO, CHOMg, and CHOSMg is displayed in their respective color with fatty chain marked as "R" in the structure. (D) Plot with m/z values vs. number of oxygen. Bubble size and color according to panel (A). Density plot on the right side displays relative abundance of compounds with specific number of oxygen.

increasing over CHO compounds but decrease again at 600°C to 1000°C. CHOMg compounds behave fairly similar in terms of variation of abundances along temperature compared to CHOSMg compounds, but they increase at the highest temperature. Consequently, it can be assumed that CHOSMg

compounds are intermediate products during the formation of CHOMg out of CHO compounds regarding heat. This trend can also be observed by comparing the fusion crust and inner matrix of meteorites.

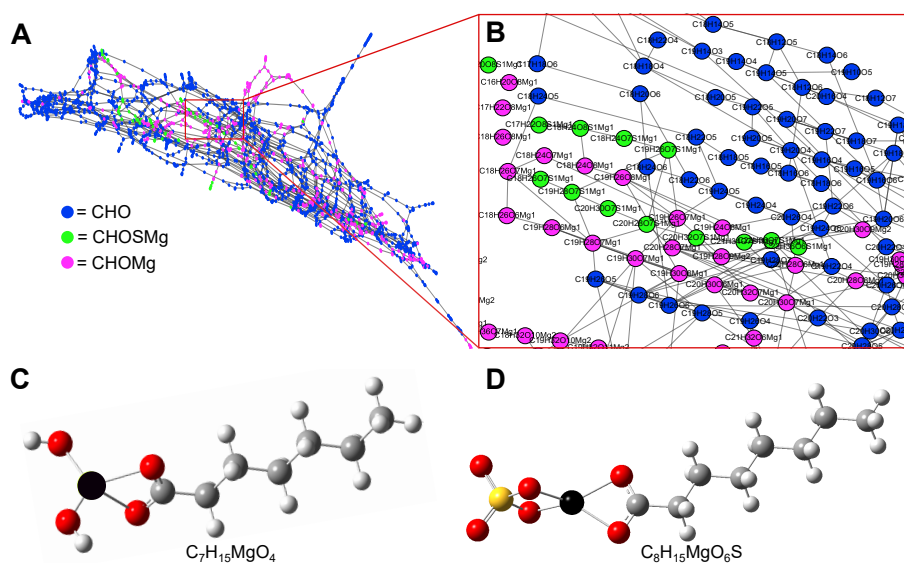


Figure 12: (A) Mass difference network of a heated Murchison sample (Murchison 250°C 3.5 hr) with (B) a zoomed-in view of a chosen position. Colored dots represent experimental masses and calculated elementary compositions of selected chemical spaces, CHO (blue), CHOSMg (green), and CHOMg (magenta). Lines between the dots present the mass differences H₂, H₄, CH₂, C₂H₄, O, H₂O, MgSO₄, MgH₂O₂, S, S₂, and Mg from a mass difference network analysis. (C) Proposed structure of CHOMg compounds as published [88]. (D) Proposed structure of CHOSMg compounds according to MS/MS experiments (see Figure A.2) and stability calculations (see Figure A.3). Colored dots represent carbon (dark gray), hydrogen (light gray), oxygen (red), magnesium (black), and sulfur (yellow).

During atmospheric entry, the outer shell of meteorites reaches temperatures of more than 2000°C, resulting in melting and evaporation of the material. It is reported that the inner matrix stays relatively cold [249]. We compared the fusion crust and the core matrix of three different meteorites to assess the effect of temperature exposure on CHOSMg compounds. The separation between fusion crust and inner matrix was performed by physical

force in an agate mortar. The heating during atmospheric entry eventually causes alteration of the carbon-containing compounds within the crust, which is seen in Figure 12. It is noteworthy that atmospheric entry is considered as heating only, neglecting the influence of pressure from the shock wave [250]. The analyzed meteorites were Aba Panu, a highly shocked (S4) L3 ordinary chondrite [251], and the CM2s Aguas Zarcas, as well as Murchison. Panel (A) of Figure 12 shows the CHOSMg compounds in the respective inner matrix (top row) and the fusion crust (bottom row) of each of the three analyzed meteorites. Aba Panu contains a higher amount of CHOSMg compounds compared to Aguas Zarcas and Murchison. This might be related to higher extents of shocks of this meteorite. The CHOSMg compounds in Aguas Zarcas contain several sulfur atoms, which reflects the diverse sulfur chemistry in this meteorite. For Murchison, the amount of CHOSMg compounds is scarce, similarly to CHOMg compounds. All three meteorites show higher abundances of CHOSMg compounds in their fusion crusts than in their inner matrices. In the Aba Panu fusion crust, more than 75% of all CHOSMg compounds contain one sulfur atom. Compared to the Aba Panu inner matrix, the newly formed homologous series of CHOSMg compounds can be observed in the Aba Panu fusion crust (see Figure 12(A)). Aguas Zarcas also exhibits new homologous series in the fusion crust compared to its inner matrix. In the Aguas Zarcas fusion crust, a significant loss of sulfur atoms in CHOSMg can be observed in comparison to the Aguas Zarcas inner matrix. While the Aguas Zarcas inner matrix contained only 10% of CHOS₁Mg compounds, the amount of CHOS₁Mg rose to closely 75% in the fusion crust. The Murchison matrix contains hardly any CHOSMg compounds. And again, similarly to Aba Panu and Aguas Zarcas, a wide diversity and complexity of new CHOSMg homologous series are increased in the Murchison fusion crust compared to the inner matrix. The boxplots of Figure 13(B) show the amount of CHOSMg compounds in the matrix and crust of the three meteorites. Compared to the matrix, the average amount of CHOSMg compounds is higher in the fusion crust. Furthermore, the distribution of oxygen (Figure 13(C)) and of sulfur

(Figure 13(D)) is different in the meteoritic fusion crust compared to the inner matrix. CHOSMg molecules in the matrix contain mostly six to eight oxygen atoms with only small differences to lower and higher amounts of oxygen. The amount of sulfur is similarly distributed over one to three sulfur atoms and shows a decrease beginning at four sulfur atoms. In fusion crust analysis, it was shown that the abundances of CHMgO_6S , CHMgO_7S , and CHMgO_8S are significantly increased compared to all other CHOSMg compounds. For sulfur in CHOSMg compounds in the crust, it can be seen that especially CHOS_1Mg compounds are strongly increased and show a steady decrease with higher amounts of sulfur.

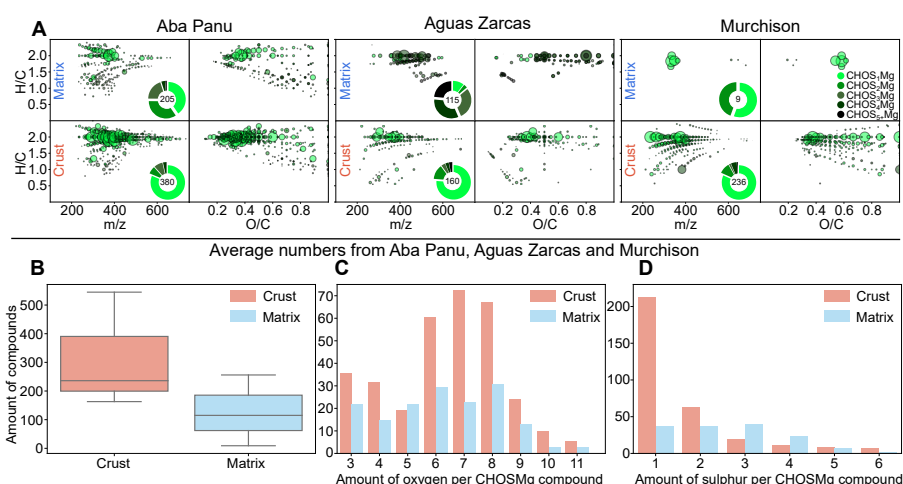


Figure 13: Difference between meteoritic matrix and fusion crust of three different meteorites. (A) Comparison between meteoritic matrix (top row) and meteoritic fusion crust (bottom row) of ordinary chondrite Aba Panu (L3) and carbonaceous chondrites Aguas Zarcas (CM2) and Murchison (CM2). Depicted are mass-edited H/C ratio diagrams (left side of each of the three panels) and O/C ratio vs. H/C ratio (van Krevelen) diagrams (right side of each of the three panels). Bubble size represents the intensity in the mass spectrum; color represents the amount of sulfur per CHOSMg compound according to the legend. The donut plot shows the total amount of CHOSMg compounds and shares of each of the five colored groups by count according to the legend. (B) Boxplot of the amount of CHOSMg compounds in the three meteorite samples, for crust (red, left side) and for matrix (blue, right side). (C) Average amount of oxygen per CHOSMg compound for crust (red) and matrix (blue). (D) Average amounts of sulfur per CHOSMg compound for crust (red) and matrix (blue). See also Figure A.8.

2.2.4 CHOSMg Compounds as a Surrogate Parameter for Temperature Incidents

We investigated a large number of meteorites (44) using partial least-squares discriminant analysis (PLS-DA) to describe structural correlations between thermal history and CHOSMg compounds. To assess the reliability of the PLS-DA, we tested the cross-validated predictive residuals through the analysis of variance. We observe a separation in three different groups, namely, a group with hydrothermal background without short-duration heating - T I (e.g., CM2 Paris), moderate short-duration heating-T II (e.g., C2 ungrouped Tagish Lake) and intense short-duration heating - T III/T IV (e.g., CR2 GRO 03116), and long-duration heating - LDH in meteorites (e.g., L6 Novato) [23,24,252]. The plot in Figure 14(A) shows a thermal gradient from T I meteorites over T II, T III, and T IV meteorites to LDH meteorites going from left to right. Three regions in the plot were determined (see Figure 14(B)) and further used to evaluate the values of loadings that characterize all of those regions. Examples of the CHOSMg signature of each region are depicted in the Appendix (see Figure A.9). Hydrothermal backgrounds without short-duration heating T I meteorites are mostly described by oxygen-rich CHOSMg compounds. Molecules with one sulfur are equally frequent as those with several sulfur atoms. Oxygen distribution (see Figure 13(C)) shows the highest amounts between seven and nine oxygen per CHOSMg compound. Notably, the O/C ratio of CHOSMg is very high compared to other compound classes owing to the fact that the magnesium-sulfur head group mostly incorporates six or more oxygen atoms, which results in high O/C ratio at low aliphatic acid chain lengths. CHOSMg compounds of more heated T II meteorites show higher contribution of sulfur atoms compared to the other regions. The oxygen numbers of T II meteorites are distributed similarly to the ones of T I meteorites. However, the number of sulfur atoms in T III/IV meteorites is strikingly high, which is also reflected in the low C/S ratio. Meteorites that experienced long-duration heating show a characteristic pattern of CHOSMg compounds. Approximately 75% of all compounds

belong to CHOS_1Mg , 25% containing more than one sulfur atom. The CHOSMg compounds of this region are mostly carbon saturated compounds, and most of the compounds contain six or seven oxygen atoms, which has been shown to be a highly stable form of CHOSMg compounds (see Figure A.3). Overall, the CHOSMg compounds show distinct characteristics according to the thermal history of the meteorite. Noteworthy is the fact that the amount of sulfur in CHOSMg compounds decreases with increasing heat. Our approach enables the discrimination between thermally stressed meteorites according to their CHOSMg signature, involving their information in carbon saturation and oxidation and the number of sulfur atoms. Some examples in predictions can be found in Figures A.10 and A.11 in the Appendix for Maribo CM2; low-temperature meteorites Orgeil CI, Ivuna CI, Mundukpura CM2, and heated Diepenveen CM2; and DHO1988 CY in validation of our approach. This motivates us to consider many more meteorites and their whole CHNOSMg chemical space to set up heating prediction models that can find their application in the analysis of novel meteorite falls and return mission samples.

2.2.5 Conclusion and Outlook

In this work, we show the presence of a new and hitherto- undescribed carbon-based chemical compound class called CHOSMg compounds. These compounds are readily formed during temperature incidents. As their amount and chemical characteristics are different when looking at the inner matrix and the fusion crust of the same meteorite, we conclude that heat is an important factor of the formation of these magnesium organosulfur compounds. Moreover, by investigating a large set of meteorites, we describe that CHOSMg compounds follow meteorites according to their thermal history. Our research reveals that hydrogen, carbon, oxygen, and magnesium, together with sulfur, are sequestered in thermostable metalorganic compounds in meteorites and can thus contribute to long-term astrochemical organic diversity. The extent of this formation is highly dependent on the thermal exposure of the asteroid parent

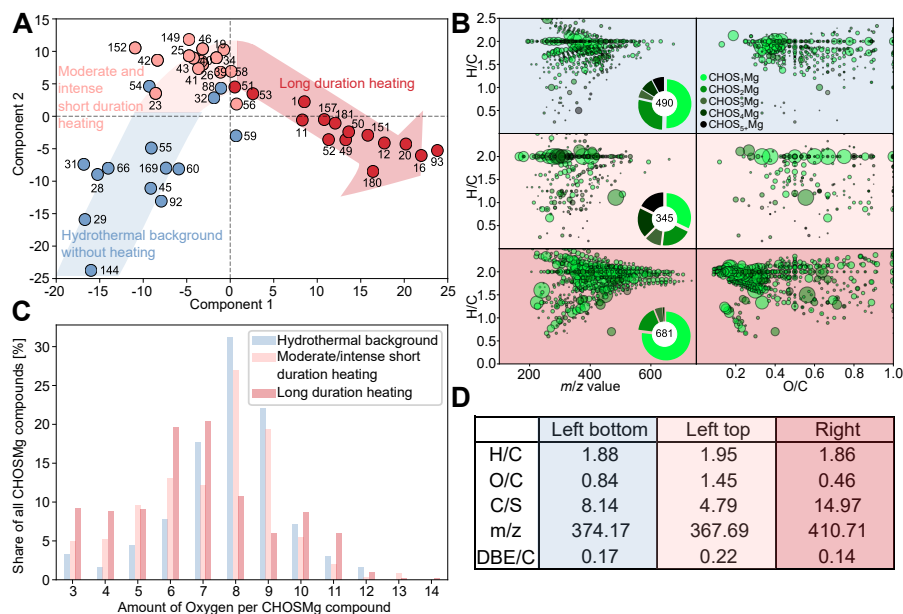


Figure 14: (A) PLS-DA of 44 different meteorites well described [23,24,252] regarding their thermal metamorphism history. Only CHOSMg compounds were used as PLS-DA loadings. Three categories were chosen according to the assigned thermal history. Hydrothermal background without short-duration heating (T I - dark blue), moderate short-duration heating (T II) and intense short-duration heating (T III/T IV - light red), and long-duration heating (LDH — dark red) [23,24]. Information on samples can be found in Table A.1. Three areas of interest were marked in different background colors, namely, hydrothermal background without short-duration heating in light blue, moderate and intense short-duration heating in light red, and long-duration heating in dark red. (B) CHOSMg loadings of PLS-DA according to the three colored regions. Top row: hydrothermal background without short-duration heating in light blue; middle row: moderate and intense short-duration heating in light red; bottom row: long-duration heating in dark red. Depicted are mass-edited H/C ratio diagrams (left side of each of the three panels) and O/C ratio vs. H/C ratio (van Krevelen) diagrams (right side of each of the three panels). Bubble size represents the intensity in the mass spectrum; color represents the amount of sulfur per CHOSMg compound according to the legend. The donut plot shows the total amount of CHOSMg compounds and shares of each of the five colored groups according to the legend. (C) Amount of oxygen per CHOSMg compound vs. share of all CHOSMg compounds for the three colored areas of the PLS-DA, hydrothermal background without short-duration heating in light blue, moderate to intense short-duration heating in light red, long-duration heating in dark red. (D) Weighted averages of descriptive ratios for the three colored areas of the PLS-DA. Double bond equivalent (DBE) calculation is explained in the paragraph "material and methods."

body. The organic footprint in CHOSMg compounds in meteorites allows us to draw conclusions regarding the thermal history of the analyzed meteorites. While meteorites having witnessed only low-temperature exposures mostly contain CHOSMg compounds with higher amounts of oxygen and sulfur per molecule, the ones in more heated meteorites converge to a six-oxygen-bearing form (CHMgO₆S), which represents the most stable form of this compound class. We show that the carbon-based CHOSMg molecules survive not only the harsh conditions of the asteroid parent body (extreme temperatures, pressures, and radiation) but also the atmospheric entry conditions where the material is heated to temperatures well above 2000°C in the meteorite crust. This illustrates the astrobiological impact of our study because these organic compounds in meteorites were continuously delivered to the early Earth's surface through meteoritic impacts and still are. Due to their stability, the pool of CHOSMg compounds might have contributed significantly to the organic diversity found on Earth today. These might have played a significant role in the emergence of life on Earth as well. The organics in meteorites might have contributed to prebiotic chemistry and the formation of protocell membranes with their extreme chemical diversity and resilience toward heat more than thought so far, particularly in very primary hot periods on early Earth such as the Hadean.

Funded by the Deutsche Forschungsgemeinschaft (DFG, German Research Foundation)—Project-ID 364653263—TRR 235 (CRC 235).

Chapter 3

Diversity of Organic Molecules in Olivine Mineral Detected with High-Resolution Analytical Techniques

Matzka, M. and Schmitt-Kopplin, P.

Unpublished manuscript

Olivine mineral contains a broad variety of organic compounds, which are widely uninvestigated to this point. In this study we present a method to analyze the variety of carbon containing molecules in olivine mineral and show their stability towards elevated temperature within the mineral matrix. Fourier transform ion cyclotron mass spectrometry was applied to evaluate the methanolic extracts of olivine rocks from Åheim, Norway. The olivines contain a complex and diverse mixture of organic molecules containing carbon, hydrogen, oxygen, nitrogen, sulfur, and magnesium. Furthermore the compounds are detectable after exposing the olivine to 600°C showing the protective characteristics of the mineral matrix. The same metalorganic compounds as already found in meteorites were detected in olivine with the same heat resistant properties. Consequently olivine mineral represents an important medium to store organic compounds in the terrestrial carbon cycle. Both olivine from outer space but also from the Earth mantle could have significantly influenced the emergence and sustainment of life on Earth. The mineral contains enough small molecules to start and fuel prebiotic chemical reactions on early Earth.

Contribution: M.M. designed and performed research, conducted experiments, analyzed the data and made figures. M.M. wrote the paper.

3.1 Introduction

Olivine ($\text{Mg,Fe})_2\text{SiO}_4$ is a neo- or orthosilicate mineral belonging to a group of magnesium iron silicates. It is the most abundant mineral in the Earth's upper mantle, followed by orthopyroxene, clinopyroxene, and garnet [1, 48]. Olivine consists of isolated silicon tetrahedra with magnesium and iron cations at the octahedral positions. From a coordination point of view, olivine mineral can be seen as an array of isolated SiO_4^{4-} tetrahedra with Me^{2+} ions in octahedral holes [42]. The mineral mostly contains a mixture of magnesium and iron cations but also the pure magnesium and pure iron forms can be found in nature. The magnesium endmember (Mg_2SiO_4) is called Forsterite, the iron endmember (Fe_2SiO_4) is called Fayalite. Besides oxygen, silicon, magnesium, and iron, the mineral also can contain nickel, calcium, aluminum, chromium, manganese, and other cations, but far fewer in amount. Also carbon was detected in different oxidation states and forms within olivine mineral.

Carbon incorporation in the olivine is controversially discussed in the literature. Carbon was discussed to be a direct substitute of silicon in the tetrahedral structure of the olivine [83, 84] or it could be dissolved in the mineral matrix, found as carbonaceous phases, graphite, silicon carbide, and other compounds as well as in sub- microscopic bubbles or cracks [85, 86]. Freund et al. suggested that H_2O and CO_2 are, to a certain extent, soluble in upper mantle olivine. These molecules can further be converted to form H_2 and reduced carbon, which then can cause the formation of C-H entities. These C-H entities either exist in the form of carboxylic acids, dicarboxylic acids, and medium chain fatty acids or are directly attached to the Mg-silicate matrix by bonding to two O⁻ moieties [87]. Depending on the used analytic technique, the amount of carbon is suggested to be approximately between 10 ppm and 30 ppm in San Carlos olivine [85, 86, 89–91]. A more recent approach reports a carbon solubility in olivine of 0.1 ppm to 1 ppm [92].

Many studies to investigate the chemical and physical properties of olivine have been performed, looking into abiotic features and mineral characteristics. Recently, olivine gained new attention due to its ability to abiotically generate

methane and elemental hydrogen, and within this topic, the connection to small organic molecules was drawn. Olivine, which comes in contact with water under 500°C undergoes serpentinization reaction, thereby forming serpentinite minerals [73]. This is a hydration reaction, during which olivine ((Mg,Fe)₂SiO₄) is hydrated to serpentinite ((Mg,Fe)₃Si₂O₅(OH)₄). Furthermore, Fe²⁺ in the olivine is oxidized to Fe³⁺ leading to the abiotic generation of molecular hydrogen [74]. Especially this process is able to promote further reactions. One of the reactions enabling the formation of methane is the Sabatier reaction [99, 100]. The Sabatier process allows the formation of methane from carbon dioxide and hydrogen under high temperature and pressure conditions. Both carbon dioxide and carbon monoxide can be educts for this reactions. Moreover, the Fischer Tropsch synthesis is also a plausible chemical way to abiotically generate alkanes, alkenes, and alcohols in mineral samples [101, 102]. Fischer Tropsch reactions require catalytic reaction surfaces such as metal oxides in combinations with metal catalysis as known from nickel and iron. Olivine is consequently a suitable matrix to help abiotic organic compound synthesis and might have contributed to the emergence of life on Earth.

In this work, we want to present the large diversity of organic compounds found in olivine mineral. In the first part of the paper, we present the method of analysing olivine mineral with Fourier transform ion cyclotron resonance spectroscopy. The second part will cover the analysis of organic compounds in olivine with LC-MS and the third part shows the analysis of organic compounds with the NMR technique.

3.2 FT-ICR-MS Analysis

3.2.1 Materials and Methods

For ESI measurements, five milligrams of olivine and for APCI and APPI, four milligrams of olivine were used respectively. The rocks were washed three times with methanol in an agate mortar. Before crushing, methanol

was added to the mortar. The olivine mineral was finely powdered and together with methanol formed a homogeneous suspension. After 30 seconds of ultrasonic bath and centrifuging, the supernatant was used for ESI-FT-ICR-MS acquisition. To ensure cleanness of the mass spectrometer, methanol blanks were acquired before measurement. The full material and methods can be found in the appendix.

3.2.2 Organic Compounds in Olivine

Most of the research regarding organic compounds within meteorites was conducted to characterize the molecules within the meteorite matrix [88, 141, 148, 253]. During the investigation of Tissint meteorite, several compartments of the meteorite were investigated to specify their respective contribution to the organic matter within meteorites. Tissint meteorite is an aluminium depleted ferroan basaltic rock, which depicts internal mineral diversity of four mayor regions. It contains (1) a fine-grained main matrix composed of pyroxene-maskelynite, chromite, ilmenite and pyrrhotite, (2) a black fusion crust resulting from the atmospheric entry, (3) a black vitrified part originated from heating and pressure during shock events, and (4) olivine mineral [254, 255].

After investigation of these four regions with FT-ICR-MS the results showed that different fractions of Tissint meteorites contained alternating amounts and characteristics of compounds. The olivine mineral of the Tissint meteorite contained by far the most amount of assigned formulae and thus the highest diversity of organic molecules. Especially CHOMg compounds were detected, which were shown to be formed from CHO compounds in proximity to magnesium mineral [88].

Olivine mineral seems to be an important factor for the formation of organic compounds within minerals. To better understand the carbon specitation in olivine mineral, a broad investigation of an olivine mineral is conducted within this work.

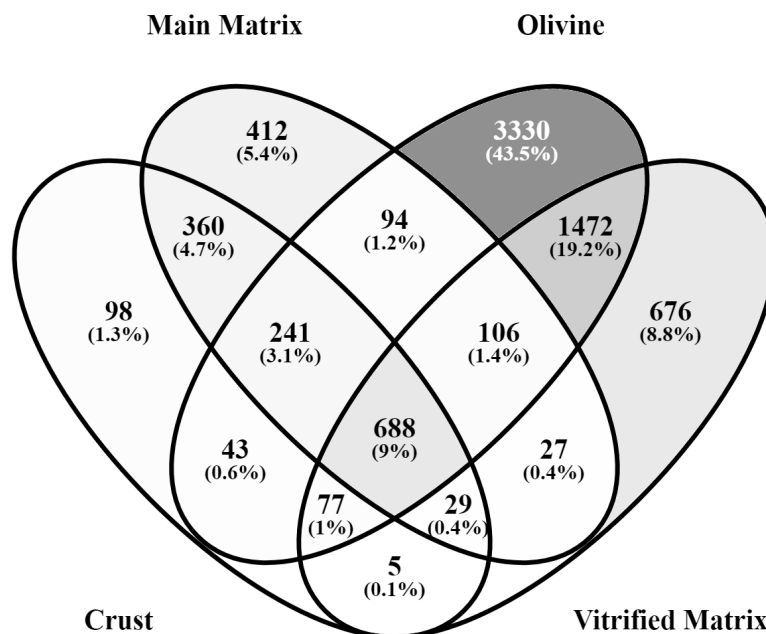


Figure 15: Total amount of assigned chemical formulae for the four different regions of Tissint meteorite. Depicted are Tissint main matrix, Tissint crust, Tissint vitrified matrix and Tissint olivine crystals. The darker the color, the more formulae are contained.

3.2.3 Comparison of Ionization Modes

Since the FT-ICR-MS measurements of organic compounds in olivine are widely uninvestigated, a systematical approach to find an ideal ionization method was conducted. The Åheim olivine extracts were measured in ESI positive and negative mode, in APPI positive and negative mode, and in APCI positive mode. The ionization methods were briefly described in the material and method section of this work. While APPI and APPI are ideal methods to ionize more lipophilic and aromatic chemical structure, the ESI ionization method is more suitable to ionize hydrophilic compounds.

The results of the ionization experiments can be seen in Fig. 16 and their respective numbers in Table 1. APPI and APCI ionization mode primarily ionized CHO and CHNO compounds. In positive mode, even some CH, so partly unsaturated and aromatic hydrocarbons were ionized and measured.

APPI positive mode was also able to ionize some CHOS compounds. The distribution of the mass as seen in Figure 16 is quite similar in both APPI positive mode and APCI positive mode, while APPI negative mode shows a reduced amount of compounds and doesn't show compounds in high m/z values over 400 m/z . The compounds are low in oxygen as seen by the average weighted O/C value of 0.09 for CHO compounds in APCI (+), 0.15 for APPI (-) and 0.1 for APPI (+). Also for CHNO compounds the average weighted O/C values are in similar ranges (0.05 for APCI (+), 0.08 for APPI (-) and 0.1 for APPI (+)), which shows that these ionization methods mostly ionize lipophilic compounds. A notable fact is also that magnesium containing compounds were not at all ionized in APPI and APCI and are only visible in ESI ionization mode. ESI shows besides a wide range of CHO, CHNO, CHOS, and CHNOS compounds also many magnesium containing compounds. The m/z range of ESI is not as high as with APPI and APCI, but stops at approximately 500 m/z . However, more oxygen containing compounds were detected. Average weighted O/C ratios of CHO compounds are 0.17 for ESI (-) and 0.26 for ESI (+) and thus significantly higher than APPI and APCI. For CHNO compounds, the average weighted O/C values are 0.1 for ESI (-) and 0.11 for ESI (+). Notably is the average weighted H/C value of CHNO compounds, which is with a value of 1.56 significantly lower than the values of all other methods.

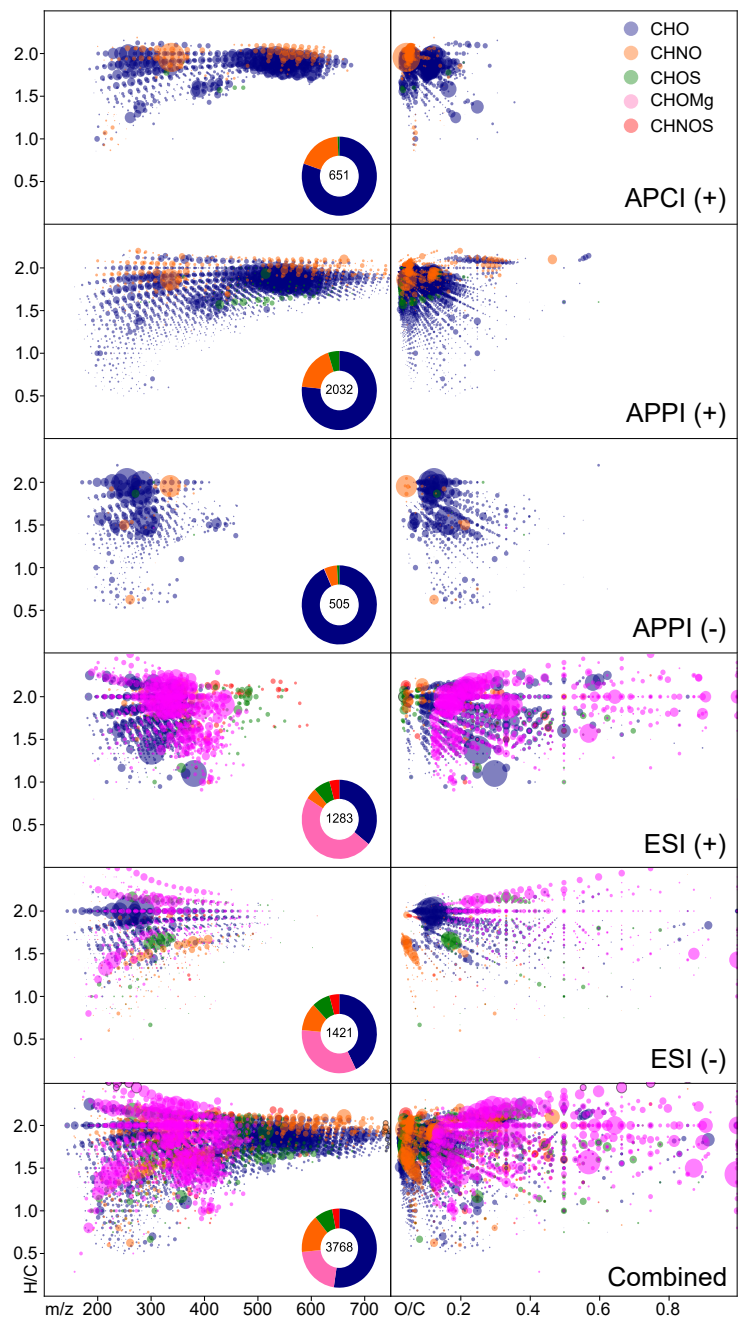


Figure 16: Van Kreveleven diagrams and mass-edited H/C diagrams of the five different ionization techniques and their combination as a diagram of all.

	APCI (+)	APPI (-)	APPI (+)	ESI (-)	ESI (+)	Combined
CH	124	0	310	0	0	322
CHO	522	471	1556	607	459	1972
CHS	2	0	27	0	0	27
CHOS	5	5	97	110	90	293
CHN	26	0	35	0	0	55
CHNO	124	28	378	163	61	592
CHNOS	0	0	1	61	55	116
CHOMg	0	0	0	480	618	795
CHOSMg	0	0	0	93	93	183
CHNOMg	0	0	0	96	163	253
CHNOSMg	0	0	0	33	35	68
Sum	803	504	2404	1643	1574	4676
Average H	0.63	0.6	0.63	0.59	0.58	0.59
Average C	0.34	0.35	0.34	0.32	0.32	0.33
Average O	0.03	0.05	0.03	0.07	0.08	0.06
Average N	0	0	0	0	0.01	0.01
Average S	0	0	0	0	0	0
Average Mg	0	0	0	0.01	0.01	0.01
HC	1.84	1.73	1.82	1.84	1.84	1.79
OC	0.08	0.14	0.09	0.3	0.28	0.27
CN	248.77	195.35	368.42	82.52	54.19	49.97
CS	7459.67	2647.91	1938.99	86.91	72.12	75.64
mass	448.11	278.95	493.06	289.46	347.22	407.49
DBE	3.25	3.39	3.7	2.17	2.62	3.4
OC CHO	0.09	0.15	0.1	0.17	0.26	0.14
OC CHOMg	0	0	0	0.6	0.3	0.47
OC CHOS	0.09	0.17	0.07	0.24	0.22	0.23
OC CHOSMg	0	0	0	0.76	0.29	0.48
OC CHNO	0.05	0.08	0.1	0.1	0.11	0.12
OC CHNOMg	0	0	0	0.32	0.32	0.32
OC CHNOS	0	0	0.13	0.16	0.27	0.25
OC CHNOSMg	0	0	0	0.41	0.34	0.35
HC CHO	1.86	1.73	1.83	1.91	1.73	1.79
HC CHOMg	0	0	0	1.86	1.91	1.82
HC CHOS	1.67	1.83	1.71	1.73	1.81	1.79
HC CHOSMg	0	0	0	1.43	1.7	1.59
HC CHNO	1.95	1.77	1.94	1.56	1.98	1.82
HC CHNOMg	0	0	0	1.62	1.82	1.8
HC CHNOS	0	0	1.94	1.67	1.88	1.84
HC CHNOSMg	0	0	0	1.81	1.93	1.91
HC CH	1.64	0	1.57	0	0	1.59
HC CHN	1.44	0	1.77	0	0	1.52
HC CHS	1.55	0	1.59	0	0	1.67

Table 1: Numbers from all Ionization techniques which were used to analyse Åheim olivine.

Overall, this all ionization methods, the organic matter of Åheim olivine can be nicely analyzed and described with different ionization methods and FT-ICR-MS. The combined picture shows a full and diverse spectra of compounds.

However, the analysis of a broad range of geological and mineral samples with all of these ionization method is hardly feasible. For one reason, the amount of sample to be used to make extracts is extremely high. This is especially problematic for meteorite analysis where material is scarce. Furthermore, the deconstruction and installation of the different sources takes time, also for the FT-ICR-MS system to adjust and for the subsequent calibration after installation. Consequently, one methods which mostly represents the samples has to be found and applied for further analysis. Figure 17 shows the comparison of the different ionization techniques.

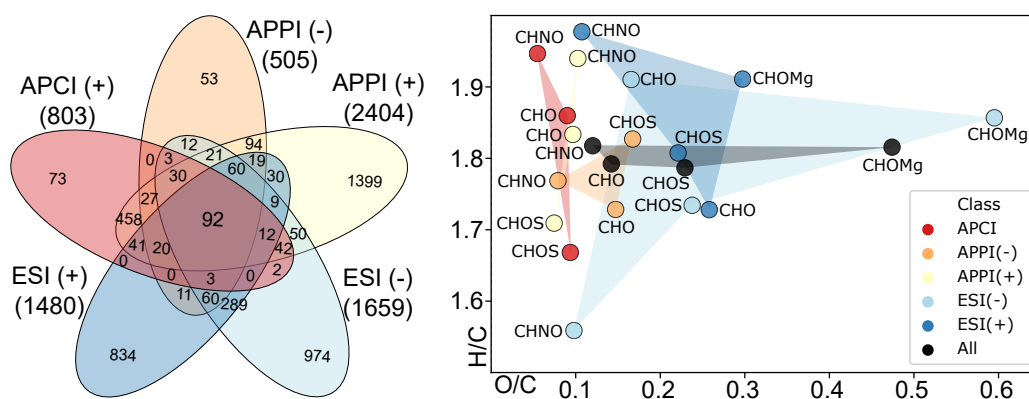


Figure 17: Left side: Venn diagram of five different ionization techniques and amounts of assigned chemical compositions with overlay to other ionization techniques. Right side: Van Krevelen Diagram of average weighted O/C and H/C values of CHO, CHNO, CHOS and CHOMg compounds for all five ionization techniques as well as the average values of all techniques combined. Colored areas represent to coverage of the ionization methods to detect compounds.

On the left side of the figure, a Venn diagram [256] of the five different ionization modes can be seen. Of all ionization methods, only 92 compounds, which are only CHO compounds, are common to all. For APCI (+) mode, only nine percent of the compounds detected are unique to this mode of

ionization. For APPI (-), 10.5% of the compounds are unique to this methods. Most of the with these methods measured compounds consequently can be also found in other ionization modes. 58.2% of the compounds of APPI (+) are unique to this method. These are mostly CH and CHO compounds, which were too lipophilic for ionization with ESI mode. However there is a large amount of unique compounds to APPI (+), the lack of magnesium containing compounds renders the method not useful as a standard ionization method if not used in combination with an ESI ionization mode. ESI (-) and ESI (+) mode both ionize a wide range of compounds and also have more than 42% overlap with other methods. The right side of Fig. 17 shows average weighted O/C and H/C values for CHO, CHNO, CHOS, and CHOMg compounds (only for ESI (+) and ESI (-)). Clearly visible are that APCI (red) and APPI(+) (yellow) do not cover a large area of the Van Krevell diagram. Both ionization methods show all their weighted averages in the left top corner, which again shows they mostly ionize oxygen-deprived compounds. APPI (-) mode features few more compounds in the region between O/C values of 0.1 and 0.2, which are slightly higher O/C values compared to APCI (+) and APPI (+). ESI (+) mode (dark blue) covers a wider range of compounds with higher O/C values up to 0.3 for CHOMg compounds. The largest area is covered by ESI(-) mode (light blue). Its O/C values for CHOMg compounds reach up to 0.6 and also H/C values below 1.6 for CHNO compounds are visible in this ionization mode. By looking at the combined values (in black), it can be seen that ESI (-) shows the largest coverage of the black area in the diagram. Consequently, for a facilitated analysis of the geological samples and also for reasons of the best coverage of all compound classes, the ESI (-) ionization mode was chosen to describe the samples within this work. It has been shown to combine the ionization of a wide range of compounds and compound classes with variable O/C and H/C values and is a readily used method at the FT-ICR mass spectrometer for an investigation of organic compounds in mineral samples such as Åheim olivine.

3.2.4 ESI Analysis of Unheated Åheim Olivine

With a S/N ratio of ≥ 3 , a total of 35360 peaks were picked (117454 with a S/N ratio of ≥ 2). At the nominal mass of m/z 319 (between m/z 318.8 and m/z 319.3), 98 resolved signals were detected with a maximal resolution of 1.4 million. At the nominal mass of 350 m/z (between 349.8 m/z and 350.3 m/z), 70 resolved signals were detected with a maximal resolution of 0.8 million. The spectrum was calibrated internally with fatty acids from the CHO fraction and some organomagnesium compounds. The calibration resulted in an error with a standard deviation of 0.095 ppm. In the final data table, the average error of the assignment is -0.017 ppm. After cleaning steps, a total of 1774 organic compounds were assigned to a chemical formula in the sample of the olivine from Åheim, Norway. They belong to the chemical spaces of CHO (683 / 38.5%), CHOS (111 / 6.2%), CHNO (166 / 9.4%), CHNOS (62 / 3.5%), CHOMg (512 / 28.9%), CHOSMg (97 / 5.5%), CHNOMg (95 / 5.4%), CHNOSMg (32 / 1.8%), and CHOMgBr (16 / 0.9%) compounds. The smallest and largest assigned m/z value is 136.96 and 721.12 respectively. The H/C values range from 0.5 to 2.5 and the values of O/C range from 0.033 to 2 in total. 386 signals (22%) were detected as $[M+Cl]^-$ adducts in the spectrum. 115 different organic compounds were detected as $[M+Cl]^-$ and $[M-H]^-$ adduct. Consequently, a total of 1659 unique chemical formulae have been found in the olivine sample.

A total of 683 CHO compounds were detected in ESI (-) mode in the olivine extract. The average weighted O/C value is 0.17, the average weighted H/C value is 1.91 for this compound class. The Figure 18 shows a descriptive visualization of the CHO compounds in Åheim olivine. Fig. 18A shows the Van Krevelen diagram. Most CHO compounds are situated in the left top corner of the diagram, with H/C values mostly between 2 and 1.4 and O/C values mostly below 0.5 in total. As seen in Fig. 9, these compounds largely belong to lipid like structures. Fig. 18C represents a zoom version of Fig. 18A with assigned compositions. Homologous series of CHO compounds can be seen which follow different lines of theoretical mass differences. Horizontal

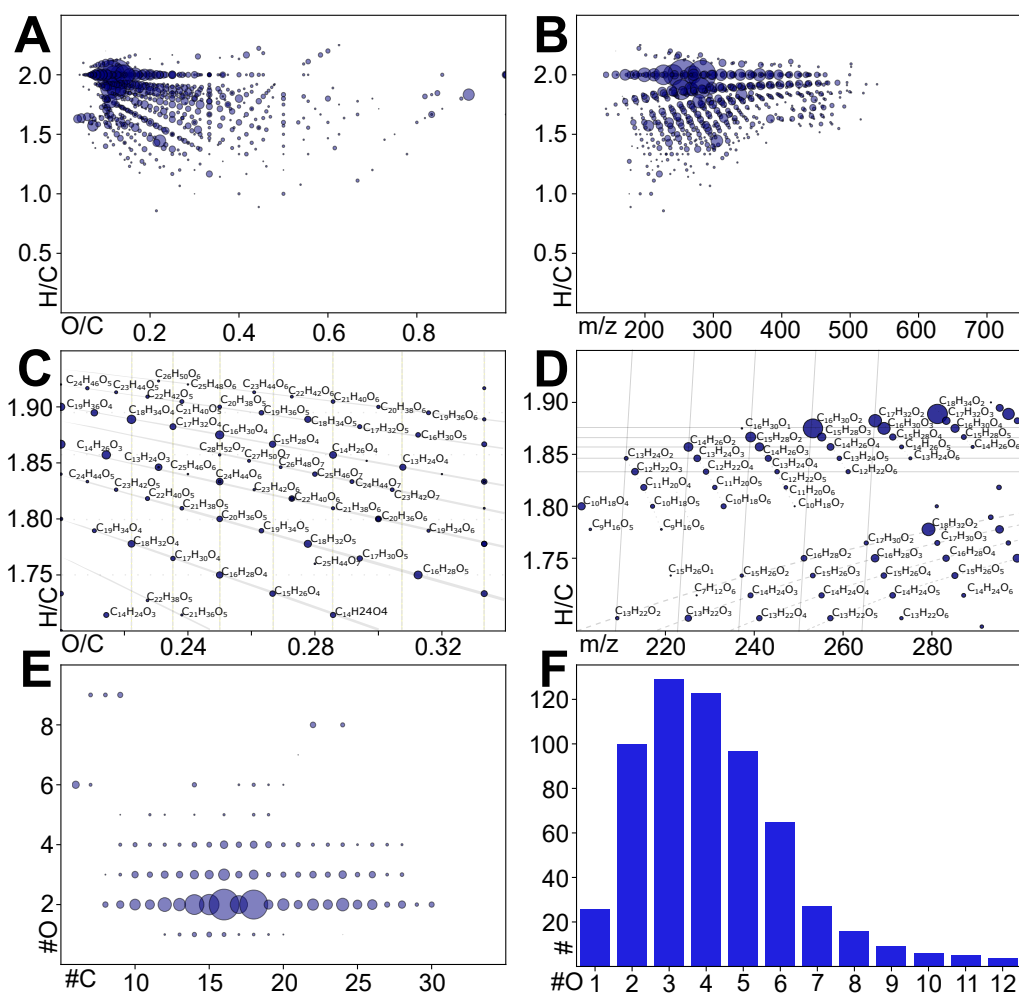


Figure 18: ESI(-) mode results for the CHO compounds of Åheim olivine. Size of bubbles represent intensity in the spectrum. **A** Van Krevelen diagram. **B** Mass-edited H/C diagram. **C** Zoomed-in area of the Van Krevelen diagram with annotations. Grey lines represent certain lines of mass differences. **D** Zoomed-in area of the mass-edited H/C diagram with annotations. Grey lines represent certain lines of mass differences. **E** Amount of carbon atoms vs. amount of oxygen atoms for H/C = 2. **F** Amounts of oxygen per compound vs. amount of compounds.

lines in the Van Krevelen diagram represent the change of one oxygen atom as for example seen from the assigned compositions of $C_{18}H_{32}O_4$ and $C_{18}H_{32}O_5$, which both lie on a horizontal line. The descending lines going from the top left corner to the bottom right edge of the graph represent changes in CH_2 , for example the sequence of $C_{24}H_{44}O_5$ going down to $C_{16}H_{28}O_5$ in methylene-

steps. Dots on the same vertical line represent similar composition with the difference of H_2 , as for example seen in the line of $C_{21}H_{40}O_6$ followed by $C_{21}H_{38}O_6$ with similar O/C ratio, but lower H/C ratio. Fig. 18B represents a mass-edited H/C diagram, with shows the properties of m/z values compared to H/C values. Similar to the Van Krevelen diagram, homologous series can be observed. The m/z range is approximately $100 m/z - 500 m/z$, with highest intensities between $250 m/z$ and $300 m/z$. To better understand the structure of this diagram, a zoomed version of the mass-edited H/C plot can be seen in Fig. 18D. Homologous series are observable from the left bottom to the right top side of the diagram. Similar to the Van Krevelen diagram, these characteristic series are coming from CH_2 mass differences, for example from $C_{13}H_{22}O_2$ to $C_{18}H_{32}O_2$ in steps of CH_2 units. Also visible are horizontal lines of assigned compositions, represented by the mass difference of one oxygen. Similar to the Van Krevelen diagram, the mass difference of H_2 can be seen as a slightly askew line due to the mass loss of $2 m/z$. Furthermore, interesting sequences in the form of the loss of CH_2 , but the gain the of O can observed going from left top to right bottom side of the diagram. The gap in between the two formations of compounds is explained for a mathematical reason, as CH_2 is chemically seen the mathematical mass difference of these types of diagrams. The space in between cannot be filled because a single H atom was a not permitted mass difference in this setting. Fig. 18E represents only compositions with a H/C value of 2. It can be seen that few compounds contain one oxygen atom, probably hydroxy structures or ether compounds. Most of the compounds contain two to four oxygen compounds, which like represents carboxyl acids and hydroxy carboxyl acids, which can be found in the top left corner of the Van Kevelen Diagram. Fig. 18F shows the distribution of the amounts of oxygen over all CHO compounds. Most compounds contain two to five oxygen atoms with a maximum at three. This could signify that, carboxylic acids, hydroxy carboxylic acids and dicarboxylic acids are the most prevalent structures in the olivine samples as these compounds have matching O/C and H/C values

as well as oxygen amounts. However mass spectrometry alone cannot confirm the presence of these structures as assigned sum formulae allow only an assumption of chemical structures, which ultimately would need confirmation from MS/MS side. Amounts of oxygen go up to 12 where already sugar-like compounds and structures could be imaginable in mineral samples. Overall, the amount and diversity of CHO compounds in Åheim olivine represents the variety of organic molecules found. Furthermore, the presence of homologous series as well as the sequence of intensities corroborated the theory that indeed FT like reactions and Sabatier-processes can be plausible reactions pathways for the formation of organic compounds in olivine.

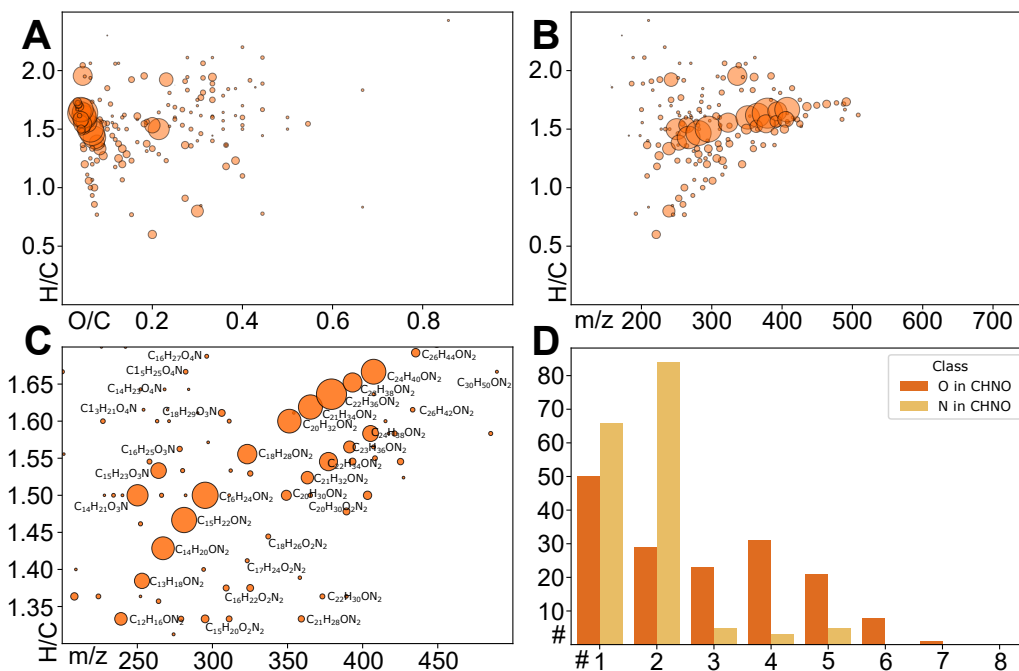


Figure 19: ESI(-) mode results for the CHNO compounds of Åheim olivine. Size of bubbles represent intensity in the spectrum. **A** Van Krevelen diagram. **B** Mass-edited H/C diagram. **C** Zoomed-in area of the mass-edited H/C diagram with annotations. **D** Amounts of oxygen per compound and amounts of nitrogen per compound vs. amount of compounds.

A total of 163 CHNO compounds was discovered in the extract of Åheim olivine. The results of the CHNO compounds can be seen in Fig. 19. The

weighted average H/C and O/C value is 1.56 and 0.1 respectively for this compound class. The Van Krevelen diagram as seen in Fig. 19A shows that the most compounds have very low amounts of oxygen and only few ones tend to go to higher O/C values of up to 0.5, but only with low intensities. Homologous series of CHNO compounds can already be detected in this Van Krevelen diagram. Fig. 19B shows the mass-edited H/C diagram, which reveals, that only a few compounds have H/C values around two and most of the CHNO compounds are located around 1.5 in the diagram. The m/z is going from approximately 200 m/z to 500 m/z and shows related compound structures forming rows of similar chemical composition. A zoomed-in version of the mass-edited H/C diagram as seen in Fig. 19C reveals that most structures belong to either the series of $C_xH_{2x-8}ON_2$, of $C_xH_{2x-10}ON_2$ or of $C_xH_{2x-10}ON_2$. Visibly, the H/C value is lower compared to CHO compounds. The underlying chemical structures with a low H/C value could derive from aromatic nitrogen containing compounds such as pyridine or pyrimidine with attached hydrocarbon chains. Also amine or amide groups are possible structures to be present in the organic matter. Fig. 19D shows that most CHNO compounds contain one or two nitrogen atoms. This could also indicate the presence of nitrogen containing aromatic rings or amine and amide structures. Most CHNO compounds contain one oxygen atom, but up to seven oxygen atoms were found in CHNO compounds which could explain the ESI (-) ionization of aromatic nitrogen structures, which usually hardly ionize in ESI (-) mode.

A total of 110 CHOS compounds were detected in the extract of Åheim olivine. With an H/C value of 1.73 and O/C value of 0.24, the CHOS compounds are slightly less aromatic than CHNO compounds, but not as aliphatic as CHO compounds. Also their O/C value is higher than those of CHNO and CHO compounds. Fig. 20 shows the visualization of the CHOS compounds. The Van Krevel diagram (Fig. 20A) and the mass-edited H/C diagram (Fig. 20B) show that the spread of compounds is larger compared to CHNO and CHO compounds, but still homologous series can

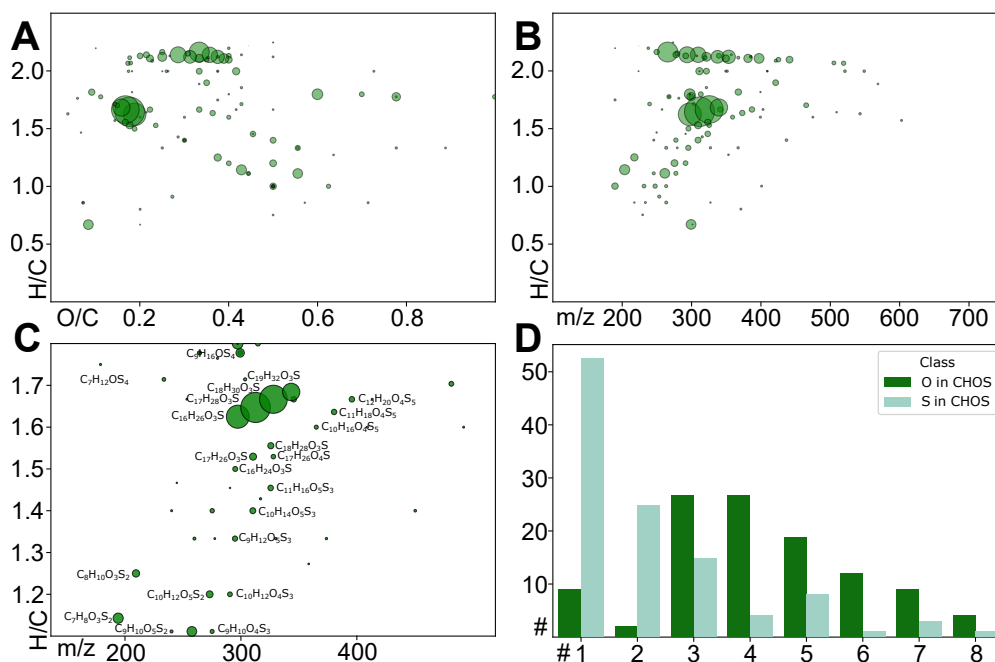


Figure 20: ESI(-) mode results for the CHOS compounds of Åheim olivine. Size of bubbles represent intensity in the spectrum. **A** Van Krevelen diagram. **B** Mass-edited H/C diagram. **C** Zoomed-in area of the mass-edited H/C diagram with annotations. **D** Amounts of oxygen per compound and amounts of sulfur per compound vs. amount of compounds.

be seen. Most compounds have a m/z value between 200 and 400 m/z with few larger compounds. Fig. 20C shows a zoomed in version of the mass-edited H/C diagram. The four largest signals seen are always present due to contamination of the methanol. Other CHOS compounds are high in oxygen and sulfur, which could come from the presents of disulfide bridges, which add two sulfur atoms to a molecule in combination with the presence of organic sulfates and sulfites, which add sulfur and many oxygen atoms to compounds. Low H/C values of some compounds allow the assumption, that sulfates attached to aromates or thiophene rings might be present in the organic matter. The distribution of sulfur and oxygen in Fig. 20D shows that most compounds contain one sulfur atom, but compounds with up to eight sulfur compounds were also detected. Oxygen numbers are higher compared

to CHNO compounds with a maximum at four oxygen atoms. This could be another hint that organic sulfates might be present in the organic matter of Åheim olivine.

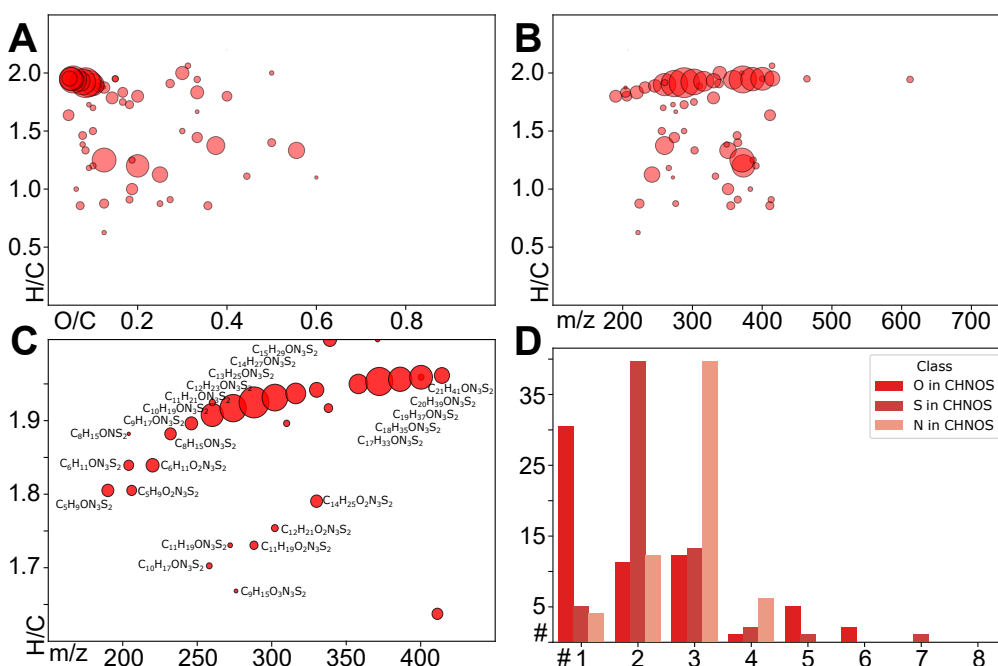


Figure 21: ESI(-) mode results for the CHNOS compounds of Åheim olivine. Size of bubbles represent intensity in the spectrum. **A** Van Krevelen diagram. **B** Mass-edited H/C diagram. **C** Zoomed-in area of the mass-edited H/C diagram with annotations. **D** Amounts of oxygen per compound, amounts of nitrogen per compound and amounts of sulfur per compound vs. amount of compounds.

CHNOS compounds in Åheim olivine organic matter are scarce, only 61 different chemical composition were found. Their average weighted H/C value is 1.67 and their average weighted O/C value is 0.16, so both values lie in between those of CHNO and CHOS compounds. The results of the CHNOS compounds are visualized in Fig. 21. The Van Krevelen diagram and the mass-edited H/C diagram show a diffuse spread of the CHNOS compounds with only one homologous series. The series is shown in Detail in Fig. 21C. The compounds of the series follow the structure of $C_xH_{2x-1}ON_3S_2$. Possible structures for such compounds are for example methyl

N-[(3-oxoindol-2-yl)amino]carbamodithioate or 5,8-bis(ethylsulfanyl)octanoyl azide, so structures with a diverse range of functional chemical groups. Only few compounds were detected in the area of amino acids. Fig. 21D shows that most compounds contain one oxygen atom, two sulfur atoms and three nitrogen atoms, but also variable numbers of heteroatoms were detected in CHNOS compounds.

A similar large group as CHO compounds are the CHOMg compounds in Åheim olivine. 480 different chemical structures from this compounds class were detected. Their average weighted H/C is 1.86 and their average weighted O/C value is 0.6, which is a lot higher than the O/C value of CHO compounds. In Fig. 22, the properties of CHOMg compounds are depicted. The Van Krevelen diagram in Fig. 22A shows, that the CHOMg compounds similar to CHO compounds demonstrate very structured homologous series. Due to the fact that CHOMg compounds have a calculated mass difference of MgO_2H_2 to CHO compounds, they naturally have higher O/C values compared to CHO compounds. Most CHOMg compound series follow the mass difference of CH_2 and are barely found in aromatic areas. They were assumed to mostly contain aliphatic hydrocarbon chains attached to a magnesium-oxygen head group, which is corroborated within Åheim olivine. A zoomed-in version of the Van Krevelen diagram can be seen in Fig. 22C. Similar to the CHO compounds, also the CHOMg compounds follow certain lines of mass differences. Horizontal lines are represented by the addition of oxygen, for example as seen at $\text{C}_{14}\text{H}_{26}\text{O}_3\text{Mg}$ and $\text{C}_{14}\text{H}_{26}\text{O}_4\text{Mg}$. Falling lines are represented by the loss of CH_2 , for example as seen by the homologous series of $\text{C}_{23}\text{H}_{42}\text{O}_5\text{Mg}$ going down to $\text{C}_{16}\text{H}_{28}\text{O}_5\text{Mg}$. Similar to CHO compounds, CHOMg compounds form close to flawless series. Fig. 22B shows the mass-edited H/C diagram, which shows that the mass range of CHOMg compounds lie in between 150 m/z and approximately 500 m/z . It can be seen that CHOMg also reach higher H/C values compared to CHO compounds, and most of them follow homologous series. A zoomed in version of this diagram can be seen in Fig. 22D. Notably, there are also compounds presents which

contain two magnesium atoms and not only one. This goes along with an additional intake on oxygen, as most of these compounds contain 7 or more oxygen atoms. Approximately 39% of the CHOMg compounds contain two magnesium ions. This is probably due to the fact that dicarboxylic acids formed magnesium head groups during shock and heat events. In the zoomed-in diagram, parallel lines are again containing alike structures with varying amount of oxygen or magnesium as this goes along with an increased m/z value. Falling lines from the left top to the bottom right are created by the mass difference of CH_2 and one oxygen, for example $\text{C}_{12}\text{H}_{22}\text{O}_4\text{Mg}$ going to $\text{C}_8\text{H}_{14}\text{O}_8\text{Mg}$. Lines from the left bottom to the right end signify the addition or loss of CH_2 , for example seen at $\text{C}_{10}\text{H}_{18}\text{O}_6\text{Mg}$ going to $\text{C}_{16}\text{H}_{30}\text{O}_6\text{Mg}$. Fig. 22E shows the distribution of oxygen atoms in CHOMg compounds with an H/C value of 2. The magnesium compounds start at a minimum of three oxygen atoms. As they are formed from CHO compounds by the formal addition of MgO_2H_2 , it explains this increase in oxygen. Most CHOMg compounds contain four and five oxygen. CHOMg compounds with four oxygen are probably carbon chain structures with one magnesium head group attached, while compounds with five oxygen atoms contain additional hydroxy groups or ether structures. Fig. 22F displays the number of oxygen in all CHOMg compounds. As similar progress was already seen in Fig. 18E, but shifted to the left by two oxygen atoms. The distribution of CHOMg compounds has a comparable shape to CHO compounds, which corroborates their chemical evolution out of CHO compounds. Most CHOMg compounds contain four to seven oxygen compounds, but also CHOMg compounds with 12 oxygen atoms were detected.

A total of 96 CHNOMg compounds were detected within the extract of Åheim olivine. Their average weighted O/C value is 0.32, which is a lot higher compared to CHNO compounds, and their average weighted H/C value is 1.62, which is near to the H/C value of CHNO compounds. The results depicted in Fig. 23. The CHNOMg compounds show two distinct areas of compounds, once at the region of $\text{H/C} = 2$ and once a series which

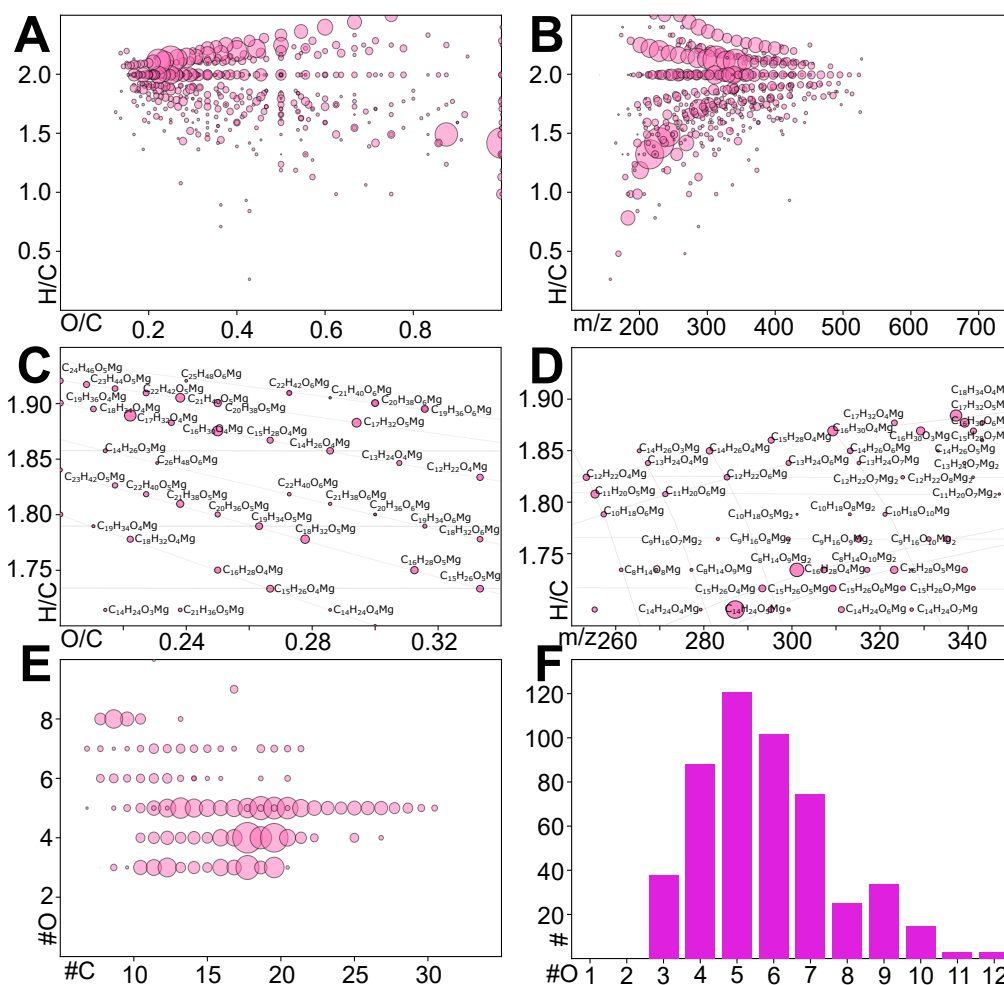


Figure 22: ESI(-) mode results for the CHOMg compounds of Åheim olivine. Size of bubbles represent intensity in the spectrum. **A** Van Krevelen diagram. **B** Mass-edited H/C diagram. **C** Zoomed-in area of the Van Krevelen diagram with annotations. Grey lines represent certain lines of mass differences. **D** Zoomed-in area of the mass-edited H/C diagram with annotations. Grey lines represent certain lines of mass differences. **E** Amount of carbon atoms vs. amount of oxygen atoms for H/C = 2. **F** Amounts of oxygen per compound vs. amount of compounds.

is evolving into a more unsaturated area of the Van Krevelen diagram (Fig. 23A). These two groups of compounds can also be observed in the mass-edited H/C diagram (Fig. 23B). The m/z values of CHNOMg compounds range from 200 m/z to approximately 450 m/z . In Fig. 23C, a zoomed-in version of the mass-edited H/C diagram can be seen. Besides some diffuse

compounds, a striking homologous series can be observed with the pattern of $C_xH_{x-10}N_2O_3Mg$, ranging from 11 to 25 carbon atoms. The chemical composition lets one assumed that a magnesium head group with nitrogen incorporation is a possible structure for these compounds. It is also feasible that CHNOMg compounds do not incorporate nitrogen on the magnesium head group, but contains aliphatic and aromatic amines or amide groups. Fig. 23D shows that most CHNOMg compounds contain two nitrogen, followed by one nitrogen, which was also seen at CHNO compounds. Oxygen amounts start at three, similar to CHOMg compounds, but show a quick decrease in amounts.

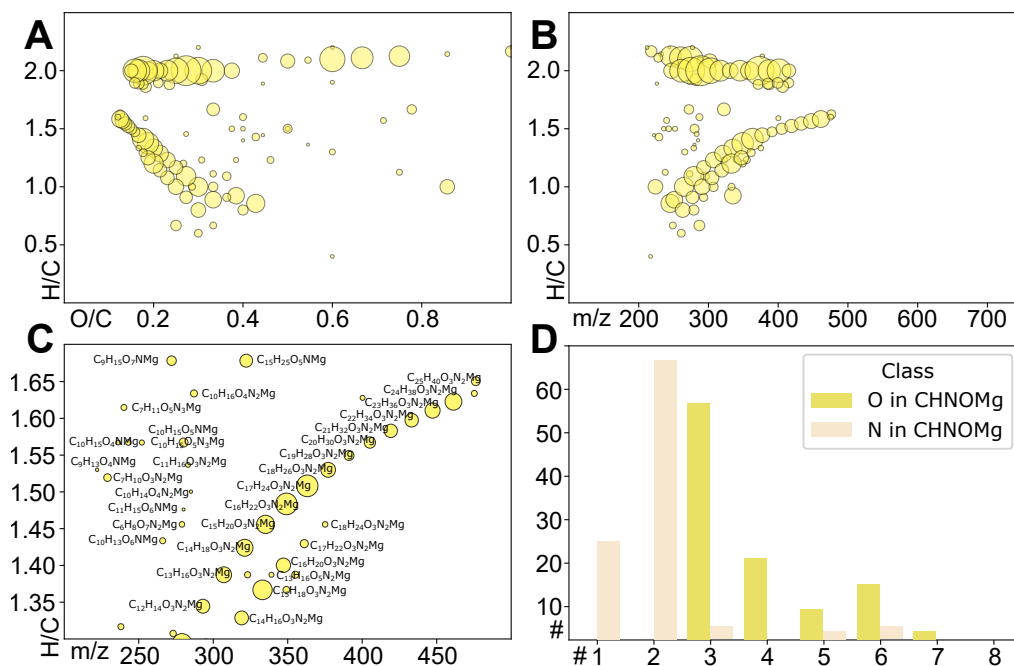


Figure 23: ESI(-) mode results for the CHNOMg compounds of Åheim olivine. Size of bubbles represent intensity in the spectrum. **A** Van Krevelen diagram. **B** Mass-edited H/C diagram. **C** Zoomed-in area of the mass-edited H/C diagram with annotations. **D** Amounts of oxygen per compound and amounts of nitrogen per compound vs. amount of compounds.

For CHOSMg compounds, a total of 93 different chemical structures were detected in Åheim olivine. Their average weighted O/C value is 0.76, which

is the highest O/C value of all compound classes, and their H/C value is 1.43, which is lowest H/C value of all compound classes. The results of CHOSMg compounds are depicted in Fig. 24. The Van Krevelen diagram shows a diffuse picture of CHOSMg, which spread over a wide range of H/C and O/C values (see. Fig. 24A). In the mass-edited H/C diagram of Fig. 24B, some series of CHOSMg compounds can be observed. Their m/z range goes from 200 m/z to 400 m/z with few exceptions. Fig.24C shows the zoomed-in version of the mass-edited H/C diagram, which shows the chemical compositions of the CHOSMg compounds. Some homologous series can be observed, but visibly most of the CHOSMg are not ordered or follow only a short homologous series. Furthermore, these are very spread out as the difference of an oxygen or sulfur results in a big mass shift over the diagram due to the mass of these atoms. Many compounds contain several sulfur and oxygen compounds. These are probably similar to CHOS compounds also organic sulfates or sulfites, and polysulfur structures such as disulfide bonds and thiol structures. Also very high amounts of oxygen can be observed, which go along with the presence of oxidized sulfur atoms. Figure 24D show that most CHOSMg compounds contain one sulfur atom with decreasing frequency at increasing amount of sulfur. Amounts of oxygen start at three oxygen with a maximum at six, while values around six are approximately equally distributed. Consequently, the most frequent CHOSMg structure should contain six oxygen atoms and one sulfur, which then is also probably the most stable structure.

The last and smallest compounds class are CHNOSMg compounds, as see in Fig. 25. 33 CHNOSMg compounds were detected in the extract of Åheim olivine, with an average weighted O/C value of 0.41 and an average weighted H/C value of 1.62 for this compounds class. The Van Krevelen diagram shows are very diffuse picture with most compounds at an H/C value of approximately two with some compounds having lower H/C values (Fig. 25A). The mass-edited H/C diagram shows one homologous series (see Fig. (Fig. 25B) which ranges from 50 m/z to 400 m/z . Only few compounds show higher m/z values than 400. In Fig. 25C, a zoomed-in version of the

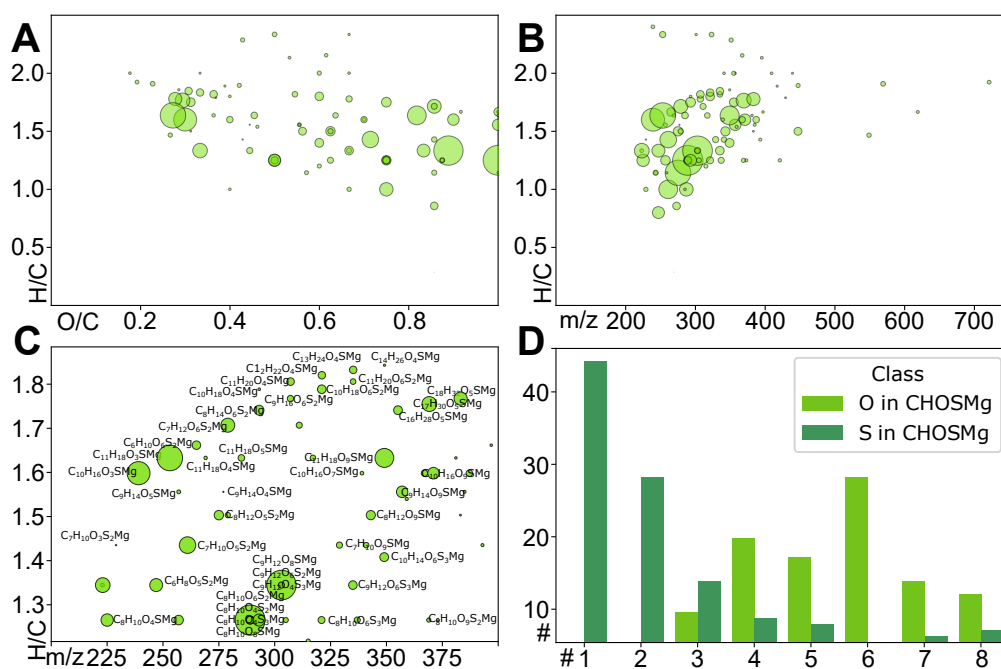


Figure 24: ESI(-) mode results for the CHOSMg compounds of Åheim olivine. Size of bubbles represent intensity in the spectrum. **A** Van Krevelen diagram. **B** Mass-edited H/C diagram. **C** Zoomed-in area of the mass-edited H/C diagram with annotations. **D** Amounts of oxygen per compound and amounts of sulfur per compound vs. amount of compounds.

mass-edited H/C diagram can be seen. The displayed homologous series with the chemical composition of $C_xH_{x+1}N_3O_3S_2Mg$ ranges from six to 14 carbon atoms. It is likely that this series evolved from the CHNOS compounds as their amount of nitrogen and sulfur is similar to the amount of the largest series of CHNOS compounds. Fig. 25D shows that most CHNOSMg compounds contain three oxygen atoms, which probably results from the addition of two oxygen atoms together with the magnesium atom. Most CHNOSMg compounds contain two or three nitrogen atoms and one or two sulfur atoms, which is slightly different from CHNOS compounds and shows that some chemical alteration took place between the transition from CHNOS compounds to CHNOSMg compounds.

The ESI (-) ionization mode enabled the detection and annotation of a broad variety of different compounds with different degrees of oxygenation,

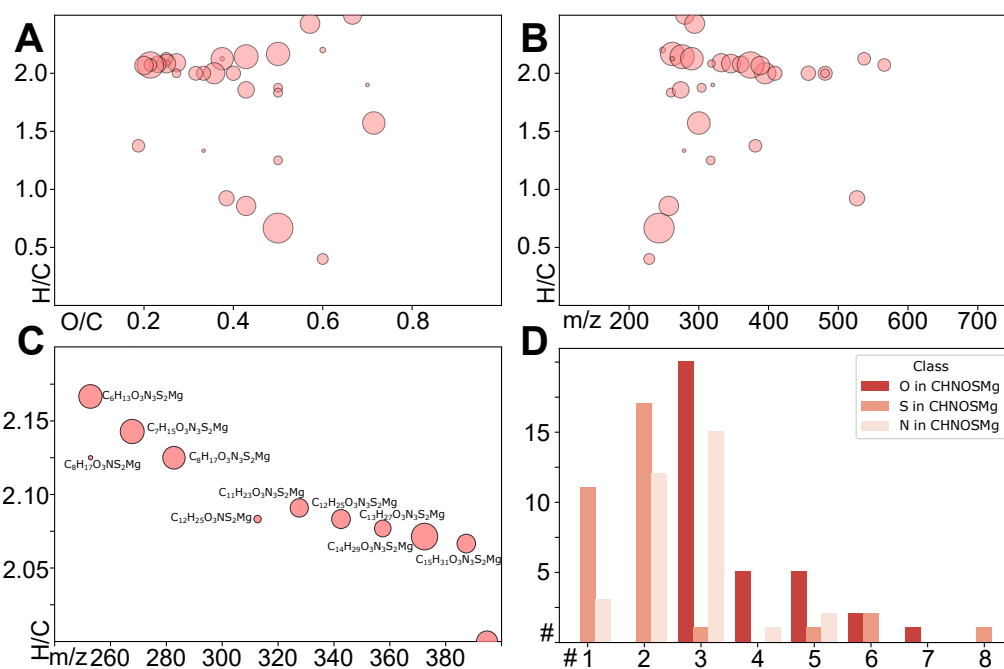


Figure 25: ESI(-) mode results for the CHNOSMg compounds of Åheim olivine. Size of bubbles represent intensity in the spectrum. **A** Van Krevelen diagram. **B** Mass-edited H/C diagram. **C** Zoomed-in area of the mass-edited H/C diagram with annotations. **D** Amounts of oxygen per compound, amounts of nitrogen per compound, and amounts of sulfur per compound vs. amount of compounds.

saturation, and incorporation of hetero- and metalatoms. This variety of organic compounds within mineral samples such as olivine was hitherto not described and analyzed in such depth. The presence of such a diversity of organic matter has implications for all geo-sciences and many questions arise from this newly discovered fact. It is now the task to find exact pathways of their emergence and factor which influence the formation, stability, alterations, and destruction of such compounds in mineral. Åheim olivine is one the first olivine samples which has been investigated and such depth, but by analyzing more olivine samples terrestrial and extraterrestrial origin, the knowledge about organic compounds in mineral will expand in the upcoming years.

3.2.5 Heated Åheim Olivine and CHOSMg Compounds

As previously described, Åheim olivine was heated to 200°C, 400°C, and 600°C degrees respectively. The mineral was heated outside its stability field, which causes alteration in surface mineralization and consequently also changes in organic cargo. The three temperatures and the non-heated olivine were analyzed with ESI (-) FT-ICR-MS in triplicates to analyze and describe the chemical evolution of the organic compounds within the olivine. The material and method part of this chapter describes the exact conditions for extraction and measurements of the olivines. The results of the measurements of all triplicates can be seen in Table 2. Given are numbers regarding amount compounds in each chemical class, percentages of elements within the samples according to the chemical classes, average weighted ratios for the whole sample and average weighted ratios for each chemical class respectively.

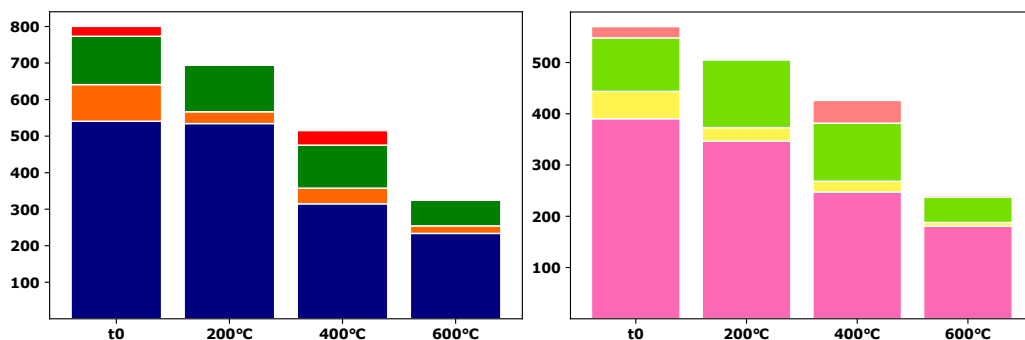


Figure 26: Average amounts of compound classes from the triplicate measurements of Åheim olivine. Left barplot: Lowest bar are CHO (blue), next are CHNO (orange), next are CHOS (green) and last are CHNOS (red). Right barplot: Lowest bar are CHOMg (magenta), next are CHNOMg (yellow), next are CHOSMg (light green) and last are CHNOSMg (light red).

The average amounts of the different chemical families are displayed in Fig. 26, where magnesium-containing are separated from non-magnesium-containing compound classes. The left barplots shows compounds which are not containing any magnesium atoms, so CHO, CHNO, CHOS and CHNOS compounds. It can be seen that the total amount of soluble organic compounds in olivine is reduced by heat. All four colored bars are less compared to the

Sample Name	OI t0 1	OI t0 2	OI t0 3	OI 200°C 1	OI 200°C 2	OI 200°C 3	OI 400°C 1	OI 400°C 2	OI 400°C 3	OI 600°C 1	OI 600°C 2	OI 600°C 3
Nr of CHO	683	576	363	692	440	471	326	334	284	228	226	247
Nr of CHOS	111	128	158	147	117	118	135	93	125	81	74	56
Nr of CHNO	166	43	92	26	31	40	47	49	33	19	13	30
Nr of CHNOS	62	6	13	1	1	0	75	9	35	0	0	5
Nr of CHOMg	543	341	287	303	373	363	205	240	297	193	164	185
Nr of CHOSMg	101	56	156	134	144	119	112	138	90	34	88	27
Nr of CHNOMg	98	29	33	8	20	52	12	26	25	7	4	11
Nr of CHNOSMg	34	5	27	0	0	7	71	8	54	2	2	6
Total number	1798	1184	1129	1311	1126	1170	983	897	943	564	571	567
Average H	0.592	0.586	0.604	0.597	0.614	0.607	0.588	0.557	0.569	0.59	0.604	0.602
Average C	0.318	0.325	0.318	0.321	0.317	0.321	0.325	0.314	0.316	0.313	0.323	0.32
Average O	0.074	0.073	0.059	0.068	0.059	0.059	0.066	0.104	0.091	0.081	0.06	0.065
Average N	0.004	0.001	0.007	0	0	0.001	0.003	0.002	0.003	0.002	0	0.002
Average S	0.004	0.01	0.006	0.009	0.004	0.006	0.011	0.009	0.011	0.006	0.008	0.006
Average Mg	0.008	0.006	0.006	0.005	0.006	0.005	0.008	0.014	0.01	0.009	0.005	0.007
HC Ratio	1.853	1.806	1.893	1.855	1.935	1.896	1.808	1.776	1.806	1.881	1.875	1.885
OC Ratio	0.321	0.323	0.297	0.263	0.216	0.212	0.275	0.255	0.242	0.442	0.238	0.298
CN Ratio	83.012	276.591	48.907	1208.965	876.895	380.206	127.675	156.488	114.069	133.454	754.71	165.597
CS Ratio	87.837	33.898	54.05	34.737	80.518	50.285	28.657	36.062	29.424	54.022	39.328	57.798
mz value	288.59	300.13	308.35	301.548	296.572	306.948	299.333	286.679	299.628	291.951	298.621	298.716
DBE	2.142	2.587	2.028	2.13	1.538	1.979	2.587	2.552	2.519	1.907	2.089	1.989
OC of CHO	0.182	0.146	0.139	0.145	0.127	0.128	0.127	0.128	0.127	0.129	0.124	0.123
OC of CHOMg	0.649	0.855	0.862	0.548	0.435	0.412	0.565	1.045	0.897	0.935	0.622	0.815
OC of CHOS	0.238	0.247	0.23	0.311	0.23	0.189	0.197	0.222	0.324	0.445	0.187	0.206
OC of CHOSMg	0.765	0.552	0.728	0.423	0.483	0.445	0.677	0.736	0.707	1.013	0.597	0.621
OC of CHNO	0.098	0.103	0.066	0.072	0.071	0.07	0.069	0.221	0.067	0.061	0.069	0.068
OC of CHNOMg	0.369	0.323	0.164	0.277	0.262	0.215	0.257	0.177	0.425	0.177	0.257	0.318
OC of CHNOS	0.158	1.079	0.637	0.364	0.176	0	0.473	0.541	0.938	0	0	0.085
OC of CHNOSMg	0.423	0.382	1.461	0	0	1.057	1.676	1.035	0.548	0.532	2.126	0.41
HC of CHO	1.91	1.928	1.927	1.906	1.942	1.942	1.954	1.91	1.947	1.948	1.98	1.951
HC of CHOMg	1.915	1.937	1.936	1.939	2.038	2.066	1.841	1.824	1.846	1.908	2.08	2.001
HC of CHOS	1.734	1.682	1.755	1.784	1.812	1.708	1.695	1.634	1.693	1.71	1.671	1.718
HC of CHOSMg	1.437	1.79	1.712	1.641	1.815	1.864	1.573	1.569	1.827	1.776	1.759	1.64
HC of CHNO	1.561	1.912	1.95	1.937	1.947	1.95	1.949	1.678	1.946	1.951	1.952	1.949
HC of CHNOMg	1.656	0.918	1.99	2.033	1.987	1.967	1.969	1.614	2.012	1.895	2.053	0.964
HC of CHNOS	1.666	2.113	2.047	1.455	1.706	0	1.619	1.419	1.994	0	0	0.763
HC of CHNOSMg	1.83	1.141	2.221	0	0	2.225	2.595	1.549	1.37	0.581	2.911	0.958

Table 2: Numbers and calculated averages of all triplicates from the ESI (-) measurements.

not-heated olivine. CHO compounds are the most abundant compounds in the organic matter of Åheim olivine. By heating the mineral to 200°C, the amount of CHO compounds is barely reduced. The relative amount is thus increased at this point. However, at 400°C, CHO compounds experience a drop in amount, and features even less CHO compounds in 600°C sample. However, their relative amount decreases strongly at 400°C as heteroatom containing compounds remain present and even increase in number. At 600°C the relative amount of CHO increases again, as heteroatom containing compounds are not withstanding the heat exposure and decrease in amount. Nitrogen containing compounds make up only a small share of the organic compounds in Åheim olivine. Compared to t0 olivine, their amount is reduced at 200°C, but increases again at 400°C. At 600°C, they are basically absent, only few compounds are left. A possible explanation is that nitrogen containing compounds are destroyed by increasing temperature, as for example aliphatic amines are thermolabile. At 400°C, CHNO and CHNOS compounds can increase because they released nitrogen from the disintegration at lower temperatures plus the energy, which is left during cooldown from 400°C allows the formation of new CHNO and CHNOS compounds by integrating nitrogen in oxygenated carbohydrate structures. At 600°C most nitrogen either has left the system by diffusion or reacted with the now also very reactive IOM and thus is removed from the system of soluble compounds. Sulfur containing CHOS compounds are very stable over a wide range of temperature. Their amount slowly decreases at lower temperatures, and show also reduced amount at 600°C compared to t0 olivine. However, their numbers are only slowly decaying with increasing temperature. Similar reactions of compounds without magnesium can be observed with their magnesium containing pendants. Looking at CHOMg compounds, they behave similar to CHO compounds. At 200°C, they are barely affected by increasing temperatures. A larger reduction can be seen at 400°C and even more reduced amounts of CHOMg compounds at 600°C. CHNOMg and CHNOSMg compounds also behave similar to CHNO and CHNOS compounds. At 200°C, their amounts is reduced compared to

t0, at 400°C, they can be again observed in the mass spectra. At 600°C, they basically completely disappear from the extract of Åheim olivine.

However, a quite unique behavior can be observed for CHOSMg compounds. Compared to t0 olivine, their amount increases with heat at 200°C and even more at 400°C, but ultimately also disappear at high temperatures outside of the stability field of the olivine. This observation is quite unique for the organic compounds of Åheim olivine, as all other compounds classes either show similar or strongly reduced numbers at increasing temperature. The CHOSMg compounds in mineral samples constitute a particular compound class which reacts different towards temperature incidents compared to all other compounds classes. Consequently, they will be further investigated within this work.

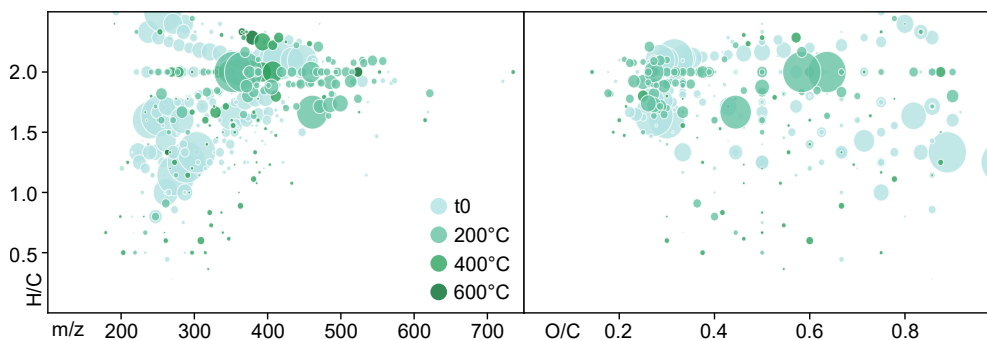


Figure 27: CHOSMg compounds of Åheim olivine. Van Krevelen diagram (left) and mass-edited H/C diagram (right) with differently colored bubbles. The color represents the temperature at which a compound appeared the first time. Bubble size represents the intensities in the spectra.

The number of CHOSMg compounds in Åheim olivine varies at different temperatures. Fig. 27 shows the different CHOSMg compounds of Åheim olivine and which CHOSMg compounds appeared first at different temperatures. The measured amount of CHOSMg compounds in the triplicates is 104 ($s = 50$) in t0 olivine, 132 ($s = 13$) in 200°C olivine, 113 ($s = 24$) in 400°C olivine, and 33 ($s = 33$) in 600°C olivine. For the triplicates, the O/C value is 0.68 ($s = 0.11$) for t0 olivine, 0.45 ($s = 0.03$) for 200°C olivine, 0.71 ($s = 0.03$) for 400°C olivine and 0.74 ($s = 0.23$) for 600°C olivine. The H/C value is 1.64

(s = 0.19) for t0 olivine, 1.77 (s = 0.12) for 200°C olivine, 1.66 (s = 0.15) for 400°C olivine and 1.72 (s = 0.07) for 600°C olivine for the triplicates. For t0 olivine, the average amount of oxygen per CHOSMg compound is 5.80 (s = 1.77) and the average amount of sulfur per CHOSMg compound is 2.16 (s = 1.61). For 200°C olivine, the average amount of oxygen is 5.91 (s = 1.33) and the average amount of sulfur is 1.61 (s = 0.90). For 400°C olivine, the average amount of oxygen is 6.07 (s = 2.49) and the average amount of sulfur is 2.21 (s = 1.36). For the highest temperature of 600°C, the average amount of oxygen is 6.79 (s = 2.58) and the average amount of sulfur is 1.73 (s = 0.93). Overall, the amount of CHOSMg compounds increases compared to t0 olivine, and only decreases at 600°C. The standard deviation of the amount of CHOSMg first drops at 200°C, but then continuously increases showing that heat causes a diffuse reaction of CHOSMg resulting in a wider range of amounts of chemical compositions of CHOSMg compounds. At 200°C, the most new CHOSMg species are formed. Over the temperature gradient, the average amount of oxygen steadily increases for CHOSMg compounds. The average oxygen amounts are passing 6 oxygen, which is the most stable form of CHOSMg compounds, and is reaching numbers below seven. The average amount of sulfur is moving between 2.21 and 1.61 for all of the temperatures. The most stable form of CHOSMg compounds is supposed to be a form with one sulfur atom, but higher amounts of sulfur atoms in other CHOSMg compounds moves this average to higher numbers. Overall, the CHOSMg compounds represent a class of compounds which is highly influenced by temperature incidents.

3.3 LC-MS Analysis

The strength of the analysis with LC-MS is its ability to give chromatographic information besides the information of time of flight (TOF) mass spectrometry. Compounds are not only described with a m/z value, but also with a retention time, which is specific for compounds in defined conditions regarding eluents and columns. Another big advantage is the automated tandem mass spectrometry (MS/MS) function which automatically fragmentates high m/z values to give structures information for these peaks. Besides these benefits, LC-MS with a TOF mass spectrometer lacks high-resolution and is not able to differentiate between for example CHO and CHOMg compounds as they have only small mass differences [88].

To optimize the output of LC-MS measurements, Åheim olivine was analyzed by two different methods. The first method used is a protocol especially used for metabolite screening with an apolar stationary phase and water and acetonitrile as eluents. The method has been developed to screen for small compounds with polar and apolar functional groups. A second method uses a protocol especially developed for lipidomics. With water, acetonitrile, and isopropanole as eluents, a run time of 25 minutes, and an apolar stationary phase, the method is able to separate lipid structures with variable carbon chains. Both methods combined were used in this work to give a structural insight into the organic compounds of olivines. In general, TOF-MS does not provide similar high-resolution as FT-ICR-MS. Thus compounds measured in TOF-MS are general higher in abundance in the olivines are a good representation over organic compounds found in the mineral.

3.3.1 Metabolite Method Results

Two olivine samples were measured and compared to two blank samples. The samples were measured in positive mode and in negative mode. In all four positive mode measurements, a total of 58309 mz -rt (m/z - retention time) pairs were counted. Of all of these, 5068 peaks were assigned with an adduct

and thus also with a neutral mass. 4845 m/z-rt pairs were assigned to $[M+H]^+$ adducts, 58 m/z-rt pairs were assigned to $[M+K]^+$ adducts, and 165 m/z-rt pairs were assigned to $[M+Na]^+$ adducts. A total of 1132 m/z-rt pairs were absent in blanks or had a three times higher intensity in the samples. By looking at the MS/2 level, a total of 607 m/z-rt pairs in sample 1 and 610 m/z-rt-pairs in sample 2 were fragmented. By checking all possible neutral mass differences, only specific ones were chosen for further evaluation. 180 interesting MS/MS spectra in sample 1 and 185 interesting MS/MS spectra in sample 2 were further considered. A total of 148 MS/MS spectra showed similar patterns, 110 MS/MS spectra were finally chosen to be further looked at.

For the negative mode, a total of 4933 m/z-rt pairs were detected. 733 of those were found to have an adduct. Most of these m/z-rt pairs (725) were assigned to $[M-H]^-$, a small amount of seven m/z-rt pairs were assigned to $[M+Cl]^-$ and once a $[M+HAc-H]^-$ adduct was found. A total of 329 m/z-rt pairs had 3x higher intensities in the samples than in the blanks or were completely absent in the blanks. At the MS/MS level, 115 and 114 different MS/MS spectra were found in both measurements. 14 of them were present in both samples.

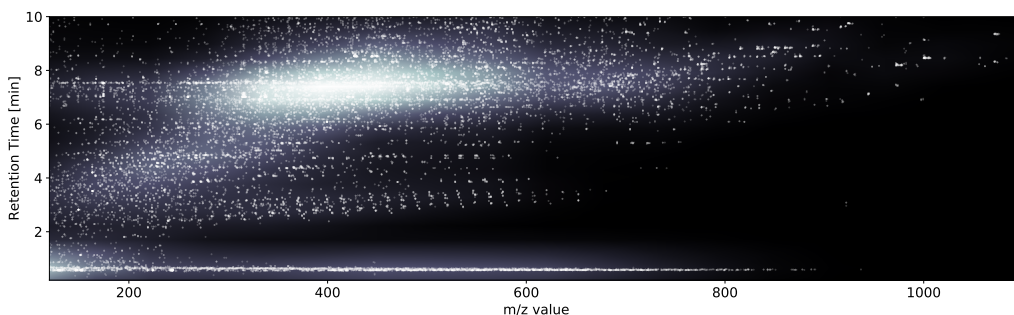


Figure 28: LC-MS chromatogram of Åheim olivine in (+)-ESI mode. White dots represent m/z-rt pairs(features). Background reflects the density of features in white.

Since an untargeted approach was used to describe the organics compounds of Åheim olivine, also the search of interesting mass differences was performed

in an untargeted manner. To search for interesting and unknown mass differences, every MS/MS spectrum was used to calculate all differences between the MS/MS peaks to the respective parent ion. These mass differences were then compared to all possible mass differences within a certain range of elements. By using this approach, the possibility to miss important mass differences by not knowing them in the beginning is excluded.

The most common mass differences were then further evaluated. The first common mass differences belonged to carbon chains, which show the characteristic loss of a CH_3 , followed by subsequent losses of CH_2 . These are possibly present as fatty acid structures, but can also be present as esters or ethers. 28,2% of all MS/MS spectra showed a loss of CH_3 . Losses of larger carbon chain fragments were also present in the samples. C_2H_5 were present in 26.4% of the samples, C_3H_7 in 22.7% and C_4H_9 in 20.0% of the samples [257]. The decrease of prevalence of larger carbon chain fragments is explained either due to less commonness in the compounds as well as the higher energy needed to fragment those structures. Overall, the loss of one of the mentioned carbon chain fragments was found in 43.6 % of all of the MS/MS spectra, making it the largest group of found mass losses. Approximately every second fragmented ion shows some kind of a mass loss typical for carbon chain, ester, or ether structures. Ester structures were also confirmed by the presence of $\text{C}_1\text{H}_4\text{O}_1$ and $\text{C}_2\text{H}_6\text{O}_1$ losses, which are typical for methyl and ethyl esters. The most common mass loss in all spectra is the loss of isobutene - C_4H_8 followed by the loss of H_2O . Isobutene loss is mostly occurring due to McLafferty rearrangement of carbon chains next to a carbonyl group such as aldehydes, ketones, carboxylic acids, amides, and esters [258]. Furthermore, it is possible to find Mc Lafferty rearrangements next to benzene structures [259]. The mass loss of water further corroborates the presence of hydroxyl- or carbonyl groups. Other losses found were acetone - $\text{C}_3\text{H}_6\text{O}_1$ which is a marker for ketone structures in the compounds, ethanol - $\text{C}_2\text{H}_6\text{O}_1$ which could derive from aldehydes, and formic acid - $\text{C}_1\text{H}_2\text{O}_2$. The mass differences of $\text{C}_2\text{H}_5\text{O}_1\text{N}_1$ and $\text{C}_2\text{H}_3\text{N}_1$ corroborate the presence of amide structures and thus nitrogen

in the organic compounds. Approximately 25% of the compounds showed mass losses containing nitrogen. Moreover, carbon monoxide and carbon dioxide were detected as present losses, which corroborate the presence of aldehyde/ketone and carboxylic acids respectively. However, basically no mass losses confirming sulfur in the compounds was detected. This could be either due to absence of sulfur containing compounds, but also due to impeded ionization of sulfur compounds in positive ESI mode. Overall, the organic compounds of Åheim olivine detected by this method show mostly carbon chain structures with carbonyl groups with contribution of nitrogen. This is in agreement with LC-MS results or FT-ICR results analyzing abiotic geological samples [141, 260].

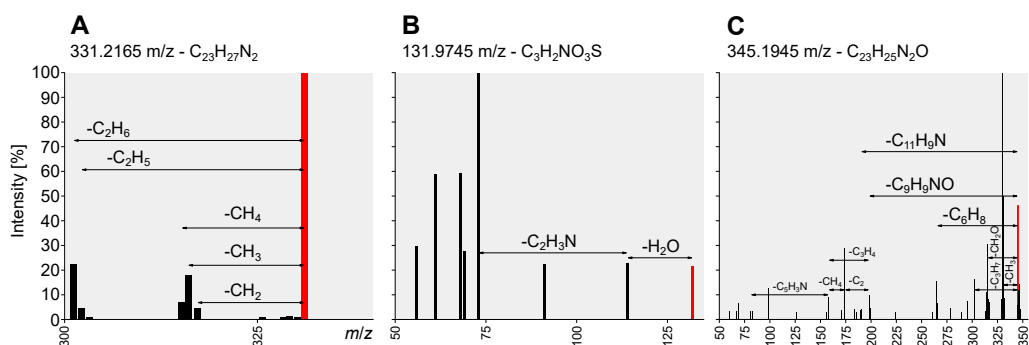


Figure 29: Exemplary MS/MS spectra from the positive mode metabolites measurements from Åheim olivine. Three masses and their fragmentation patterns with neutral mass losses are given. The precursor ion is marked in red, other peaks are depicted in black.

In Fig. 29, some examples of MS/MS spectra from the metabolites methods are given. Figure 29A shows the typical fragmentation pattern of aliphatic carbon chains which lose variable amounts of carbon and hydrogen during fragmentation. The also before mentioned peaks of C_1H_3 and C_2H_5 are present in the spectrum. The peak of 331.2165 m/z is putatively assigned to the chemical formula $C_{23}H_{27}N_2$, which could have a structure such as 1-[(Z)-Stilbene-4-yl]-3-hexyl-1H-imidazole-3-ium. Besides aromatic features, also aliphatic carbon chains are present which show characteristic MS/MS fragments as seen in Figure 29A. In 29B, the peak of 131.9745 m/z showed a

mass loss of water which indicates the presence of carboxylic acids, aldehydes or esters. The subsequent neutral loss of $C_2H_3N_1$ is a typical loss for nitrile groups. In 29C, a more complex MS/MS spectrum is depicted. The mass of 345.1945 m/z is assigned to the chemical formula $C_{23}H_{25}N_2O$. The neutral losses of C_1H_3 , C_3H_7 , and C_6H_8 indicate the presence of an aliphatic carbon chain in the structure. Moreover, two large neutral losses were observed in the MS/MS spectrum. The loss of $C_{11}H_9N$ is present. A possible neutral loss would be a sort of 2-Phenylpyridine or 2-Vinylquinoline. The presence of benzene rings is also likely due to the H/C value of 1.1 for the suggested chemical composition, which would be a highly aromatic one. The neutral loss of C_9H_9NO could structurally be seen as the loss of cinnamic acid amide. A possible fragmentation pathway is the cleavage in alpha position of the amide. Subsequent losses to these neutral losses are C_3H_4 which could be propene. The neutral loss of C_5H_3N could be a loss of 3,4-Didehydropyridine. Overall the chemical structure of the mass 345.1945 m/z shows a variety of features and represents the diversity of chemical compounds which are present in olivine samples.

In negative mode, the MS/MS spectra were mostly empty not showing many mass differences of interest. The most common mass difference found in the spectra was the mass difference of SO_2 , which is only observed in negative mode coming from sulfonic acids and sulfonates. Moreover, the typical mass differences of H_2O , CO , CO_2 , and CH_2O were detected. Overall the olivine samples did not show many fragmented m/z -rt pairs and thus an evaluation is difficult. The compounds present in the mineral samples are likely more ionizable in positive mode with the applied LC-MS method. In contrast to nitrogen containing compounds, organic species containing sulfur are readily ionized in negative mode which also explains the higher abundance of fragments coming from organic sulfur species.

3.3.2 Lipid Method Results

Similar to the metabolites method, two olivine samples were measured in positive and negative and compared to two blank samples. In all 4 measurements, a total of 87110 m/z-rt pairs were counted. A total of 18419 peaks were assigned with an adduct and thus neutral masses for these adducts were given. 17820 m/z-rt pairs were assigned to $[M+H]^+$ adducts, 209 m/z-rt pairs were assigned to $[M+K]^+$ adducts, and 390 m/z-rt pairs were assigned to $[M+Na]^+$ adducts. A total of 5276 m/z-rt pairs were absent in blanks or had a three times higher intensity in the olivine samples. At the MS/MS level, a total of 1266 m/z-rt pairs in sample 1 and 1285 m/z-rt-pairs in sample 2 were fragmented. By checking all mass differences, only specific ones for lipids positive mode were chosen. Within the two measurements, a total of 537 MS/MS spectra showed similar patterns and 174 MS/MS spectra were finally chosen to be further looked at.

For the negative mode, 1771 m/z-rt pairs were found in the spectra. 281 adducts were assigned, all of them as $[M-H]^-$ adducts besides one, which was found as a $[M+Cl]^-$ adduct. 130 of these m/z-rt pairs were 3x higher in intensities of absent in the blanks. The MS/MS level showed but five MS/MS spectra in both samples.

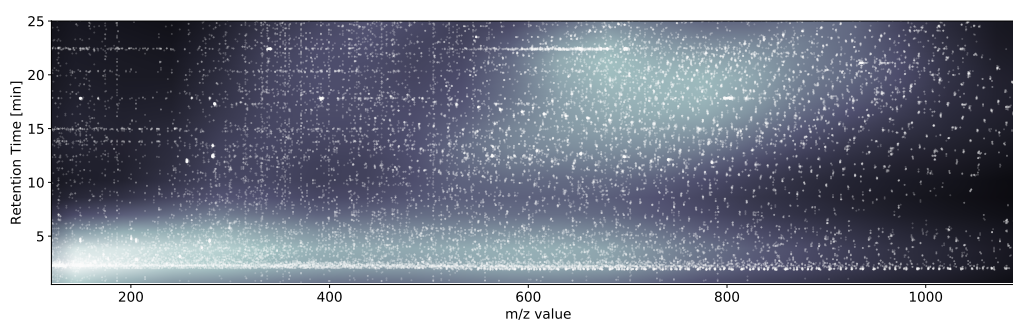


Figure 30: LC-MS chromatogram of Åheim olivine with the lipid method in (+)-ESI mode. White dots represent m/z-rt pairs(features). Background reflects the density of features in white.

The most common mass difference in the lipids positive mode is reduction

seen as a loss of H₂. This is a typical reaction for carbon chains as found in fatty acids in ESI positive mode fragmentation [261]. A similar frequent neutral loss is the loss of NH₃, which is observed in the presence of aliphatic amines and oximes. Similar to the metabolites method, also many neutral losses in connection with aliphatic carbon chains were detected such as C₁H₃, C₂H₅, and C₃H₇ were detected in large amounts. Also the mass loss of C₄H₈, which is the most abundant neutral loss from the metabolites method, was detected. Furthermore, Isobutanol (C₄H₁₀O), Propen (C₃H₆), Butanolate (C₄H₉O), Ethan (C₂H₆), and Ethen (C₂H₄) mass losses were detected. Besides the loss of H₂O and CO₂, also the mass loss of CH₄ was detected, which is a sign of the conversion from Isopropene to Ethene. Moreover, the neutral loss of methanesulfinic acid (CH₄O₂S) and of H₂S were detected as sign of the presence of sulfur containing organic compounds. Other mass differences and in different amounts were detected by the lipids positive method, which shows, that both metabolites and lipids methods are complementary to each other and reveal a broad set of compounds in the olivines samples.

Some MS/MS spectra from the lipids method were chosen to visualize the fragmentation of the compounds (see Fig. 31). In Fig. 31A, the fragmentation mass 209.1550 m/z is shown, which is annotated to C₁₂H₂₁HO. The loss of water is probably coming from a carboxylic acid or alcohol group, the mass losses of CH₂ and CH₄ are probably resulting from a carbon chain fragmentation. The pattern let's one suggest that this compounds probably has a fatty acid like structure, which is branched or unsaturated. A similar pattern is seen in Fig. 31B, where C₄H₈ losses are frequent as well as H₂O, which suggest the presence of carboxylic acid, and CH₂O₂, which is a know mass loss of alpha hydroxy acids. A possible structure could contain a carboxylic acid group with one or two hydroxy groups attached to a long carbon chain. Fig. 31C shows a even larger compound at mass 427.3801 m/z which is putatively annotated as C₂₆H₅₁O₄. Interestingly, the neutral loss of C₈H₁₆ with subsequent loss of H₂O is observed two times, which could suggest the presence of two similar chemical structures attached to a fatty

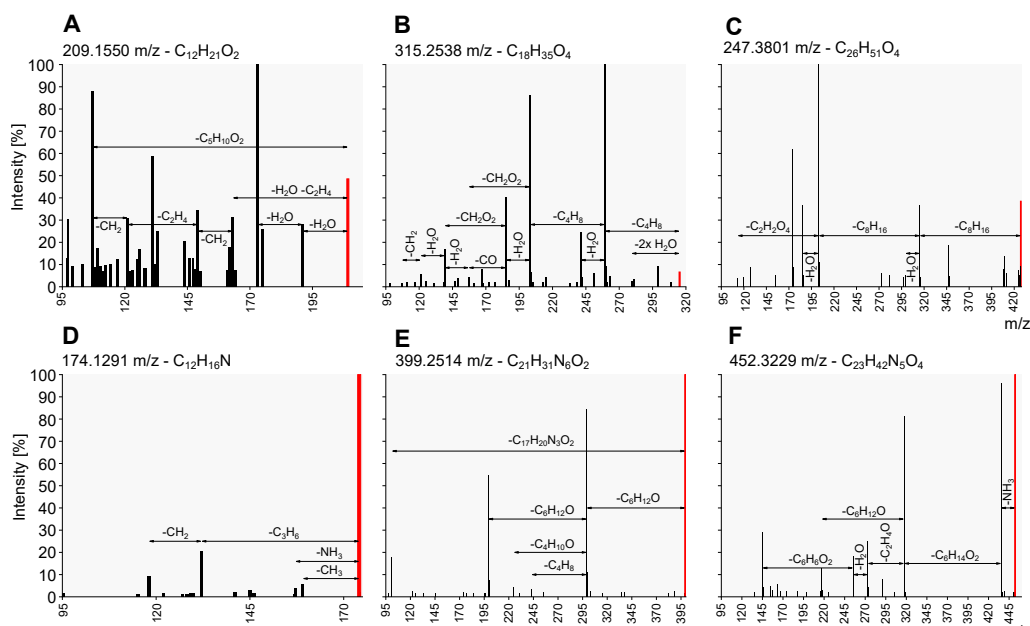


Figure 31: Exemplary MS/MS spectra from the positive mode lipids measurements from Åheim olivine. Six masses and their fragmentation patterns with neutral mass losses are given. The precursor ion is marked in red, other peaks are depicted in black.

acid chain body. In Figure Fig. 31D, a rather small nitrogen compound has been analyzed. The loss of NH_3 , which is often observed in amino acid analysis, suggests the presence of aliphatic nitrogen compounds. Besides, also aliphatic carbon chains are suggested to be present. In Fig. 31E, a similar thing to Fig. 31C can be observed. The feature of 399.2514 m/z has a putatively assigned chemical composition of $\text{C}_{21}\text{H}_{31}\text{N}_6\text{O}_2$. Here, the neutral loss of $\text{C}_6\text{H}_{12}\text{O}$ can be observed two times with very high intensities. Two similar structures, supposedly Capronaldehyde, are attached to this molecule, probably as amides due to the high number of nitrogen in this compound. The last analyzed MS/MS spectrum (Fig.31F) contains probably an aliphatic amine due to the high intensity of a signal after the neutral loss of NH_3 . From that peak, several other neutral losses can be observed, mostly alcohol, carboxylic acids or aldehyde losses. The remaining nitrogen atoms are probably incorporated into a aromatic structure as no other neutral loss containing nitrogen were observed in the MS/MS spectrum. Overall, the

lipids methods revealed a broad variety of different chemical structures in the organic matter of Åheim olivine. Especially carbon chains and nitrogen containing compounds are readily analyzed with the lipids method in positive mode.

In lipids negative mode, basically no usefull ms/ms spectra were generated. Most of the compounds detected were contamination from the methanol and preprocessing steps. The organic compounds in Åheim olivine are supposedly hampered in ESI negative ionization and thus do not show good intensities compared to positive mode. A further evaluation of the lipids negative mode was not performed.

3.3.3 Discussion of the LC-MS Results

LC-MS is a suitable method to detect and analyze the broad variety of organic compounds which can be found in olivine mineral. The here presented methods revealed a large amount of versatile compounds with different fragmentation patterns, retention times and m/z values. The liquid chromatography separation allows a refined analysis of the organic compounds and - in combination with MS/MS fragmentation - revealed many details over their underlying chemical structures.

The LC-MS method is able to analyze the SOM of olivine mineral, in this case the Åheim olivine. The detection of a broad variety of chemical structures from various chemical compounds classes is indicating towards the theory that olivine harbors carbon containing compounds. This fact was hitherto not properly investigated. Further, the organic matter can be assumed to contain aliphatic structures, various functional groups in different oxidation states, and also heteroatoms to a certain amount. To sum up, this discovery implies that geological samples have to be investigated with different analytical techniques to not only describe mineral features, but also to report the complex and diverse chemistry within the mineral.

The fact that carbon in different oxidation states can be readily detected in olivine changes given facts about the carbon cycle of our planet. If only

trace amounts of carbon is stored in olivine, the pure mass of terrestrial olivine would contain more carbon than all living creatures combined. Also, the organic signature can be analyzed and further used for classification of mineral samples regarding their origin and their temperature history on earth and also in space.

However in this work, only standardized methods were used to investigate the SOM of Åheim olivine. As NOM is a special kind of organic compound mixture, the amelioration of the LC and the MS parameters and settings could possibly reveal an even larger amount of compounds to ultimately unravel more of the exact chemical structures behind NOM in olivine. The here presented compounds are just exemplary for the broad variety which is yet to discover. With column settings, choice of solvent, gradients and refined detection parameters, it is to be expected that olivine contains even more compounds which are hitherto undiscovered. Furthermore, many compounds are insoluble, so the here presented results can just speak for the SOM, which is directly measurable in this LC-MS approach. Consequently it can be said that LC-MS is a viable method to investigate the SOM of a broad variety of mineral samples, and, with more refined and adapted methods, the yield of qualitative and quantitative data can be improved by a lot.

Future research should follow the line of these experiments to develop methods especially created to evaluate the soluble organic matter in an untargeted manner, but the probability of targeted analysis could be given as well after refined analysis has been performed. Methods have to be validated and tested on many different olivine samples to obtain a reliable data set on organic compounds in olivine. Furthermore, metabolomic data bases could be used to evaluate the possible structures of compounds on MS and MS/2 level to shed light on the chemical complexity and diversity of organic compounds in olivine.

3.4 NMR Analysis

3.4.1 NMR Spectrum of Åheim Olivine

The ^1H NMR spectrum of unheated Åheim olivine shows a broad variety of organic compounds in different regions of the spectrum which represents different chemical structures within the mineral (see Fig. 32). The integrals of the NMR spectrum were normalized to 100 %. From high to low field (from right to left), the first dominant signals can be found at $\delta_{\text{H}} \sim 0.72$ ppm - 0.97 ppm. Signals in this area indicate the presence of abundant ethyl groups ($-\text{C}-\text{CH}_2-\text{CH}_3$) as well as less abundant $-\text{C}-\text{C}(\text{C})\text{H}-\text{CH}_3$ units. With 13 % of all integrals, this represents a large class of protons in the organic matter within the olivine. At $\delta_{\text{H}} \sim 1.05$ ppm - 1.13 ppm methyl groups within aliphatic chains ($-\text{C}-(\text{HC}-\text{CH}_3)-\text{CH}$) show a small abundance of 2.4 % of all organic compounds. The largest group of proton signals is coming from methylene groups or other pure aliphatics with sp^3 hybridized carbon ($\text{R}-\text{CH}_2$) at $\delta_{\text{H}} \sim 1.14$ ppm - 1.44 ppm. 44.9 % of all signals in the organic matter of Åheim olivine derive from this chemical structure. Alicyclic rings with or without attached methyl groups can be seen between $\delta_{\text{H}} \sim 1.4$ ppm and 1.7 ppm. With 8.1% these chemical structures are fairly abundant. Acetate derivatives ($\text{H}_3\text{C}-\text{C}(=\text{O})-\text{O}-$) are seen as three separated groups between $\delta_{\text{H}} \sim 2.0$ ppm and 2.4 ppm. They make up 5.7 % of the extracted organic matter. The following signals from $\delta_{\text{H}} \sim 3.2$ ppm and 4.8 ppm belong to different units, namely carbohydrates, alcohols, esters, ethers, and others. In this region, the solvent MeOD and its contamination MeOH show intense peaks between $\delta_{\text{H}} \sim 3.2$ ppm and 3.45 ppm. This area was left out due to the solvent. However, the proton peaks around still accounted for 23.7 % of all compounds. Between $\delta_{\text{H}} \sim 5$ ppm and 7.8 ppm, only 1.6% of all signals were detected. This area shows olefinic protons as well as aromatic protons. Above 8 ppm, carboxylic acid peaks can be observed, but were left out for evaluation as they usually belong to contamination.

The results of the ^1H NMR spectrum of Åheim olivine corroborates the

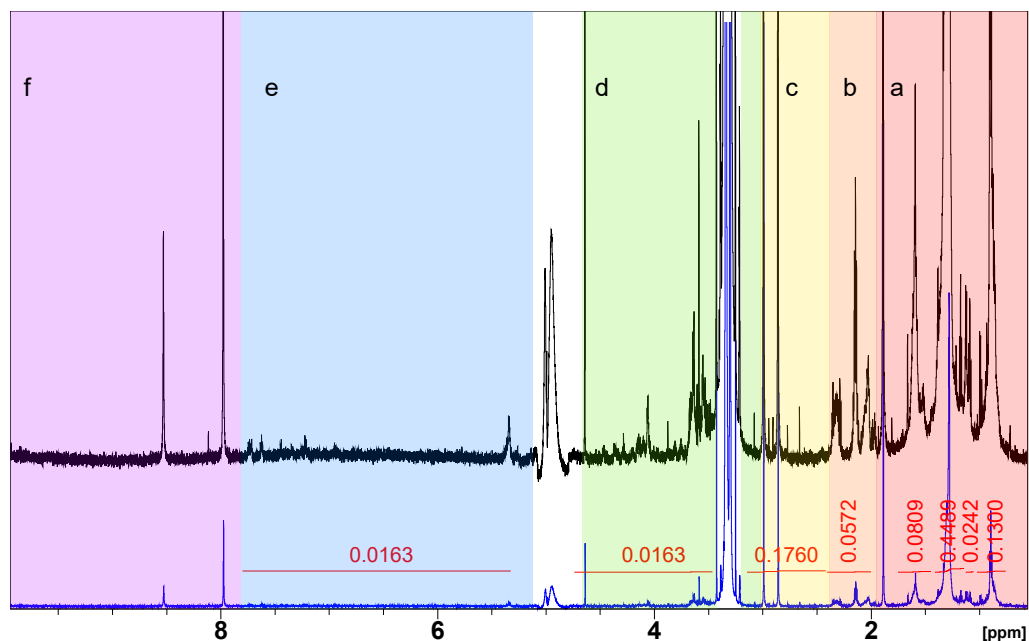


Figure 32: ^1H NMR spectrum of Åheim olivine. The blue spectrum serves as an overview while the black spectrum is a zoomed-in version. Red numbers represent the size of the integrals normalized to 100%. Colored areas represent (a) aliphatics, (b) acetate analogues, (c) carbonyl-rich alicyclic materials, (d) carbohydrate-like and methoxy, (e) olefinic and aromatic, and (f) carboxyl acids.

results as already seen in FT-ICR-MS and LC-MS. A large proportion of the SOM of the olivine mineral belongs to aliphatic structures with different degrees of saturation and branching within the compounds. Organic structures largely consist of hydrocarbon chains with contribution of heteroatoms. The majority of the hydrogen atoms belong to methyl groups or branched aliphatics, which was also seen in the fragmentation pattern of the LC-MS fragmentation results. Also FT-ICR-MS showed mostly aliphatic structures with only minimal content of aromatic compounds, similar to the ^1H NMR spectrum. The abundance of different compounds classes as seen in the ^1H NMR spectrum was similar to the MS/MS fragmentation patterns as the distribution of the organic compounds in the Van Krevelen Diagram. Consequently, ^1H NMR spectroscopy sheds more light on the organic compounds of Åheim

olivine and furthermore allows a more distinct description of the underlying organic structures.

2D NMR techniques enable a refined analysis of the underlying molecules because they reveal couplings and inter connectivity between protons in a molecule. For the 200°C Åheim olivine, a TOCSY and a J-resolved Spectroscopy (JRES) 2D NMR spectrum were acquired. Parts of the spectra can be seen in Fig. 33. In panel A, the aliphatic protons up to 2.4 ppm can be observed in this JRES spectrum. JRES allows to observe the couplings of protons. Triplets can be seen as three equidistant signals in the areas of A1 and A3 while doublets are visualized as two equidistant signals in the area of A2. Fig. 33 Aa shows the proton attached to carbonyl groups, for example COOH groups. Panel Ab shows a broad signal, which belongs to formic acid. Panel Ac and Ad represent signals from proton further away from a carbonyl group. Besides singlets, doublets and triplets, also couplings can be observed which cause even more differentiated patterns. Panel Ae mostly shows the triplet as observed by a methyl group next to a CH₂ unit.

Fig. 33B shows the aliphatic region of a TOCSY spectrum. The signals show a large range of different proton signals. Signal 1 is a methyl group attached to a carbon hydrogen chain, which can be more or less branched. However, signal 1 is at the end of this possible chain. Signal 2,3,4, and 5 represent signals with in the carbon chain and shows interactions between the different protons from the main molecule body and its branches. Signal 6,7,8, and 9 are signals resulting from an α carbon proton and its coupling with nearby protons from the main chain or the branches. However, these couplings are differently shielded compared to protons at the end of a carbon hydrogen chain.

Fig. 33C represents a TOCSY spectrum of the aromatic protons in Åheim olivine. However their amount is scarce, some signals can be observed. Fig. 33 C1 shows the signals from para substituted aromatic structures. Their abundance compared to aliphatic features is relatively scarce. Also mono- and ortho-substituted aromatic structures are sparse in the organic matter of

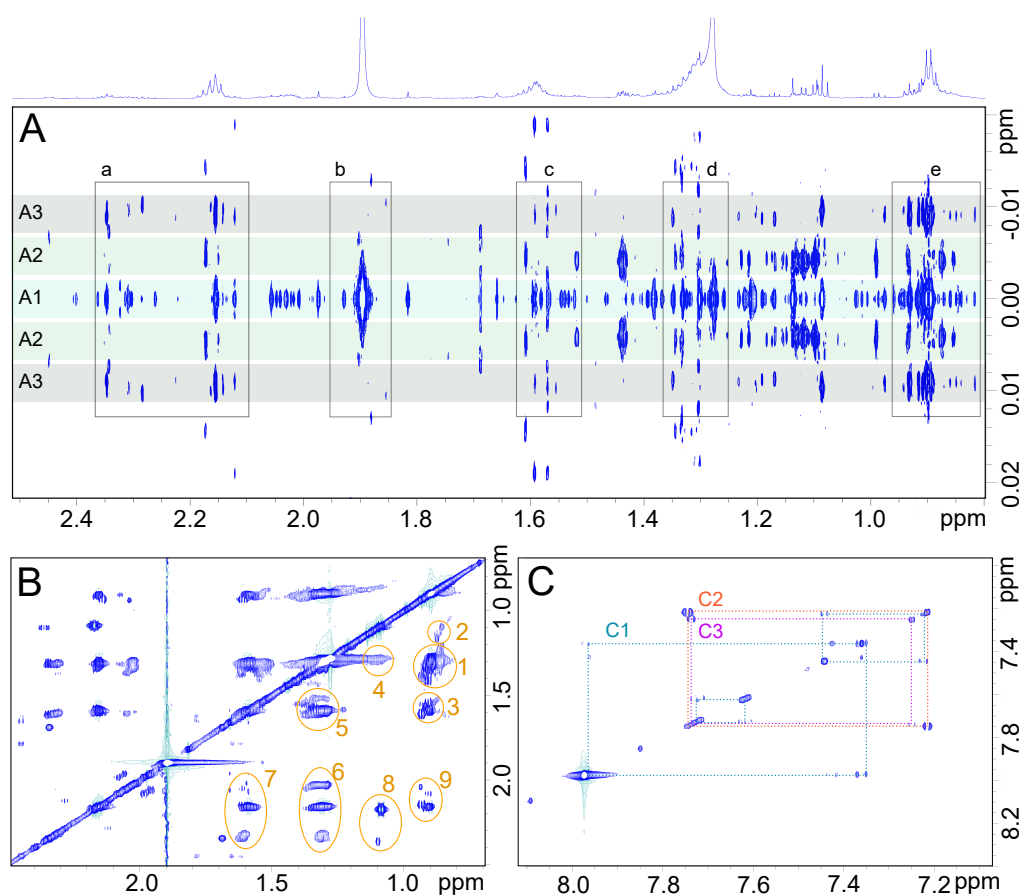


Figure 33: **A** JRES NMR spectrum. A1: $\text{CH}_3\text{-CH}_2/\alpha\text{-C}$, A2: $\text{CH}_3\text{-CH-C}$, A3: $\text{CH}_3\text{-CH}_2\text{-C}$, a: α carbon protons, b: formic acid, c: β carbon protons, d: γ,δ,ϵ carbon protons, e: CH_3 protons; **B** $^1\text{H},^1\text{H}$ TOCSY NMR spectrum. Aliphatic protons are marked with numbers. 1: $^3\text{J } \zeta\text{CH}_3 \zeta\text{H}$, 2: $^3\text{J } \epsilon\text{CH}_3 \epsilon\text{H}$ and $^5\text{J } \zeta\text{CH}_3 \epsilon\text{CH}_3$, 3: $^3\text{J } \beta\text{H } \gamma\text{CH}_3$, 4: $^3\text{J } \epsilon\text{H } \delta\text{CH}_3$ and $^4\text{J } \epsilon\text{CH}_3 \delta\text{H}$, 5: $^4\text{J } \gamma\text{H } \beta\text{CH}_3$, 6: $^4\text{J } \gamma\text{H } \alpha\text{H}$, 7: $^3\text{J } \alpha\text{H } \beta\text{H}$, 8: $^3\text{J } \alpha\text{H } \delta\text{H}$, 9: $^4\text{J } \alpha\text{H } \beta\text{CH}_3$; **C** $^1\text{H},^1\text{H}$ TOCSY NMR spectrum with aromatic protons. C1: para-substituted aromatic system (e.g. Terephthalic acid), C2: ortho-substituted aromatic system (e.g. Phthalic acid), C3: mono-substituted aromatic system (e.g. Benzoic acid).

Åheim olivine. These results were already shown by FT-ICR-MS and thus confirmed by NMR.

While the application of 2D NMR techniques is only shown in a concise manner for this work, the application possibilities, especially in targeted approaches and chemical structure elucidation is immense. For targeted approaches, 2D NMR techniques can give an overview over abundant chemical

couplings and may allow to assume chemical properties of the analyzed sample. However, the possibilities are limited as many signals are overlaying each other and a precise analysis of compounds groups or even single compounds is hampered. To improve the possibilities in this area, a pre-processing methode such as preparative HPLC would be beneficial to separate compounds classes from each other in order to achieve more precise results over specific chemical compound groups in the NOM sample.

3.4.2 NMR Spectra of Heated Olivine

Similar to FT-ICR-MS and scanning electron microcopy (SEM), also the heated Åheim olivine samples were measured with ^1H NMR spectroscopy. The extraction is described in the material and methods chapter of this section. All four different olivine samples were measured similarly to ensure comparability. For most of the signals, no difference could be observed within the samples. However, some of regions showed significant differences in signal intensity as well as in integral area. In Fig. 34, some areas with different peak intensities are depicted. Fig. 34A shows the abundance of CH_3 groups. The unheated t0 olivine has the highest intensity in this group, which decreases with heat. Also the integral has a high value compared to the other temperatures.

Region	t0	200°C	400°C	600°C
0.80 - 1.00 ppm	0.1286	0.1045	0.1163	0.1131
1.00 - 1.15 ppm	0.0306	0.0324	0.0262	0.0344
1.20 - 1.45 ppm	0.4574	0.2897	0.4689	0.3519
1.50 - 1.70 ppm	0.0765	0.0623	0.0939	0.0637
1.90 - 2.37 ppm	0.0641	0.0639	0.1233	0.0685
2.40 - 3.10 ppm	0.1786	0.3439	0.0410	0.2900
3.46 - 4.75 ppm	0.0549	0.0543	0.0759	0.0597
5.12 - 7.91 ppm	0.0093	0.0489	0.0544	0.0187

Table 3: Integrals of eight distinct regions normalized to 100%. Share of the integral to 100% is given for t0, 200°C, 400°C and 600°C olivine.

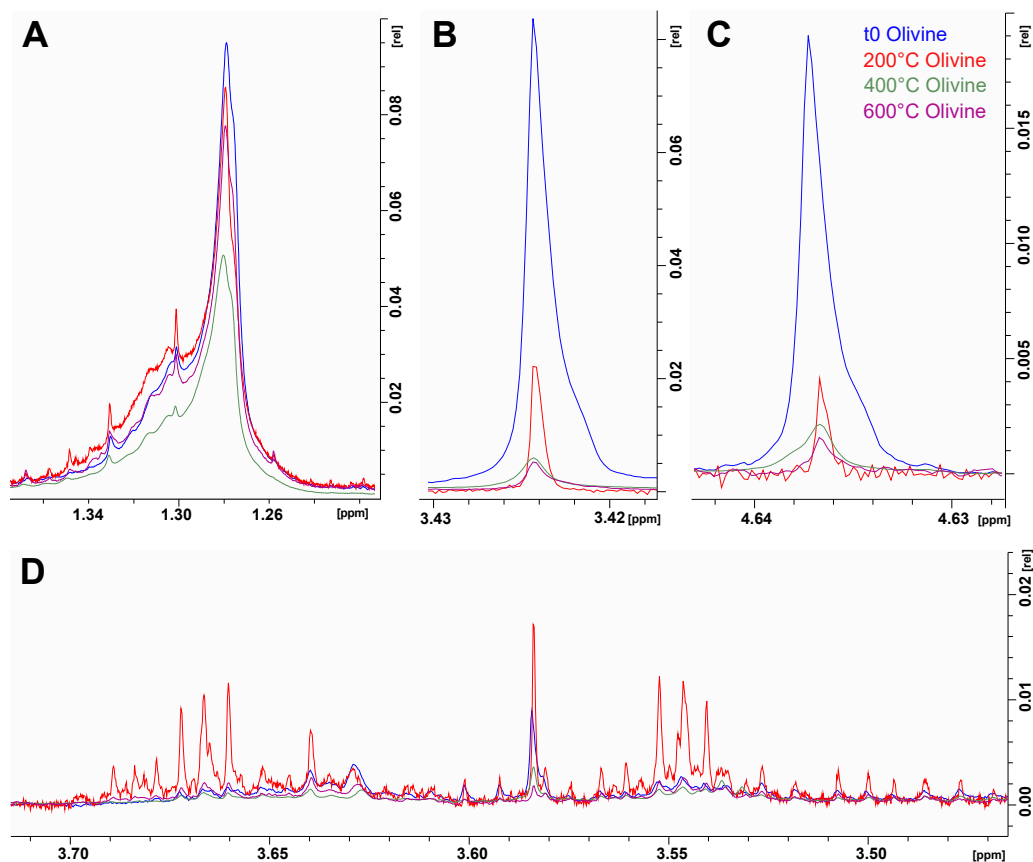


Figure 34: Comparison of ^1H spectra of t0 olivine (blue), 200°C olivine (red), 400°C olivine (green) and 600°C olivine (purple). Four panels represent different areas of the spectra between **A** 1.22 and 1.36 ppm, between **B** 3.42 and 3.43 ppm, between **C** 4.63 and 4.64 ppm and between **D** 3.45 and 3.70 ppm.

Two examples at 3.424 ppm (Fig. 34B) and at 4.636 ppm (Fig. 34C) show, that the effect of temperature exposure can be even more drastic, as peaks in the heated samples nearly disappeared compared to the t0 olivine. In this region, mostly protons of carbohydrates, alcohols, esters, and ethers generate signals. An opposite trend can be observed in Fig. 34D. In this region, especially the signals of the 200°C spectrum are higher and more distinct compared to other temperatures. By looking at Table 3, the ratios of the different integrals at different temperatures can be seen. The first to regions between 0.80 ppm and 1 ppm as well as between 1.00 ppm and 1.15 ppm shows

highest numbers in t0 olivine and decreases with higher temperature. Region three (1.20 ppm to 1.45 ppm), region four (1.50 ppm to 1.70 ppm), and region six (2.40 ppm to 3.10 ppm) show no real trend in the data, the ratio of the integral is ambiguous. However, the trend of the last three regions, region five, seven, and eight, shows that the integral increases until 400°C and then drops in amount at 600°C. A similar trend for some compounds could be observed in the FT-ICR-MS data, where some compounds classes showed an increase in numbers at 400°C, whereas 600°C depleted those organic compounds. Consequently, also NMR can provide information regarding the evaluation of organic compounds in olivine samples. Furthermore, temperature differences could be observed within the data showing that the organic molecules in olivine are sensitive to temperature alteration and that this alteration can be measured and qualitatively evaluated by NMR spectroscopy.

3.4.3 Discussion of the NMR Results

Both ^1H NMR and 2D NMR techniques have been shown to be suitable methods for analyzing the organic matter embodied in olivine mineral. In this untargeted approach, NMR spectroscopy revealed a variety of organic compounds and also allowed to make assumptions regarding their chemical structure. Especially 2D NMR methods such as TOCSY and JRES spectra allowed to see couplings between hydrogen atoms and thus revealed possible chemical connections of organic matter found in olivine. Furthermore, the comparison of differently heated olivines showed that organic compounds are susceptible for heating incidents and changes in chemical functionality can be observed. Ultimately, also meteorite extracts can be suspect to NMR spectroscopy [148]. Solely or in combination with other high-resolution techniques, the analysis of NOM and the identification of organic compounds in the pool of molecules in NOM and DOM is highly improved by the use of NMR.

In the case of NOM and DOM, NMR is especially valuable as the technique not only enables the detection of various chemical structures, but also

facilitates chemical structure elucidation as hydrogen couplings can be seen in the spectra. The information of how carbon and hydrogen atoms are chemically connected will be a key technology in the compound identification process of the mass of organic compounds which is found in olivine.

However, the broad mass of organic compounds impedes also the investigation of the chemical structures as many signals overlap. Previous refined samples preparation such as LC fractionation with subsequent NMR analysis of these fractions can be a solution to overcome overlapping signals.

The results shown here are just valid for the Åheim olivine and its heated specimen. Different olivines from different origin will probably show a particular distribution of signals depending on its emergence and heating history. It is to be expected that olivine from volcanic origin contains a distinctive signature which distinguishes it from Åheim olivine, as it is a mantle olivine. For precise statements of what exactly happens with organic compounds while heating, the experiments should be repeated with many kinds of olivines in multiple measurements. However the extraction of two grams of olivine gives an optimal average over the alteration of organic matter in the sample, the repetition of experiments could outrule variance cause by measurements inaccuracies. Ultimately, also sample preparation methods will have to be refined to enable reproducible and meaningful results from the NMR spectroscopy.

3.5 Discussion and Conclusion

Olivine mineral, which is highly abundant on earth, but also present in many meteorites, contains a diverse matrix of organic matter. FT-ICR-MS revealed the high abundance and complexity of organic compounds contained in olivine. The method is able to not only measure a broad variety of these organic compounds, but also assign elemental formulae to the measured peaks for a better elaboration of the organic matter. However, an exact structure elucidation with FT-ICR-MS is not possible. Complementary techniques such as LC-MS to perform MS/MS experiments and NMR spectroscopy to elaborate the chemical connectivity would be necessary to better describe the organic compounds and to ultimately be able to annotate specific chemical compounds. Organic matter is enclosed within olivine and not directly available to nature, but also protected from heat combustion and other harsh environments. The olivine mineral itself can change in a high temperature environment, which also enables the organic matter to change accordingly. Nevertheless FT-ICR-MS showed the broad variety of compounds which are present in olivine despite heat incidents. These stable molecules could have contributed to prebiotic chemistry and might be a missing link in regards to questions of the emergence and sustainment of life on Earth.

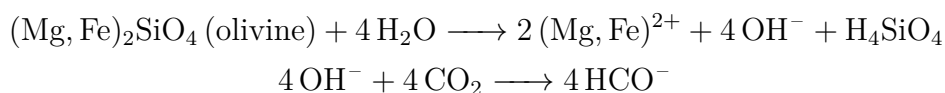
Chapter 4 - Conclusion and outlook

4.1 Implications for the Emergence of Life

This work was written in the context of the emergence and sustainment of life on Earth. The research of this field focuses on possible ways how life in our universe can start and how it could have evolved over time until today. Three major topics are looked at in this field, namely early synthesis, replication and translations, and early metabolism and cells. Replication and translation research focuses on DNA and RNA formation and their replication as well as peptides and proteins with catalytic functions. Early metabolism and cell research is focused on amplification, self-replication, and physical and chemical conditions, which were present at early Earth and how they could have promoted life. The research field where this work contributes to is the early synthesis. The topic focuses on the stability of compounds and how early synthesis could have worked in the primordial soup. The theories of this research field either represent the hypothesis that early Earth provided enough small molecules to start and fuel chemical reactions, or state that small and medium sized molecules already emerged in space and were brought to Earth by carriers.

The presented results of this work are a combination from both theories, that larger molecules were built on Earth, but also that they came from outer Space. Meteorites and olivines were shown to be carriers of organic compounds of various size with contribution of heteroatoms like nitrogen and sulfur. These organic compounds survive the atmospheric entry and are released to the surrounding environment after the meteorite lands on Earth and maybe was destroyed during this process. Consequently, landing sites of meteorites are in a way destroyed due to the large amounts of energy which is released by the impact, but also bear the potential of the emergence of new life as this abundance of organic compounds facilitates metabolism and synthesis nearby. It was also shown that organic compounds can intrinsically arise from Sabatier-processes and FT reactions in olivine. As olivine was already present

in Hadean times, the mineral matrix of olivine could have provided shelter and protection for organic compounds from the harsh exterior environments of Hadean Earth. Furthermore, olivine acclimates the surrounding water for improved survival of organic compounds, explicitly for the survival of CHOMg and CHOSMg compounds as these are easily degenerated at acidic pH values. A group showed the effects of olivine degradation and erosion in tap water [262]. Differently grained olivine was eroded in tap water by movement and the pH value was measured as an indicator of the reaction of olivine with water. During the process of degradation, the pH value of tap water increase over time. Naturally, tap water decreases its pH at air exposure, so it can be assumed that erosion of the olivine is the reason for the pH increase. Reactions of olivine with water are described by the following equations.



To corroborate these findings, the experiment was reproduced in this work. Four Erlenmeyer flasks were filled with 250 mL tap water and 30 g of Åheim olivine. The flasks were shaken for 1 d, 4 d, 7 d, and 10 d respectively and the pH value of all water samples was measured. Furthermore, 1 mL of the water was sampled after experiment, centrifuged and mixed with 5 mL of methanol. This extract was then subject to FT-ICR-MS measurements. The results of the pH measurements and the results of the FT-ICR-MS measurements can be seen in Table 4. The picture of the Erlenmeyer flasks after the experiment can be seen in Fig 35C.

Similar to the experiment as published in the paper of Schuiling et al. [262], the pH value of the water increased the more, the longer the olivine was present in the water samples. The increase of the pH value was explained by two reactions as shown before. Therefore it can be assumed that olivine when exposed to water in combination with erosion can increase the pH value of water locally. This allows the creation of a less hostile environment, both

Days of Experiment	Final pH	New CHO formulae	New CHOMg formulae	New CHOSMg formulae
One	8.98	124	6	2
Four	9.23	2	2	0
Seven	9.28	111	10	1
Ten	9.36	198	64	11

Table 4: Results of the erosion experiments with olivine in tap water

for living creatures, but also for organic compounds. Furthermore, the water samples showed an increase of CHO, CHOMg, and CHOSMg compounds over time (Figure 35A and B). While at first, the amount of compounds is variable and not notably increasing, the compounds show a strong increase in the water at seven and ten days. It is possible that the erosion of the olivine liberated organic compounds to their surroundings. Furthermore, these compounds were stable long enough to be measured with FT-ICR-MS which shows their stability at higher pH values towards degradation.

Olivine when in contact with water can create a local environment, even on Hadean Earth, which is locally more suitable to harbor life and stable organic compounds. The crater of a meteorite or local spots in the ocean can be more suitable to promote the development of life and organic compounds than other spots on the same planet. A widely investigated example of this may be the lost city underwater field of black and white smokers. The shown results indicate that organic matter could have survived on the harsh conditions on Early Earth and therefore it is possible that olivine and meteorites together promoted the emergence of life. Not only does olivine provide an friendly environment towards organic compounds, but also liberates compounds due to the erosion of the material. The shown data is only a small section of the reactions schemes happening of olivine when in contact with water. Especially CHO compounds are also prone to be added through air. Therefore, CHNO compounds were not looked at as they can easily enter the open system and thus cannot be seen as reliable markers for olivine degradation. However, CHOMg and CHOSMg compounds are unlikely to be added by air and thus allow the conclusion that olivine itself provides necessary organic compounds

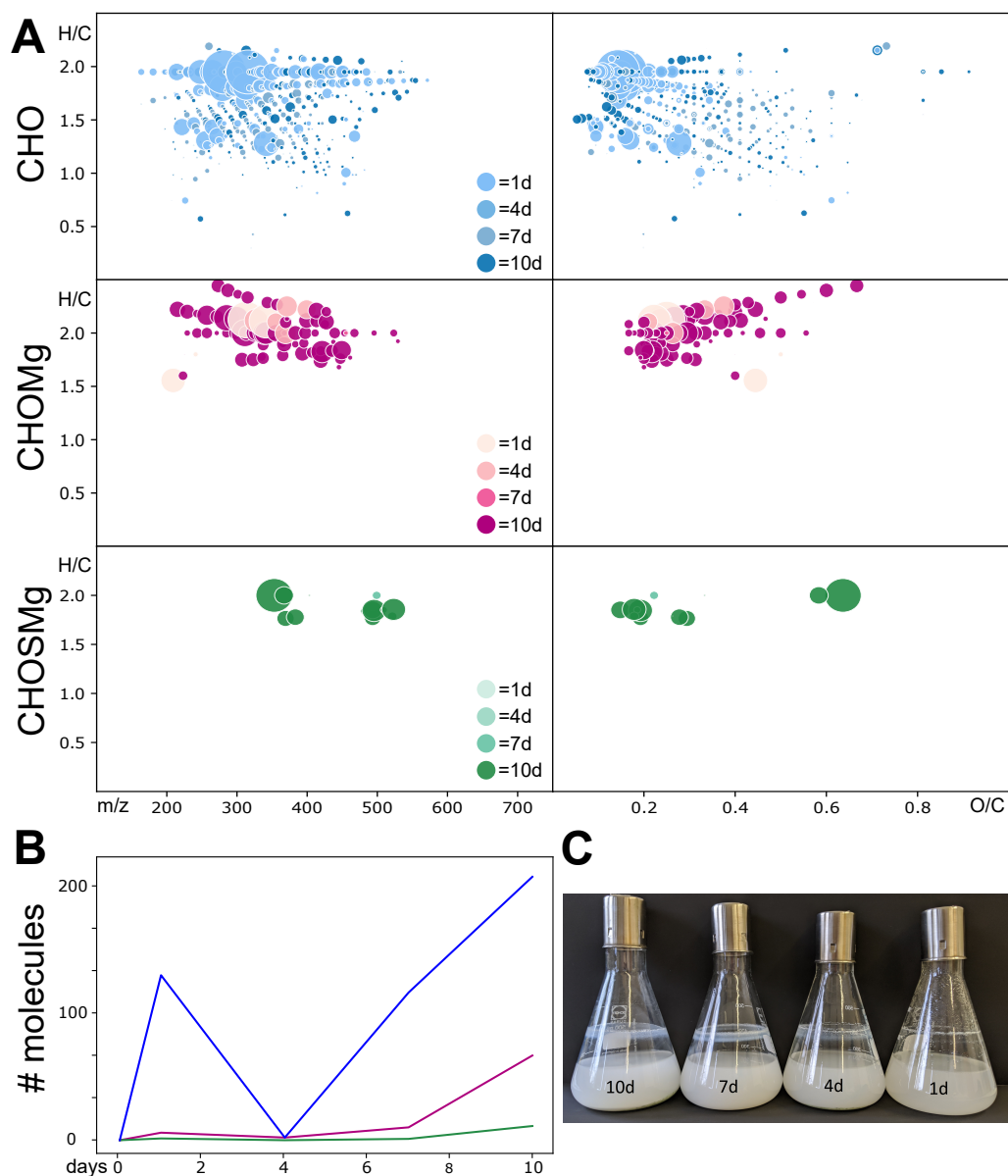


Figure 35: Results from the water erosion experiment with olivine. **A** Van Krevelen diagrams and mass-edited H/C diagrams of CHO, CHOMg, and CHOSMg compounds in water. Legend indicates at which timepoint a formula was first detected within the spectra. **B** Absolute amounts of new CHO (blue), CHOMg (magenta), and CHOSMg (green) compounds at different timepoint. **C** Picture of the Erlenmeyer flasks at different timepoint with shortest exposure (right) to longest exposure (left).

to its surrounding to create life. Further research should include a larger dataset of more olivines, more water types, atmospheres, and reactions conditions. It can be assumed that the degradation of olivine follows certain rules and that also serpentinization plays an important role in the processes of olivine in contact with water.

4.2 Further Research on Metalorganic Compounds

Until now, especially the class of CHOMg and CHOSMg compounds has been described as important proxies for heat incidents, shock, and thermal alteration in meteorites. Due to the fact that meteorites contain a far larger number of hetero atoms and metal ions as yet described in literature, it can be expected that more compounds will be discovered in the upcoming periods. Especially selenium and tellurium can be assumed to be incorporated in organic compounds as these elements share similar chemical properties like sulfur. The whole class of CHNOMg and CHNOSMg is also not yet described. Their appearance and absence might as well be an important marker for meta data. It could be assumed that nitrogen especially could be a marker for comet ice models as these often are closely related to compounds with nitrogen contribution.

The existence of halogen atoms within these kinds of molecules is also plausible as chlorine, bromine, and iodine can chemically easily be replaced with chemical groups such as OH groups. As halogens are also available in meteorites and show a characteristic isotope pattern, some olivine samples were searched and some compounds containing bromine were detected in the FT-ICR-MS in the sample of Kilauea 1959 eruption olivine. The isotopic pattern of this peak of mass 735.13907 Da was investigated and assigned to the chemical formula $C_{16}H_{33}O_3MgBr$. The isotopic pattern as seen in Fig. 36 confirms the presence of a bromine atom as its isotope of ^{81}Br (abundance 50 %) shows equally high intensity as the monoisotopic peak. Also some combinations of bromine peaks together with other isotopes can be observed. The presented peak thus includes besides magnesium also a

bromine atom, which was hitherto not reported. The depicted chemical structure is an assumption which is drawn from the chemical properties of CHOMg compounds, where one OH group was replaced by bromine. This structure however is not confirmed, but seems plausible due to the chemical structure of CHOMg and CHOSMg compounds.

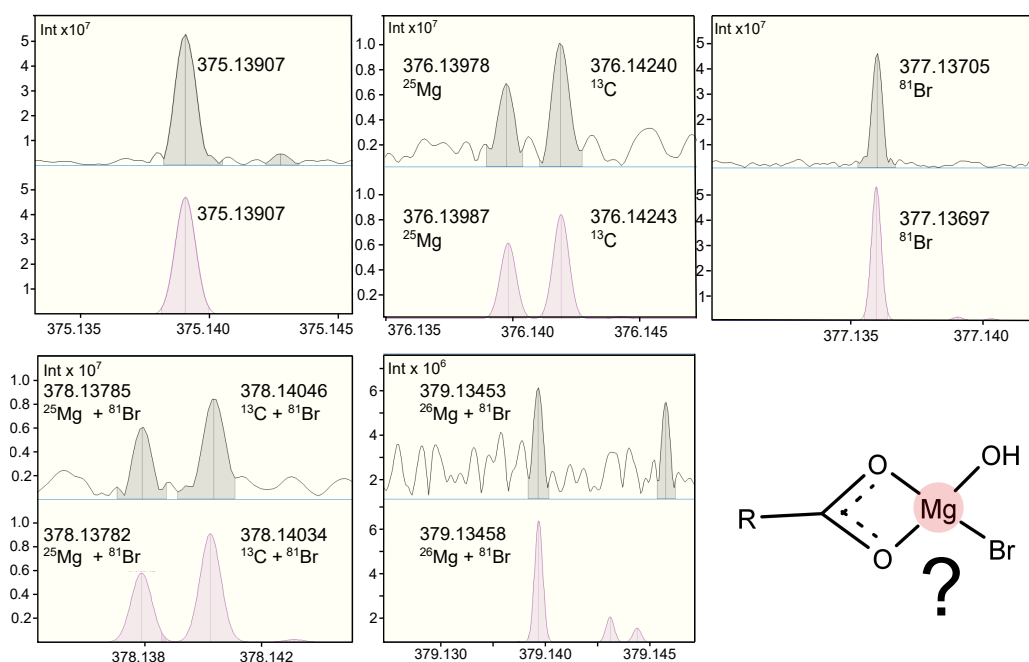


Figure 36: Isotopic pattern of the peak of m/z 375.13907, to which the chemical formula of $\text{C}_{16}\text{H}_{33}\text{O}_3\text{MgBr}$ was assigned. Isotopic pattern of this peak is depicted. A suggested chemical structure is given.

This finding and the presence of CHNOMg and CHNOSMg compounds confirms that more metal containing compounds from meteorites can be expected to be found in the upcoming future. However, it is noteworthy that size and shape of these compounds can vary to a great extent. More organo metallic compounds signify their importance to the carbon speciation in geological samples such as meteorites and olivine. These compounds furthermore also may have contributed to the emergence of life on Earth and provided chemical environments for catalysis of chemical reactions. At

this point the scope of what we know about these compounds is small and what we do not know about them is large. Future research will use further high-resolution techniques to identify more unknown compound classes and also can correlate them to chemical processes on Earth and Space. It is likely that in the upcoming twenty year, a manifold of more compounds are detected in meteorites as well as in the many return missions which have been launched in the recent years and will bring back pristine samples to Earth from Mars, from Asteroid, and other celestial bodies.

4.3 High Content Screening

High content screening (HCS) is a technique which combines automated microscopy with quantitative image analysis [263]. It is used to address biological questions in the fields of academia or pharmaceutical industry especially in the context of toxicology including all of its sub fields such as genotoxicity or neurotoxicity. By exposing relevant systems such as stem cells to chemical agents followed by application of cell dyes, antibodies, or proteins, cell characteristics data can be acquired by analyzing and measuring image parameters [263]. Critical cell alterations can be compared to known effects of drugs on cells and furthermore can be compared to zero controls of cells to display relevant changes. HCS enables a quick and broad method to test also complex systems for biological activity in cells and allows to choose for drug candidates without resolving biological pathways in the first step.

HCS is consequently a suitable platform to test for biological activity of compounds is a mixture of molecules as it is present in the SOM of meteorites and olivines. Extracts from the meteorites and olivines can be directly applied to the HCS cell models to check for biological activity within these geological samples. As the SOM of geological samples is mostly not investigated regarding chemical structures and composition, it is feasible to discover new relevant molecules for drug discovery in geological samples as these function as a novel chemical library with unknown chemical characteristics.

To test the hypothesis that meteorites and olivine contain biological active

organic compounds, the Kilauea 2018 olivine was tested for HCS. The extract of the SOM of Kilauea 2018 was applied to three plates with sufficient number of zero controls to compare the effects of the organic matter from the olivine. To improve the validity, triplicates were measured and compared to all blanks. Some important results of the HCS analysis can be seen in Figure 37.

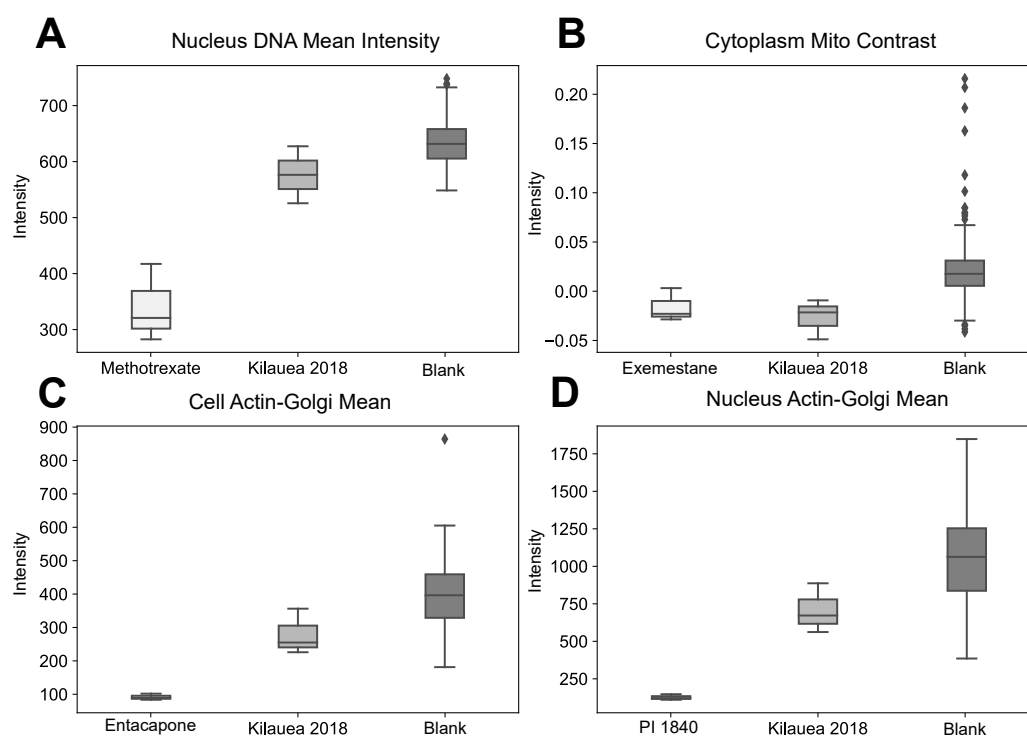


Figure 37: Important results from the HCS screening of Kilauea 2018. Analysed are **A** Nucleus DNA Mean Intensity, **B** Cytoplasm Mito Contrast, **C** Cell Actin-Golgi Mean, and **D** Nucleus Actin-Golgi Mean.

The SOM of Kilauea 2018 Olivine shows some changes compared to the blanks which are untreated cell lines. The DNA mean intensity of the olivine treated cells is lowered compared to most blanks (37A). A similar effect was seen in cells after methotrexate exposure, which is a potent inhibitor of the dihydrofolate reductase. Furthermore the drug inhibits the enzyme aminoimidazolecarboxamidoadenosineribonucleotide (AICAR) transformylase, which is involved in the purine biosynthesis, and causes apoptosis. Also PFI-1,

a highly selective BET (bromodomain-containing protein) inhibitor for BRD4, which is researched for cancer therapy, causes this effect on cells. Cytoplasmic contrast (37B) is also lowered in the cells treated with Kilauea 2018 extract. This effect can also be seen in the cells treated with Exemestane, which is an aromatase inhibitor. Besides that, the Kilauea 2018 extract also shows activity towards the actin-golgi structures in the cell (37C) and also in the nucleus (37D). A similar effect was observed in the Entacapone treated cells, which is a potent inhibitor of alpha-syn and beta-amyloid oligomerization and fibrillogenesis, and also in cells which were treated with PI-1840, a chymotrypsin-like inhibitor.

The Kilauea 2018 olivine contains organic compounds which show biological activity in the HCS cell models. The SOM of olivine and possibly also the SOM of meteorites can function as a chemical library for new biological active chemical structures or compounds which can be used as blueprints for drug discovery. The data shown is recorded in triplicates and shows changes compared to blank measurements. However, the cells show less intense cellular response towards the Kilauea 2018 extract as they do for most drugs. As the drugs are highly purified chemical agents with a defined metabolic pathway, it is likely that Kilauea 2018 extract shows a milder effect compared to the drugs. Nevertheless, some effects in the olivine extract can be observed which implies that the organic matter of Kilauea 2018 olivine contains some biological active compounds. To investigate these chemical active compounds, a method such as solid phase extraction and subsequent preparative chromatographic separation could increase the chances to firstly enrich the biological active substances and secondly to isolate them from non biological active substances. By this method, olivine and meteorites can serve as novel chemical libraries to discover new potent chemical agents for the pharmaceutical industry.

4.4 Research Questions

"Do geological samples contain the suitable compounds to fuel and sustain the emergence of life on Earth?" Geological samples contain

suitable compounds to have a significant influence on the emergence of life on Earth. The vast variety of organic compounds, especially those one containing nitrogen and sulfur can act as organic precursors for life on earth.

"Do organic compound survive harsh conditions and how are these conditions influencing the molecules within the geological samples?" Organic compound within a mineral matrix can survive harsh conditions for a long period of time without largely changing their composition. Although high temperature influences the organic compounds within the geological samples, organic compounds never completely disappear.

"Where are organic compounds located within geological samples?" The most likely answer to this are microinclusions which bear the of the organic compounds within geological samples. Olivine represents a suitable matrix to contain and protect organic compounds from harsh external conditions and thus constitute a suitable place for organic compounds within geological samples.

"Are organic compounds in geological samples more dependent on their origin or are there others factors which have to be considered?" The research concludes that both the origin of the geological sample as well as their temperature history influences that organic cargo. Organic compounds within the samples give give clues about the origin of the samples, but also allow assumptions to be made about their temperature history.

Appendix

A.1 Material and Methods to Chapter 2

A.1.1 FT-ICR-MS Five milligrams of each meteorite sample were washed three times with methanol in an agate mortar. Before crushing, 750 μ l methanol was added to the sample. The meteorite was further crushed until meteorite powder and methanol formed a homogeneous suspension. The suspension was transferred to an Eppendorf vial and left in an ultrasonic bath for 30 s. After centrifuging, the supernatant was transferred to another Eppendorf vial and ultimately used for ESI-FT-ICR-MS acquisition. The system was calibrated with L-Arginine clusters in negative mode. To ensure cleanness of the system, pure methanol blank spectra were acquired before measurement of samples. Relevant peaks for this study are absent in methanol blanks.

A.1.2 Data Treatment Spectra were internally calibrated with common fatty acids. Peaks were picked with signal-to-noise ratio of 3. All picked peaks were aligned respective to their m/z value with a 1 ppm error window. Assignment of elemental compositions was conducted with an in-house built software, NetCalc (Marianna et al. 2011). Only CHOSMg compounds were considered for further evaluation, which were present in more than 5

A.1.3 FT-ICR-MS Five milligrams of each meteorite sample were washed three times with methanol (Merck-Nr.106009) in an agate mortar. The washing methanol was disposed after each wash step to reduce contamination from handling. Before crushing, 750 μ L methanol was added to the sample. The meteorite was further crushed until meteorite powder and methanol formed a homogeneous suspension. The suspension was transferred to an Eppendorf tube (3810X; 1.5 mL) and left in an ultrasonic bath for 30 s. Subsequent to the ultrasonic bath followed centrifugation with a small table centrifuge. After centrifuging, the supernatant was transferred to another Eppendorf tube and ultimately used for ESI-FT-ICR-MS acquisition. The measurements were performed on a high-field Fourier Transform Ion Cyclotron

Resonance mass spectrometer from Bruker Daltonics—Solarix. The magnet is a 12 T magnet from Magnex. Parameters were optimized with FTMS-Control V 2.2.0 from Bruker Daltonics. The mass spectra were acquired with a 4 megaword (MW) time domain. The system was calibrated with L-Arginine clusters in negative mode (5 mg/L L-Arginine solved in methanol). To ensure cleanness of the system, pure methanol blank spectra were acquired before measurement of samples. Relevant peaks for this study are absent in methanol blanks. For each sample, scans were accumulated in the mass range of 122–1000 amu. Ions were accumulated for 300 ms in normal measurements mode and 1 s for MS/MS measurements. The pressure in the hexapole was 3×10^{-6} mbar, and the pressure in the ICR vacuum chamber was 6×10^{-6} mbar. As the source, we used the Apollo ii (Bruker Daltonics), which is an ESI source. The supernatant from the extraction was directly injected via a microliter pump system (flowrate: 120 μ L/h). The source heating temperature was 200°C.

A.1.4 Data Analysis All spectra were internally calibrated with a mass list of common fatty acids. Average errors of calibration were below 0.5 ppm. Peaks were picked with a signal-to-noise ratio of three. All peaks were aligned in a 1 ppm error window according to their m/z value. The elemental composition of all m/z values was calculated with an in-house built program, NetCalc (Marianna et al. 2011). Assignments were computed with an average accuracy window of ± 0.2 ppm. Only compounds that contain one Mg atom and one or more S atom were considered as CHOSMg compounds for further evaluation. CHOSMg compounds have to be present in at least 5% of the samples to delete unique annotations. The representation of the van Krevelen diagram and H/C-edited m/z diagram was used to visualize the data. From the exact elemental compositions, the O/C and H/C ratio was calculated for each of the CHOSMg compounds. By plotting and comparing the O/C, H/C, and m/z values, the compounds can be characterized regarding saturation and oxidation levels (Van Krevelen 1950; Hertkorn et al. 2008).

A.1.5 Computations The electronic structure calculations were per-

formed on a server computer by running ab initio quantum mechanical computations, based on density functional theory (DFT), as implemented in Gaussian 09. The hybrid DFT-functional B3LYP was implemented with d-polarization functions for each heavy atom and 1 p for each hydrogen atom in all geometry optimization calculations with a 6-31+G(d,p) basis set. Frequency calculations were done for each optimized geometry with the same 6-31+G(d,p) basis set to obtain the zero-point vibrational energy. This value was multiplied by a scaling factor of 0.9804 to correct for vibrational anharmonicities. Another intention for performing the frequency analysis is the identification of transition states. Detecting imaginary frequencies implies that the optimized geometry is not fully relaxed as a stationary point (energy minimum) on the potential energy surface. The single-point energy calculations were done at the 6-311+G(d,p) level of theory. The use of diffuse functions was important to represent the correct geometry and thermodynamic properties of anionic species. Stability tests were performed to ensure that the used wave function represents the lowest-energy solution of the self-consistent field equations. For geometry optimization, the Berny analytical gradient optimization routines were used. The requested convergence value in the density matrix was 10^{-8} , the threshold value for maximum displacement was 0.0018 Å, and the threshold value for the maximum force was 0.00045 H B-1. The nature of the stationary points was established by calculating and diagonalizing the Hessian matrix (force-constant matrix). All geometries of electronic structures calculated were viewed with the GaussView program (Dennington et al. 2003). The network in Figure 3 was designed with Gephi version 0.9.2.

A.1.6 Statistical Evaluation A total of 44 meteorites were aligned in a matrix, and the putative formulae were calculated with an in-house software (Marianna et al. 2011). We took into consideration the CHOSMg compounds detected in more than 5% of the meteorites. Signal intensities were normalized for each meteorite, dividing each peak intensity by the sum of all intensities of one measurement. We excluded from further elaboration

the 10% highest and lowest intensities, to neglect extremely high and low values. The values were scaled by UV (unit variance) scaling. A principal component analysis (PCA) was applied to have an overview of the data. PCA analysis reduces the dimensionality of the data without losing important information. Ultimately, the analysis gives a representation of components that best describe the variance found in the data and separate samples accordingly. Furthermore, from metadata, we categorized the meteorites in three groups, namely, hydrothermal background without short-duration heating (T i), moderate short-duration heating (T ii) and intense short-duration heating (T iii/T iv), and long-duration heating (LDH) (Quirico et al. 2018) (see Table A1). These data were analyzed with (PLS-DA) regressions models.

A.2 Figures and Tables to Chapter 2

ID Number	Meteorite description	Type Class	Number of CHOSMg formulae	Number of total assignments	Percent CHOSMg of Total	Ratio CHOSMg/CHO	Ratio CHOMg/CHOSMg	Heating History	Shock Status
152	Tagish Lake	C2-ung	353	6429	5.49	0.45	1.64	T II	1
19	Yamato 86720	C2-ung	516	11386	4.53	0.37	1.08	T III / T IV	4
32	MET 01070	CM1	36	8644	0.42	0.04	2.78	T I	-
23	Cold Bokkeveld	CM2	1587	16335	9.72	0.91	0.68	T II	1
25	EET 87522	CM2	294	1918	15.33	5.76	0.08	T II	-
26	EET 96029	CM2	104	1373	7.57	4.33	0.03	T II	-
31	MCY 05230	CM2	831	16272	5.11	1.07	0.05	T I	-
34	MIL 07700	CM2	227	4747	4.78	0.6	0.39	T II	-
39	PCA 02010	CM2	120	1521	7.89	2.79	0	T III / T IV	-
40	PCA 02012	CM2	118	1329	8.88	2.03	0.04	T III / T IV	-
43	WIS 91600	CM2	771	3778	20.41	2.03	0.5	T II	-
45	Yamato 791198	CM2	818	14867	5.5	0.76	0.35	T I	-
46	Yamato 793321	CM2	163	3496	4.66	1.96	0.4	T II	-
66	DOM 08003	CM2	579	10141	5.71	0.85	0.11	T I	-
88	Murchison	CM2	9	13762	0.07	0.01	2.22	T I	2
92	Nogoya	CM2	795	7865	10.11	0.63	0.93	T I	1
144	Paris	CM2	579	7984	7.25	0.78	0.26	T I	0
149	Sutter's Mill	C	809	4127	19.6	0.81	0.25	T III / T IV	-
28	LEW 85311	CM2-an	117	8199	1.43	0.58	0.04	T I	-
29	LEW 85312	CM2-an	231	10518	2.2	1.19	0.12	T I	-
41	PCA 91008	CM2-an	93	2055	4.53	1.78	0.01	T III / T IV	-
42	QUE 93005	CM2-an	523	5009	10.44	0.72	0.49	T II	-
51	Yamato 81020	CO3.0	46	2678	1.72	0.03	4.33	LDH	-
49	Kainsaz	CO3.2	1066	12301	8.67	0.85	1.3	LDH	1
52	Yamato 82050	CO3.2	1340	14582	9.19	1.16	0.78	LDH	-
50	Yamato 791717	CO3.3	1093	16326	6.69	0.77	1.55	LDH	1
53	Yamato 82094	CO3.5	386	4153	9.29	0.35	1.17	LDH	2
54	GRO 95577	CR1	695	4371	15.9	1.48	0.22	T I	-
55	EET 92042	CR2	396	10019	3.95	0.36	0.7	T I	-
56	GRA 06100	CR2	1086	5386	20.16	1.77	0.93	T III / T IV	-
58	GRO 03116	CR2	144	2026	7.11	0.26	1.91	T III / T IV	-
59	MET 00426	CR2	540	7075	7.63	0.62	1.46	T I	-
60	QUE 99177	CR2	729	14523	5.02	0.64	0.7	T I	-
11	Allende	CV3	509	4918	10.35	0.4	2.31	LDH	-
169	Kaba	CV3	494	5611	8.8	0.37	0.67	T I	-
1	Aba Pamu	L3	433	5723	7.57	0.22	1.62	LDH	4
180	Renchen	L5-6	1249	9917	12.59	0.53	2.4	LDH	4
12	Battle Mountain	L6	656	11032	5.95	0.56	1.68	LDH	4
16	Braunschweig	L6	829	4708	17.61	1.25	1.17	LDH	4
93	Novato	L6	1673	11229	14.9	1.48	1.37	LDH	4
151	Soltmany	L6	501	7699	6.51	0.55	3.83	LDH	2
157	Vicencia	LL3.2	304	5411	5.62	0.24	2.04	LDH	1
20	Chelyabinsk	LL5	2266	14667	15.45	1.69	0.96	LDH	4
181	Stubenberg	LL6	828	5988	13.83	0.69	1.4	LDH	3

Table A.1: Where data on heating history are present, the samples were used for the PLS-DA of Figure 14 [264]

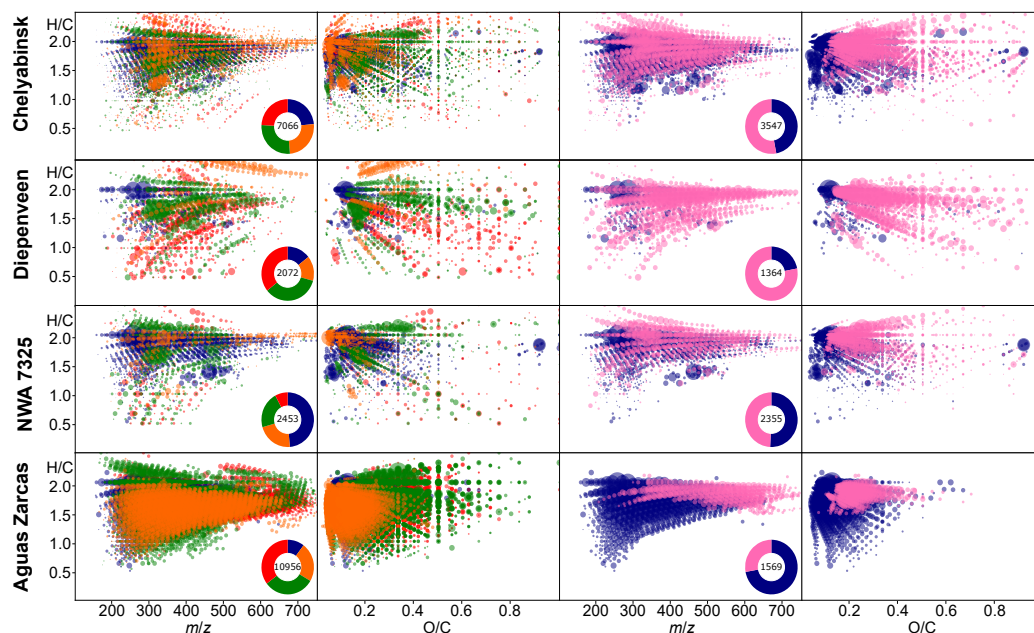


Figure A.1: Depicted are mass-edited H/C ratio diagrams (left side of each of the two panels) and O/C ratio vs. H/C ratio (van Krevelen) diagrams (right side of each of the two panels) of the four meteorites from Figure 10. Bubble size represents the intensity in the mass spectrum; color represents the chemical space. CHO = blue, CHNO = orange, CHOS = green, CHNOS = red, CHOMg = magenta. The donut plot shows the total amount of each of the chemical spaces according to the color code as described in this legend.

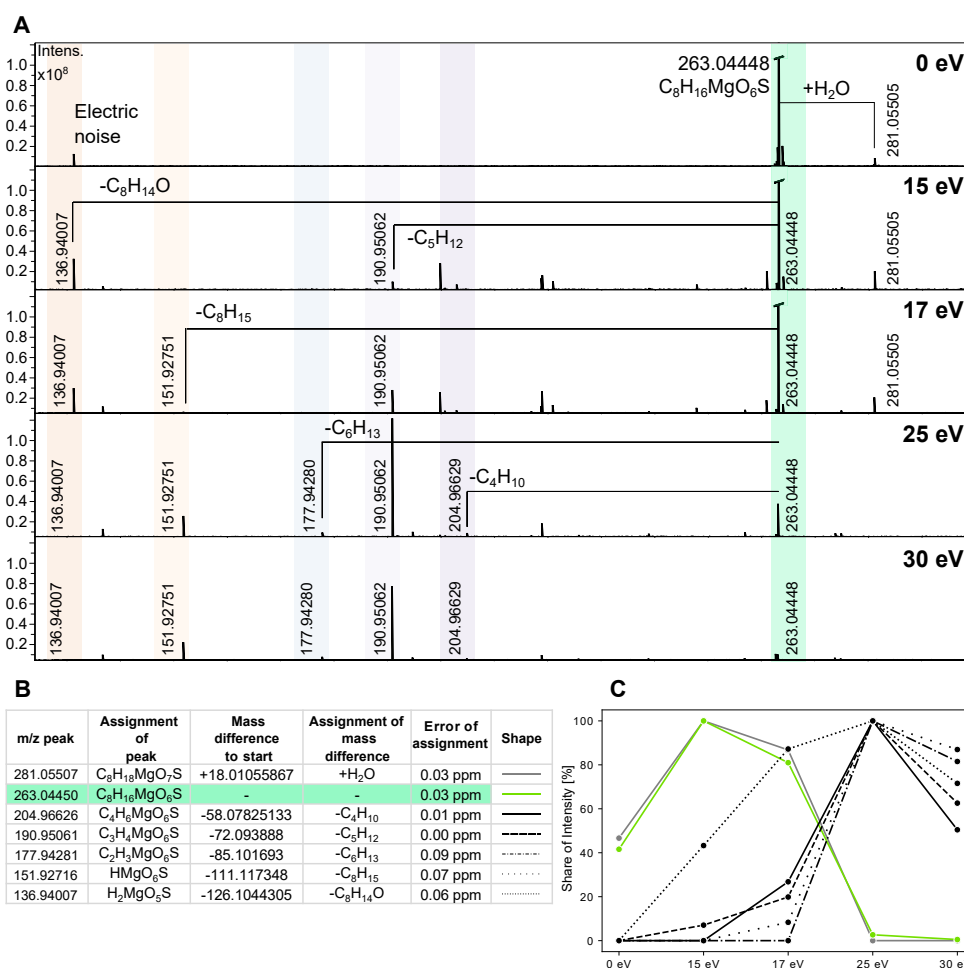


Figure A.2: MS/MS experiments of CHOSMg compounds. (A) (-) ESI-FT-ICR-MS spectra of methanolic extract of Nogoya meteorite. Quadrupole Q1 mass was set to m/z 263 to isolate m/z 263.04448, which is annotated as $C_6H_{16}MgO_6S$. Spectra with different electron volt (eV) voltage is displayed. At 15 eV, fragments of charge remote fragmentations can be observed, while the intensity of the CHOSMg decreases. (B) All annotated peaks belonging to the initial isolated peak. Only the carbon chain is shortened by charge remote fragmentation, showing the high stability of the magnesium-sulfur head group. Loss of SO_2 , SO_4 , MgO_4S , or MgO_6S were not observed. (C) Intensity of all detected fragment peaks in the MS/MS measurements. A decrease of the isolated peak can be observed, while the fragmentation results in an increase in intensity. Ultimately, all peaks decrease in intensity at high voltage.

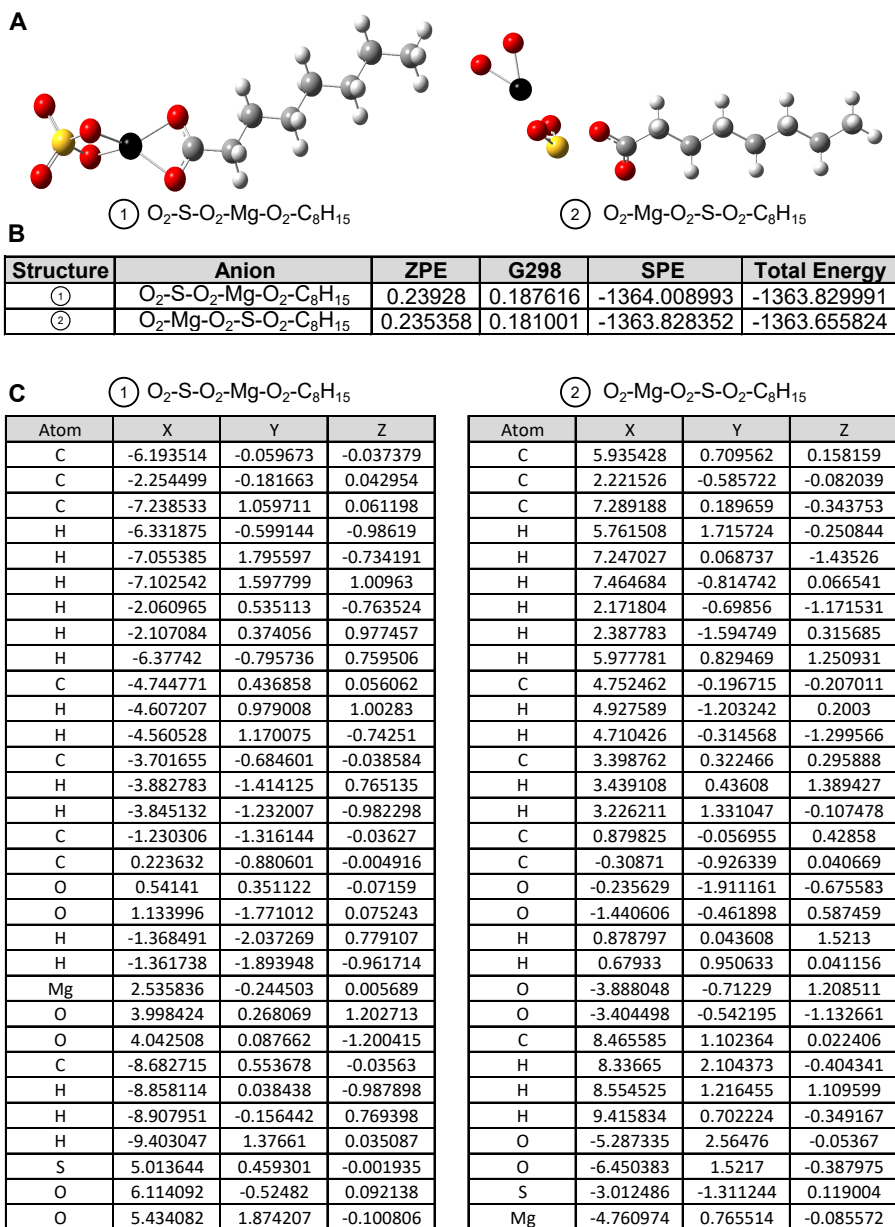


Figure A.3: (A) According to MS/MS results as seen in Figure A.2, two different possible chemical structures were tested for their stability. (B) Gas-phase total energy difference (δG) between circle1 $C_8H_{15}OOMgSO_4$ and circle 2 $C_8H_{15}OOSO_2MgO_2$ anions were calculated. The zero-point vibrational energy (ZPE) and the Gibbs free energy at room temperature $T = 298$ K (G298) were calculated on the B3LYP/6-31+G(d,p) level of theory and given in Hartrees. The single-point energy (SPE) was calculated at a higher 6-311+G(d,p) level of theory and is given in Hartrees. The energy difference between both anions is 109.3 kcal/mol. (C) XYZ coordinates of the proposed two anions in their relaxed geometry.

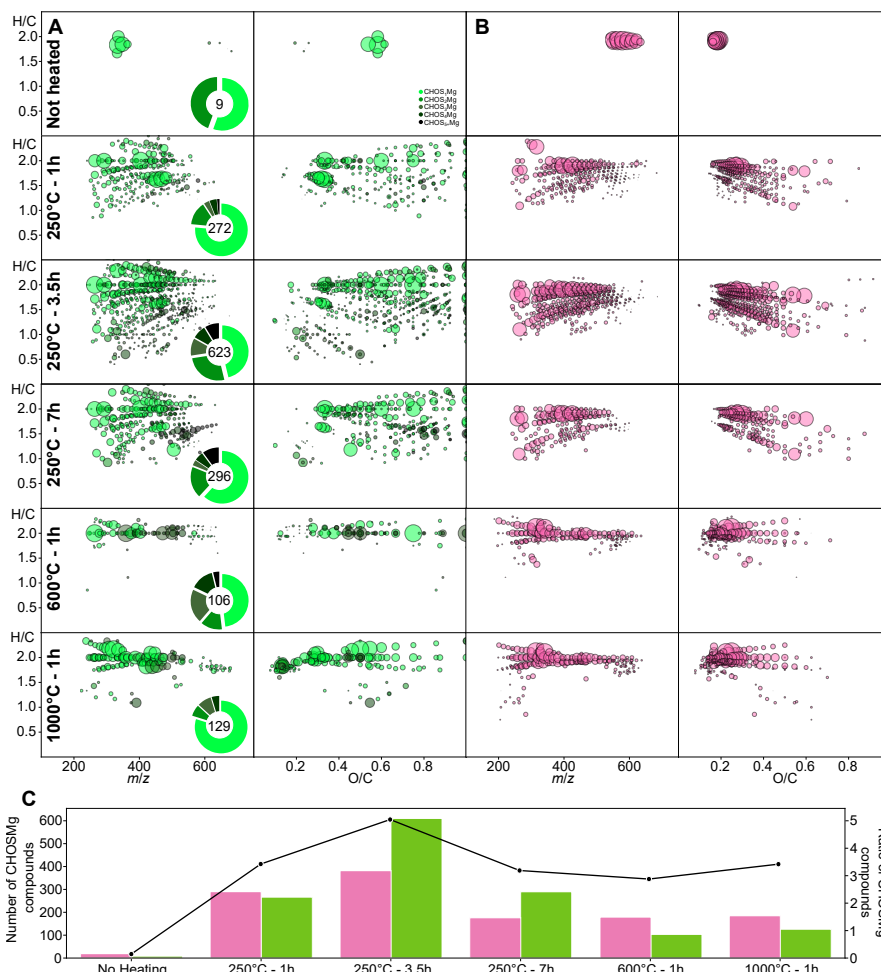


Figure A.4: Heating experiment with Murchison meteorite. Similar-sized fragments of Murchison Meteorite were heated to 250°C for different durations, and also to 600°C and 1000°C for 1 hr. Depicted are mass-edited H/C ratio diagrams and O/C ratio vs. H/C ratio (van Krevelen) diagrams of (A) CHOSMg compounds (left side in green) and (B) CHOMg compounds (right side in magenta). Bubble size represents the intensity in the mass spectrum; color represents the amount of sulfur per CHOSMg compound according to the legend in the left panel. An increase of CHOSMg compounds and CHOMg compounds with higher temperatures and heating duration can be observed. (C) Absolute amount of CHOSMg compounds (green bar charts) and CHOMg compounds (magenta bar charts) for each of the six measurements (left Y-axis) and ratio of CHOSMg compounds (line plot) to all measured compounds (right Y-axis) are shown. Absolute amount of CHOSMg compounds and the ratio increase with temperature but decrease again with very high temperature. CHOMg compounds increase with temperature and are more stable at the highest temperatures than CHOSMg compounds.

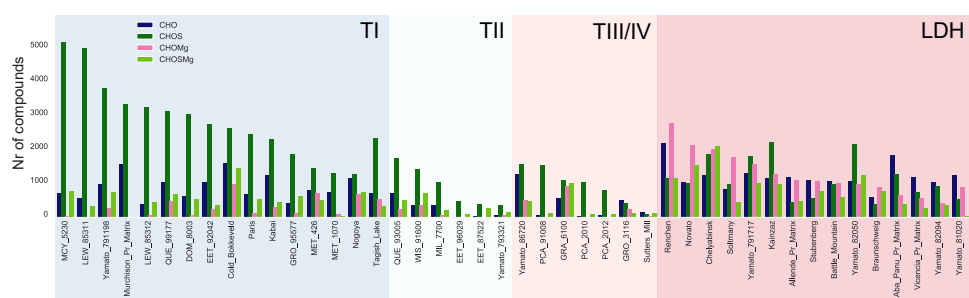


Figure A.5: Barchart with the total amount of CHO (blue), CHOS (dark green), CHOMg (magenta), and CHOSMg (light green). Lower heated samples are more to the left, and higher heated samples are placed more to the right. Information on the samples can be found in Table A.1.

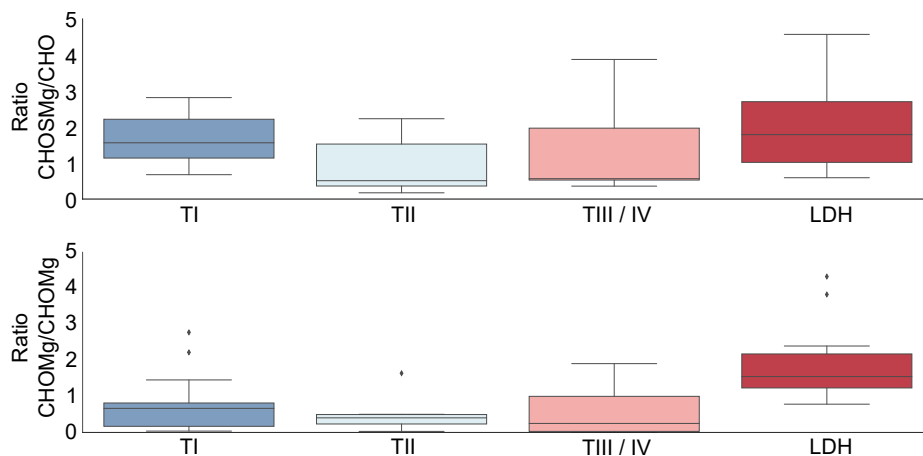


Figure A.6: Boxplots of the ratio of CHOSMg to CHO compounds (top chart) and of the ratio of CHOMg to CHOSMg compounds (bottom chart) of the respective meteorites as seen in Table A.1.

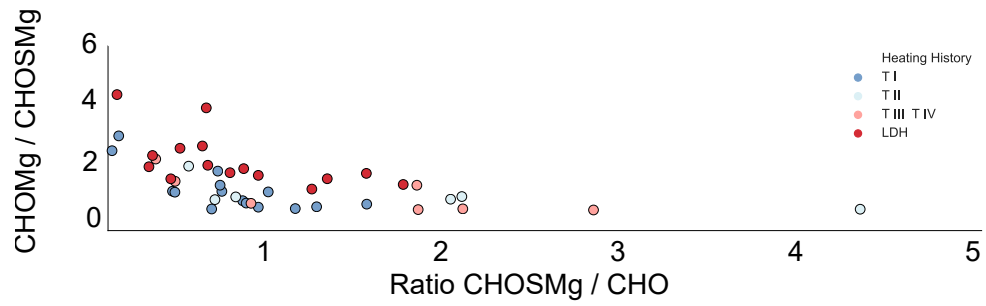


Figure A.7: Scatterplot of ratios of CHOSMg to CHO (X-axis) and of CHOMg to CHOSMg (Y-axis) of the respective meteorites as seen in Table A.1.

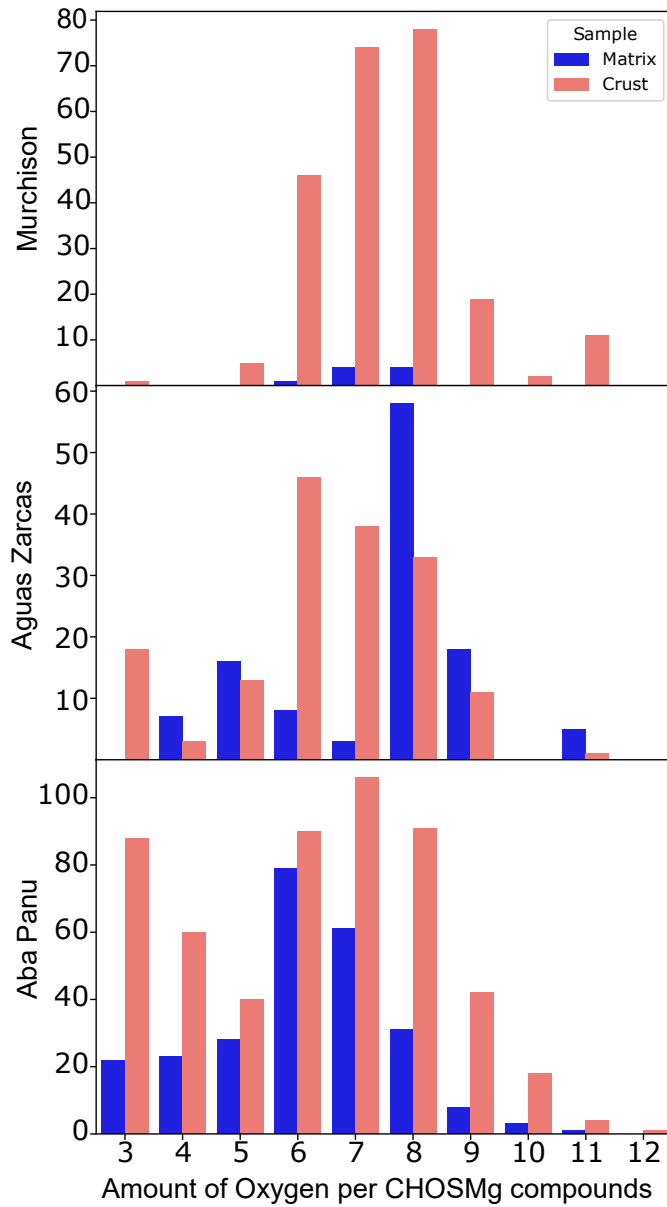


Figure A.8: Detailed view of Figure 13 in the main text. All three meteorites are depicted by different bar charts. Amounts of CHOSMg compounds in matrix (blue bars) and in crust (red bars) are depicted on the Y-axis; amounts of oxygen per CHOSMg compounds are depicted on the X-axis.

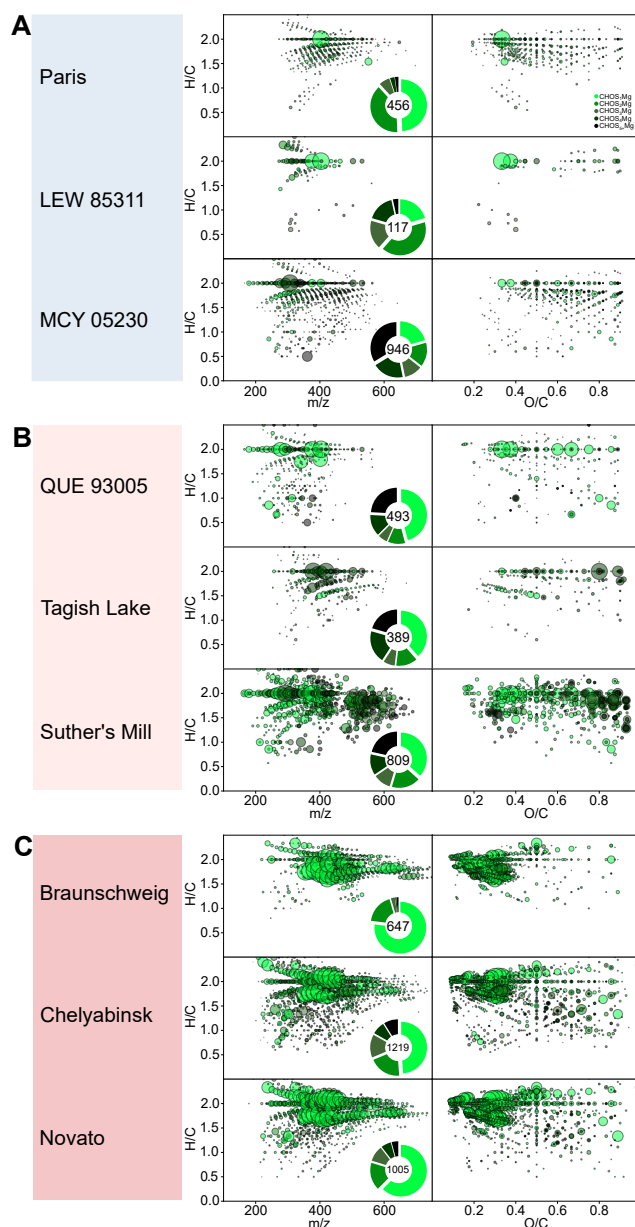


Figure A.9: Detailed view of selected meteorites from the PLS-DA of Figure 14 in the main text. (A) Three meteorites from the T I heated ones. (B) Three meteorites from the T II and T III/T IV. (C) Three meteorites from the long-duration heating. Depicted are mass-edited H/C ratio diagrams (left side of each of the six panels) and O/C ratio vs. H/C ratio (van Krevelen) diagrams (right side of each of the six panels). Bubble size represents the intensity in the mass spectrum; color represents the amount of sulfur per CHOSMg compound according to the legend.

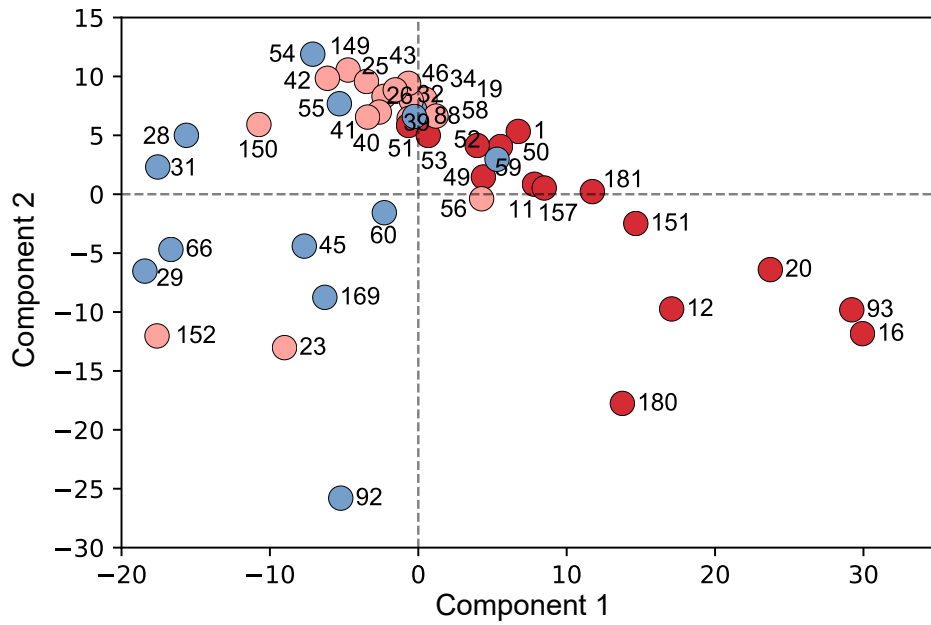


Figure A.10: PCA of similar data is found in the PLS-DA in Figure 14. PCA of 44 different well-described meteorites according to their thermal metamorphism history. Only CHOSMg compounds were used as PCA loadings. Three categories were chosen according to the assigned thermal history. Hydrothermal background without short-duration heating (T I; dark blue), moderate short-duration heating (T II) and intense short-duration heating (T III/T IV; light red), and long-duration heating (LDH; dark red). Information on samples can be found in Table A.1.

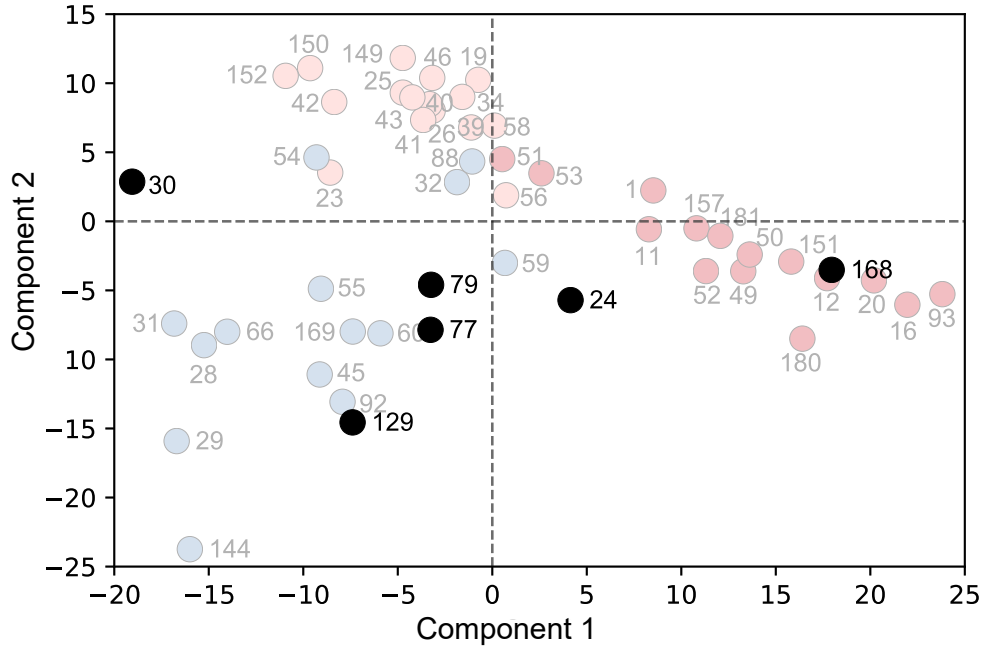


Figure A.11: Prediction with the PLS-DA from Figure 5. The PLS-DA model was used to predict the positioning of samples that were not classified in the T i, T ii, T iii/iv LDH system yet. Classified samples are Orgueil (129—CI), Ivuna (77—CI), Mukundpura (79—CM2), Maribo (30—CM2), Diepenveen (24—CM2-an), and Dhofar 1988 (168—CM2-an). The CI meteorites Orgueil and Ivuna have seen almost hardly any heat; thus, their CHOSMg signature is similar to those of T i meteorites. Maribo and Mukundpura are more similar to Murchison and thus move away from T i meteorites more into the direction of T ii and T iii/iv meteorites. Diepenveen and Dhofar 1988 both experienced some heating; thus, their CHOSMg signatures cluster them to LDH meteorites. Dhofar 1988 especially was recently reclassified as CY and shows subsequent thermal alteration [265], which is also corroborated by the positioning with the LDH meteorites in the PLS-DA.

B.1 Material and Methods to Chapter 3

B.1.1 Material and Methods - FT-ICR-MS

For ESI measurements, five milligrams of olivine crystals were first washed with methanol (Merck, EMSURE, ACS, ISO, Reag. Ph Eur) and then crushed for extraction in an agate mortar with 1 mL methanol. The achieved extracts were successively recovered in an Eppendorf tube (Nr. 0030120086), centrifuged with a table centrifuge and the supernatant was directly injected in the FT-ICR-MS. The measurements were carried out with a 12 T FT-ICR mass spectrometer Solarix (Bruker Daltonics) and the parameters were optimized via software FTMS-Control V2.2.0 (Bruker Daltonics).

For APPI and APCI measurements, 4 g of olivin crystals were washed with methanol, then crushed for extraction in an agate mortar with 1ml methanol, and the supernatant was transferred into an Eppendorf tube. The 4 g of olivine were extracted four times with methanol and all supernatants were evaporated in a speed vacuum concentrator. After being dried, the residue was redissolved in 0.1 mL methanol in an ultrasonic bath. This process was done twice, which yielded eight Eppendorf tubes with 0.1 mL extract. At the end, all extracts were combined to 0.8 mL extract which was directly used for APPI and APCI measurements. For enhanced ionization, 4% of toluene was added to the extract.

For ESI experiments, the mass spectra were acquired with a 4 megaword time-domain. Prior to acquisition, the mass spectrometer was externally calibrated with arginine clusters (10 mg/L in methanol). The ESI source (Apollo II, Bruker Daltonics) was used in negative-ion mode. The methanolic solution was infused with a flow rate of 2 $\mu\text{L}/\text{min}$ with a syringe pump. The mass spectrum ranges from m/z 122.9 to m/z 1000 and results from the accumulation of 1500 scans. For ESI (-) measurement, the capillary voltage was set at 4.0 kV, the drying gas temperature and the flow rate were kept at 200°C and 4 L/min, respectively, and the pressure of the nebulizer gas was 2.0 bar.

The APPI source (APPI II, Bruker) and the APCI source (APCI II, Bruker) were used to perform the acquisition in positive and negative mode for APPI detection mode and positive for APCI detection mode. A 900 μ L/h flow rate was used for sample infusion. The drying gas temperature and the flow rate were kept at 200°C and 2 L/min, respectively. The pressure of the nebulizer gas was 2.5 bar. The capillary voltage was 1.5 kV and the source was heated at 350°C. The mass spectrum was acquired between m/z 92 and 1200 and 300 scans were accumulated.

The achieved data were analysed using Data Analysis 5.0 (Bruker Daltonics). The FT-ICR mass spectra were internally calibrated by using reference mass lists of known components (fatty acids and some organomagnesium compounds). The mass spectra were exported to peak lists at a $S/N \geq 3$. Satellite peaks and signal related to magnetron signals were removed according to the algorithm developed by Kanawati et al. [191]. Assignment of the resulting peak lists was performed by using an in-house software, Netcalc [223]. C, H, N, O, S and Mg elements were used for assignments. Chlorine adducts were considered in negative-ion mode. Sodium adducts were considered in positive-ion mode.

B.1.2 Material and Methods - LC-MS

LC-MS analysis was performed using a maXis instrument (TOF-MS), (Bruker Daltonics, Bremen, Germany) in combination with an UHPLC system (Acquity, Waters, Eschborn, Germany) equipped with a photodiode array detector.

For the measurement of small molecules and metabolites, the following conditions were used: The used column for metabolite experiments was a Acquity BEH C8 column (1.7 μ m, 2.1 \times 150 mm, Acquity, Waters, Eschborn, Germany). Eluent A consisted of water with 5 mM ammonium formiate and 0.1% formic acid and eluent B of acetonitrile. The gradient started with 95% solvent A and % solvent B and was kept for one minute. Afterwards, the gradient changed to 100% solvent B over the course of 5 minutes. At 6

minutes with 100% solvent B2, the gradient was kept at 100% solvent B2 until the end at 10 minutes [266].

For the measurement of lipids and lipophile structures, the following conditions were used: The column used for lipids is a Cortecs C18 column (1.7 μm , 2.1×150 mm, Acquity, Waters, Eschborn, Germany). Eluent A consisted of 60% acetonitrile and 40% water and eluent B of 90% isopropanole and 10% acetonitrile, both with 10 mM ammonium formiate and 0.1% formic acid. The gradient started with 68% solvent A and 32% solvent B and was kept for one minute. Afterwards, the gradient changed to 3% solvent A and 97% solvent B over the course of 20 minutes. At 21 minutes with 97% solvent B2, the gradient was kept at 3% solvent A and 97% solvent B2 until the end at 25 minutes [267].

A pre-run time of 2 min was also set before every injection to stabilize the system. The column oven temperatures was set to 40°C. For the final measurements, the injection volume with a full loop injection was set to 10 μl . The flow rate was set to 0.350 mL/min. The samples were stored at +4°C in the sample manager. Mass spectra were acquired using MaXis TOF-MS in protonated positive mode ((+) TOF-MS) and in deprotonated negative mode ((-) TOF-MS). Samples were introduced into the ESI source at a nitrogen flow rate of 8 L/min (200 °C). The nebulizer gas pressure was set to 2 bar. Capillary voltage was set to 4000 V and measurements were performed with an acquisition rate of 5 Hz. MS/MS experiments were performed in automated MS/MS mode of the TOF-MS instrument. Ions with *intensity* ≥ 1000 were subjected to MS/MS and were limited to 5 precursor ions in every MS scan.

Data processing was done using Compass DataAnalysis 5.0 (Bruker Daltonics GmbH, Bremen, Germany) and Genedata Expressionist 13.5 (GeneData AG, Basel, Switzerland). Furthermore, Python 3.8 was used to analyze, compare, and visualize the data.

B.1.3 Material and Methods - NMR

For NMR measurements, 2 g of olivine crystals were washed with methanol, then crushed for extraction in an agate mortar with 1ml methanol and the supernatant was transferred into an Eppendorf tube. The 2 g of olivine were extracted four times with methanol and all supernatants were evaporated in a speed vacuum concentrator. After being dried, the residue was dissolved in 0.1 mL methanol in an ultrasonic bath. This process was done twice, which yielded eight Eppendorf tubes with 0.1 mL extract. At the end, all extracts were combined to 0.8 mL extract which was again dried in a speed vacuum concentrator. The dried extract was then dissolved in CD₃OD (Merck 99.95 % 2H). Proton-detected NMR spectra of methanolic extract of crushed Åheim olivine rocks were acquired using a Bruker Avance III NMR spectrometer at 800.13 MHz (B₀ = 18.7 T) and 283 K. Proton NMR spectra were acquired in 180 µL of CD₃OD (Merck. 99.96% 2H) solution with a 5-mm z-gradient 1H/13C/15N/31P QCI cryogenic probe (1H 90° excitation pulses: 10 µs) in a sealed 3-mm Bruker MATCH tube. The 1D 1H NMR spectrum was recorded with a “noesypr1d” pulse sequence, using 256 scans (5 s acquisition time, 5 s relaxation delay, 10 ms mixing time; 0.3 Hz exponential line broadening).

Absolute value JRES (with solvent suppression: jresgpprqf; 1 s acquisition time, 0.5 s relaxation delay, 70 ms mixing time) was acquired with 112 scans.

Phase-sensitive echo-antiecho TOCSY spectra (without solvent suppression: dipsi2etgps; 1.83 s acquisition time, 0.67 s relaxation delay, 70 ms mixing time) was acquired with 12 scans.

References

- [1] Weertman, J., Weertman, J.R., High temperature creep of rock and mantle viscosity, *Annual Review of Earth and Planetary Sciences*, 3(1):(1975) pp. 293–315
- [2] Gérard, O., Jaoul, O., Oxygen diffusion in san carlos olivine, *Journal of Geophysical Research: Solid Earth*, 94(B4):(1989) pp. 4119–4128, doi:10.1029/JB094iB04p04119
- [3] Donn, B., Organic molecules in space.
- [4] Winnewisser, G., Herbst, E., Organic molecules in space, in *Organic Geo-and Cosmochemistry*, pp. 119–172, (Springer1987)
- [5] Ehrenfreund, P., Charnley, S.B., Organic molecules in the interstellar medium, comets, and meteorites: a voyage from dark clouds to the early earth, *Annual Review of Astronomy and Astrophysics*, 38(1):(2000) pp. 427–483
- [6] Phillips, K.J., *et al.*, *Ultraviolet and X-ray Spectroscopy of the Solar Atmosphere*, volume 44, (Cambridge University Press Cambridge2008)
- [7] Hayes, J.M., Organic constituents of meteorites—a review, *Geochimica et Cosmochimica Acta*, 31(9):(1967) pp. 1395–1440
- [8] Anders, E., Origin, age, and composition of meteorites, *Space Science Reviews*, 3(5-6):(1964) pp. 583–714
- [9] Weisberg, M.K., *et al.*, Systematics and evaluation of meteorite classification, *Meteorites and the early solar system II*
- [10] Wikipedia commons, https://commons.wikimedia.org/wiki/File:Meteorite_Classification_after_Weissberg_McCoy_Krot_2006_Stony_Iron.svg, [Online; Accessed 2021-01-14]
- [11] Mason, B., The carbonaceous chondrites, *Space Science Reviews*, 1(4):(1963) pp. 621–646
- [12] Meteoritical bulletin, <https://www.lpi.usra.edu/meteor/metbull.php>, [Online; Accessed: 2020-08-24]
- [13] Cronin, J.R., Chang, S., Organic matter in meteorites: Molecular and isotopic analyses of the murchison meteorite, in *The chemistry of life’s origins*, pp. 209–258, (Springer1993)
- [14] Botta, O., Bada, J.L., Extraterrestrial organic compounds in meteorites, *Surveys in Geophysics*, 23(5):(2002) pp. 411–467
- [15] Sephton, M.A., Organic compounds in carbonaceous meteorites, *Natural product reports*, 19(3):(2002) pp. 292–311
- [16] Cronin, J.R., *et al.*, ^{13}C nmr spectroscopy of the insoluble carbon of carbonaceous chondrites, *Geochimica et Cosmochimica Acta*, 51(2):(1987) pp. 299–303
- [17] Remusat, L., *et al.*, The insoluble organic matter in carbonaceous chondrites: Chemical structure, isotopic composition and origin, *Comptes Rendus Geoscience*, 339(14-15):(2007) pp. 895–906
- [18] Cody, G., *et al.*, Solid-state (^1H and ^{13}C) nuclear magnetic resonance spectroscopy of insoluble organic residue in the murchison meteorite: a self-consistent quantitative analysis, *Geochimica et Cosmochimica Acta*, 66(10):(2002) pp. 1851–1865

-
- [19] Anders, E., Meteorites and the early solar system, *Annual Review of Astronomy and Astrophysics*, 9(1):(1971) pp. 1–34
- [20] Busemann, H., *et al.*, Characterization of insoluble organic matter in primitive meteorites by microraman spectroscopy, *Meteoritics & Planetary Science*, 42(7-8):(2007) pp. 1387–1416
- [21] Cody, G.D., Alexander, C.M.D., Nmr studies of chemical structural variation of insoluble organic matter from different carbonaceous chondrite groups, *Geochimica et Cosmochimica Acta*, 69(4):(2005) pp. 1085–1097
- [22] Derenne, S., Robert, F., Model of molecular structure of the insoluble organic matter isolated from murchison meteorite, *Meteoritics & Planetary Science*, 45(9):(2010) pp. 1461–1475
- [23] Quirico, E., *et al.*, Prevalence and nature of heating processes in cm and c2-ungrouped chondrites as revealed by insoluble organic matter, *Geochimica et Cosmochimica Acta*, 241:(2018) pp. 17–37
- [24] Quirico, E., *et al.*, Origin of insoluble organic matter in type 1 and 2 chondrites: New clues, new questions, *Geochimica et Cosmochimica Acta*, 136:(2014) pp. 80–99, doi:<https://doi.org/10.1016/j.gca.2014.03.025>
- [25] Sephton, M.A., Organic compounds in carbonaceous meteorites, *Natural product reports*, 19(3):(2002) pp. 292–311
- [26] Cronin, J.R., Pizzarello, S., Amino acids in meteorites, *Advances in Space Research*, 3(9):(1983) pp. 5–18, doi:[https://doi.org/10.1016/0273-1177\(83\)90036-4](https://doi.org/10.1016/0273-1177(83)90036-4)
- [27] Koga, T., Naraoka, H., A new family of extraterrestrial amino acids in the murchison meteorite, *Scientific Reports*, 7(1):(2017) p. 636, doi:[10.1038/s41598-017-00693-9](https://doi.org/10.1038/s41598-017-00693-9)
- [28] Kvenvolden, K.A., *et al.*, Nonprotein amino acids in the murchison meteorite, *Proceedings of the National Academy of Sciences*, 68(2):(1971) pp. 486–490
- [29] Sephton, M.A., Organic matter in ancient meteorites, *Astronomy & Geophysics*, 45(2):(2004) pp. 2–8
- [30] Burton, A.S., *et al.*, Understanding prebiotic chemistry through the analysis of extraterrestrial amino acids and nucleobases in meteorites, *Chemical Society Reviews*, 41(16):(2012) pp. 5459–5472
- [31] Callahan, M.P., *et al.*, Carbonaceous meteorites contain a wide range of extraterrestrial nucleobases, *Proceedings of the National Academy of Sciences of the United States of America*, 108(34):(2011) pp. 13995–13998, doi:[10.1073/pnas.1106493108](https://doi.org/10.1073/pnas.1106493108)
- [32] Martins, Z., *et al.*, Extraterrestrial nucleobases in the murchison meteorite, *Earth and planetary science Letters*, 270(1-2):(2008) pp. 130–136
- [33] Cooper, G., *et al.*, Carbonaceous meteorites as a source of sugar-related organic compounds for the early earth, *Nature*, 414(6866):(2001) pp. 879–883
- [34] Furukawa, Y., *et al.*, Extraterrestrial ribose and other sugars in primitive meteorites, *Proceedings of the National Academy of Sciences*, 116(49):(2019) pp. 24440–24445, doi:[10.1073/pnas.1907169116](https://doi.org/10.1073/pnas.1907169116)
-

-
- [35] Aponte, J.C., *et al.*, Extraterrestrial organic compounds and cyanide in the cm2 carbonaceous chondrites aguas zarcas and murchison, *Meteoritics & Planetary Science*, 55(7):(2020) pp. 1509–1524
- [36] Lawless, J.G., Yuen, G.U., Quantification of monocarboxylic acids in the murchison carbonaceous meteorite, *Nature*, 282(5737):(1979) pp. 396–398
- [37] Yuen, G.U., Kvenvolden, K.A., Monocarboxylic acids in murray and murchison carbonaceous meteorites, *Nature*, 246(5431):(1973) pp. 301–303
- [38] Ruf, A., *et al.*, Data-driven astrochemistry: One step further within the origin of life puzzle, *Life*, 8(2):(2018) p. 18
- [39] Kawaguchi, J., *et al.*, Hayabusa—its technology and science accomplishment summary and hayabusa-2, *Acta Astronautica*, 62(10-11):(2008) pp. 639–647
- [40] Lauretta, D., *et al.*, Osiris-rex: sample return from asteroid (101955) bennu, *Space Science Reviews*, 212(1-2):(2017) pp. 925–984
- [41] Brown, G., Olivines and silicate spinels, *Reviews in mineralogy*, 5:(1980) pp. 275–381
- [42] Nakamura, A., Schmalzried, H., On the nonstoichiometry and point defects of olivine, *Physics and Chemistry of Minerals*, 10(1):(1983) pp. 27–37, doi:10.1007/BF01204323
- [43] Longwell, C.R., *et al.*, *Physical geology*, (John Wiley & Sons1969)
- [44] Smyth, J.R., *et al.*, Comparative crystal chemistry of orthosilicate minerals, *Reviews in mineralogy and geochemistry*, 41(1):(2000) pp. 187–209
- [45] Hirakawa, N., *et al.*, Aqueous alteration without initial water: possibility of organic-induced hydration of anhydrous silicates in meteorite parent bodies, *Earth, Planets and Space*, 73(1):(2021) pp. 1–11
- [46] Elmasry, W., *et al.*, Synthesis of organic matter in aqueous environments simulating small bodies in the solar system and the effects of minerals on amino acid formation, *Life*, 11(1):(2021) p. 32
- [47] Hirakawa, N., *et al.*, Effects of minerals on metamorphism of organic matter during thermal processes in meteorite parent bodies, *Icarus*, p. 114167
- [48] Christensen, U., Effects of phase transitions on mantle convection, *Annual Review of Earth and Planetary Sciences*, 23(1):(1995) pp. 65–87
- [49] Farina, V., Investigation of mechanically induced co2 storage and conversion driven by olivine weathering process
- [50] Gordeychik, B., *et al.*, Growth of, and diffusion in, olivine in ultra-fast ascending basalt magmas from shiveluch volcano, *Scientific Reports*, 8(1):(2018) p. 11775, doi:10.1038/s41598-018-30133-1
- [51] Fournelle, J., An investigation of “san carlos olivine”: Comparing usnm-distributed material with commercially available material, *Microscopy and Microanalysis*, 17(S2):(2011) pp. 842–843, doi:10.1017/S1431927611005083
- [52] Frey, F.A., Prinz, M., Ultramafic inclusions from san carlos, arizona: Petrologic and geochemical data bearing on their petrogenesis, *Earth and Planetary Science Letters*, 38(1):(1978) pp. 129–176, doi:https://doi.org/10.1016/0012-821X(78)90130-9
-

-
- [53] Jarosewich, E., *et al.*, Reference samples for electron microprobe analysis*, *Geostandards Newsletter*, 4(1):(1980) pp. 43–47, doi:10.1111/j.1751-908X.1980.tb00273.x
- [54] Palme, H., Fegley Jr, B., High-temperature condensation of iron-rich olivine in the solar nebula, *Earth and Planetary Science Letters*, 101(2-4):(1990) pp. 180–195
- [55] Mason, B., Olivine composition in chondrites, *Geochimica et Cosmochimica Acta*, 27(10):(1963) pp. 1011 – 1023, doi:https://doi.org/10.1016/0016-7037(63)90062-0
- [56] Ireland, T., *et al.*, Magnesium isotopic compositions of olivine, spinel, and hibonite from the muchison carbonaceous chondrite, *Geochimica et Cosmochimica Acta*, 50(7):(1986) pp. 1413 – 1421, doi:https://doi.org/10.1016/0016-7037(86)90314-5
- [57] Cruikshank, D.P., Hartmann, W.K., The meteorite-asteroid connection: Two olivine-rich asteroids, *Science*, 223(4633):(1984) pp. 281–283
- [58] Sunshine, J.M., *et al.*, Olivine-dominated asteroids and meteorites: Distinguishing nebular and igneous histories, *Meteoritics & Planetary Science*, 42(2):(2007) pp. 155–170
- [59] Hoefen, T.M., *et al.*, Discovery of olivine in the nili fossae region of mars, *Science*, 302(5645):(2003) pp. 627–630
- [60] Mustard, J.F., *et al.*, Olivine and pyroxene diversity in the crust of mars, *Science*, 307(5715):(2005) pp. 1594–1597
- [61] Norman, M., *et al.*, Magnesium isotopic composition of olivine from the earth, mars, moon, and pallasite parent body, *Geophysical research letters*, 33(15)
- [62] Isaacson, P.J., *et al.*, Remote compositional analysis of lunar olivine-rich lithologies with moon mineralogy mapper (m3) spectra, *Journal of Geophysical Research: Planets*, 116(E6)
- [63] Palme, H., Fegley, B., High-temperature condensation of iron-rich olivine in the solar nebula, *Earth and Planetary Science Letters*, 101(2):(1990) pp. 180–195, doi:https://doi.org/10.1016/0012-821X(90)90152-N
- [64] Buseck, P.R., Goldstein, J.I., Olivine compositions and cooling rates of pallasitic meteorites, *Geological Society of America Bulletin*, 80(11):(1969) pp. 2141–2158
- [65] Donohue, P.H., *et al.*, Experimentally determined subsolidus metal-olivine element partitioning with applications to pallasites, *Geochimica et cosmochimica acta*, 222:(2018) pp. 305–318
- [66] Mason, B., *Meteorites* wiley, New York, New York, USA
- [67] Boesenberg, J.S., *et al.*, A petrological and chemical reexamination of main group pallasite formation, *Geochimica et Cosmochimica Acta*, 89:(2012) pp. 134–158
- [68] Hsu, W., Minor element zoning and trace element geochemistry of pallasites, *Meteoritics & Planetary Science*, 38(8):(2003) pp. 1217–1241
- [69] Leitch, C., *et al.*, Minor elements in pallasites: Zoning in springwater olivine, in *Lunar and Planetary Science Conference*, volume 10, pp. 716–718
- [70] Miyamoto, M., Chemical zoning of olivine in several pallasites, *Journal of Geophysical Research: Planets*, 102(E9):(1997) pp. 21613–21618
-

-
- [71] Tomiyama, T., Huss, G., Minor and trace element zoning in pallasite olivine: modeling pallasite thermal history, in 37th Annual Lunar and Planetary Science Conference, volume 37
- [72] Bondar, Y.V., Perelygin, V., Cosmic history of some pallasites based on fossil track studies, Radiation measurements, 36(1-6):(2003) pp. 367–373
- [73] McCaig, A.M., *et al.*, Serpentinite in the earth system, Philos Trans A Math Phys Eng Sci, 378(2165):(2020) p. 20190332, doi:10.1098/rsta.2019.0332
- [74] Klein, F., *et al.*, Magnetite in seafloor serpentinite—some like it hot, Geology, 42, doi:10.1130/G35068.1
- [75] Berndt, M.E., *et al.*, Reduction of co₂ during serpentinization of olivine at 300 degrees c and 500 bar (vol 24, pg 351, 1996), Geology, 24(7):(1996) pp. 671–671
- [76] Holm, N.G., *et al.*, Serpentinization and the formation of h₂ and ch₄ on celestial bodies (planets, moons, comets), Astrobiology, 15(7):(2015) pp. 587–600, doi:10.1089/ast.2014.1188
- [77] McCollom, T.M., *et al.*, The effect of ph on rates of reaction and hydrogen generation during serpentinization, Philos Trans A Math Phys Eng Sci, 378(2165):(2020) p. 20180428, doi:10.1098/rsta.2018.0428
- [78] McCollom, T.M., Seewald, J.S., A reassessment of the potential for reduction of dissolved co₂ to hydrocarbons during serpentinization of olivine, Geochimica et Cosmochimica Acta, 65(21):(2001) pp. 3769–3778, doi:https://doi.org/10.1016/S0016-7037(01)00655-X
- [79] Allen, D.E., Seyfried Jr, W., Serpentinization and heat generation: constraints from lost city and rainbow hydrothermal systems, Geochimica et Cosmochimica Acta, 68(6):(2004) pp. 1347–1354
- [80] Reeves, E.P., Fiebig, J., Abiotic synthesis of methane and organic compounds in earth’s lithosphere, Elements: An International Magazine of Mineralogy, Geochemistry, and Petrology, 16(1):(2020) pp. 25–31
- [81] Boetius, A., Lost city life, Science, 307(5714):(2005) pp. 1420–1422
- [82] Mumma, M.J., *et al.*, Strong release of methane on mars in northern summer 2003, Science, 323(5917):(2009) pp. 1041–5, doi:10.1126/science.1165243
- [83] Ernst, T., *et al.*, High pressure experiments on the equilibrium olivine–co₂–enstatite–carbonate in natural system, High Pressure in Geosciences
- [84] Fyfe, W., Lattice energies, phase transformations and volatiles in the mantle, Physics of the Earth and Planetary Interiors, 3:(1970) pp. 196–200
- [85] Oberheuser, G., *et al.*, Carbon in olivine single crystals analyzed by the 12c(d, p)13c method and by photoelectron spectroscopy, Geochimica et Cosmochimica Acta, 47(6):(1983) pp. 1117–1129, doi:https://doi.org/10.1016/0016-7037(83)90242-9
- [86] Varela, M.E., Metrich, N., Carbon in olivines of chondritic meteorites, Geochimica Et Cosmochimica Acta, 64(19):(2000) pp. 3433–3438, doi:Doi10.1016/S0016-7037(00)00432-4
- [87] Freund, F., *et al.*, Organic protomolecule assembly in igneous minerals, Proc Natl Acad Sci U S A, 98(5):(2001) pp. 2142–7, doi:10.1073/pnas.061513298
-

-
- [88] Ruf, A., *et al.*, Previously unknown class of metalorganic compounds revealed in meteorites, *Proc Natl Acad Sci U S A*, 114(11):(2017) pp. 2819–2824, doi:10.1073/pnas.1616019114
- [89] Hanon, P., *et al.*, High carbon concentrations in meteoritic chondrules: A record of metal-silicate differentiation, *Geochimica Et Cosmochimica Acta*, 62(5):(1998) pp. 903–913, doi:10.1016/S0016-7037(97)00385-2
- [90] Mathez, E., *et al.*, Carbon in olivine: Results from nuclear reaction analysis, *Journal of Geophysical Research: Solid Earth*, 92(B5):(1987) pp. 3500–3506
- [91] Tingle, T.N., *et al.*, Organic compounds on crack surfaces in olivine from san carlos, arizona and hualalai volcano, hawaii, *Geochimica et Cosmochimica Acta*, 54(2):(1990) pp. 477–485, doi:https://doi.org/10.1016/0016-7037(90)90337-K
- [92] Keppler, H., *et al.*, Carbon solubility in olivine and the mode of carbon storage in the earth’s mantle, *Nature*, 424(6947):(2003) pp. 414–6, doi:10.1038/nature01828
- [93] Dasgupta, R., Hirschmann, M.M., The deep carbon cycle and melting in earth’s interior, *Earth and Planetary Science Letters*, 298(1-2):(2010) pp. 1–13
- [94] Lee, C.T.A., *et al.*, A Framework for Understanding Whole-Earth Carbon Cycling, pp. 313–357, (Cambridge University Press2019)
- [95] Orcutt, B.N., *et al.*, Deep Carbon: Past to Present, (Cambridge University Press2019)
- [96] Yokochi, R., Marty, B., Geochemical constraints on mantle dynamics in the hadean, *Earth and Planetary Science Letters*, 238(1):(2005) pp. 17–30, doi:https://doi.org/10.1016/j.epsl.2005.07.020
- [97] Ménez, B., *et al.*, Life in the hydrated suboceanic mantle, *Nature Geoscience*, 5(2):(2012) pp. 133–137, doi:10.1038/ngeo1359
- [98] Templeton, A.S., Ellison, E.T., Formation and loss of metastable brucite: does fe(ii)-bearing brucite support microbial activity in serpentinizing ecosystems?, *Philosophical Transactions of the Royal Society A: Mathematical, Physical and Engineering Sciences*, 378(2165):(2020) p. 20180423, doi:10.1098/rsta.2018.0423
- [99] Leonzio, G., Process analysis of biological sabatier reaction for bio-methane production, *Chemical Engineering Journal*, 290:(2016) pp. 490–498, doi:10.1016/j.cej.2016.01.068
- [100] Sabatier, P., *La catalyse en chimie organique*, librairie polytechnique
- [101] Adesina, A.A., Hydrocarbon synthesis via fischer-tropsch reaction: travaux and triumphs, *Applied Catalysis A: General*, 138(2):(1996) pp. 345–367
- [102] Masters, C., The fischer-tropsch reaction, *Advances in Organometallic Chemistry*, 17:(1979) pp. 61–103
- [103] McGeoch, M., *et al.*, Hemolithin: a meteoritic protein containing iron and lithium, arXiv preprint arXiv:200211688
- [104] Smith, K.E., *et al.*, Organometallic compounds as carriers of extraterrestrial cyanide in primitive meteorites, *Nature Communications*, 10(1):(2019) p. 2777, doi:10.1038/s41467-019-10866-x
-

-
- [105] Nebbioso, A., Piccolo, A., Molecular characterization of dissolved organic matter (dom): a critical review, *Analytical and bioanalytical chemistry*, 405(1):(2013) pp. 109–124
- [106] Dittmar, T., *et al.*, A simple and efficient method for the solid-phase extraction of dissolved organic matter (spe-dom) from seawater, *Limnology and Oceanography: Methods*, 6(6):(2008) pp. 230–235
- [107] Derrien, M., *et al.*, Comparing discrimination capabilities of fluorescence spectroscopy versus ft-icr-ms for sources and hydrophobicity of sediment organic matter, *Environmental Science and Pollution Research*, 25(2):(2018) pp. 1892–1902
- [108] Wang, H., *et al.*, Molecular transformation of crude oil contaminated soil after bioelectrochemical degradation revealed by ft-icr mass spectrometry, *Environmental Science & Technology*, 54(4):(2020) pp. 2500–2509
- [109] Gonsior, M., FT-ICR MS and Orbitrap mass spectrometry approaches in environmental chemistry, pp. 407–423, (Elsevier2019)
- [110] Bae, E., *et al.*, Identification of about 30 000 chemical components in shale oils by electrospray ionization (esi) and atmospheric pressure photoionization (appi) coupled with 15 t fourier transform ion cyclotron resonance mass spectrometry (ft-icr ms) and a comparison to conventional oil, *Energy & Fuels*, 24(4):(2010) pp. 2563–2569, doi:10.1021/ef100060b
- [111] Gonsior, M., *et al.*, Molecular characterization of effluent organic matter identified by ultrahigh resolution mass spectrometry, *Water Research*, 45(9):(2011) pp. 2943–2953, doi:https://doi.org/10.1016/j.watres.2011.03.016
- [112] Shakeri Yekta, S., *et al.*, Characterization of dissolved organic matter in full scale continuous stirred tank biogas reactors using ultrahigh resolution mass spectrometry: A qualitative overview, *Environmental Science & Technology*, 46(22):(2012) pp. 12711–12719, doi:10.1021/es3024447
- [113] Zhang, H., *et al.*, Study on transformation of natural organic matter in source water during chlorination and its chlorinated products using ultrahigh resolution mass spectrometry, *Environmental science & technology*, 46(8):(2012) pp. 4396–4402
- [114] Lavonen, E.E., *et al.*, Selective chlorination of natural organic matter: identification of previously unknown disinfection byproducts, *Environmental science & technology*, 47(5):(2013) pp. 2264–2271
- [115] Tseng, L.Y., *et al.*, Molecular characteristics and differences of effluent organic matter from parallel activated sludge and integrated fixed-film activated sludge (ifas) processes, *Environmental Science and Technology*, 47(18):(2013) pp. 10277–10284, doi:10.1021/es4002482
- [116] Gonsior, M., *et al.*, Changes in dissolved organic matter during the treatment processes of a drinking water plant in sweden and formation of previously unknown disinfection byproducts, *Environmental science & technology*, 48(21):(2014) pp. 12714–12722
- [117] Zhai, H., *et al.*, Formation of brominated disinfection byproducts during chloramination of drinking water: new polar species and overall kinetics, *Environmental science & technology*, 48(5):(2014) pp. 2579–2588

-
- [118] Zhang, H., *et al.*, Characterization of unknown brominated disinfection byproducts during chlorination using ultrahigh resolution mass spectrometry, *Environmental science & technology*, 48(6):(2014) pp. 3112–3119
- [119] Bletsou, A.A., *et al.*, Targeted and non-targeted liquid chromatography-mass spectrometric workflows for identification of transformation products of emerging pollutants in the aquatic environment, *TrAC Trends in Analytical Chemistry*, 66:(2015) pp. 32–44, doi:<https://doi.org/10.1016/j.trac.2014.11.009>
- [120] Gonsior, M., *et al.*, Bromination of marine dissolved organic matter following full scale electrochemical ballast water disinfection, *Environmental science & technology*, 49(15):(2015) pp. 9048–9055
- [121] Leendert, V., *et al.*, Trends in liquid chromatography coupled to high-resolution mass spectrometry for multi-residue analysis of organic micropollutants in aquatic environments, *TrAC Trends in Analytical Chemistry*, 67:(2015) pp. 192–208, doi:<https://doi.org/10.1016/j.trac.2015.01.010>
- [122] Picó, Y., Barceló, D., Transformation products of emerging contaminants in the environment and high-resolution mass spectrometry: a new horizon, *Analytical and Bioanalytical Chemistry*, 407(21):(2015) pp. 6257–6273, doi:10.1007/s00216-015-8739-6
- [123] Schymanski, E.L., *et al.*, Non-target screening with high-resolution mass spectrometry: critical review using a collaborative trial on water analysis, *Analytical and Bioanalytical Chemistry*, 407(21):(2015) pp. 6237–6255, doi:10.1007/s00216-015-8681-7
- [124] Dvorski, S.E.M., *et al.*, Geochemistry of dissolved organic matter in a spatially highly resolved groundwater petroleum hydrocarbon plume cross-section, *Environmental Science & Technology*, 50(11):(2016) pp. 5536–5546, doi:10.1021/acs.est.6b00849
- [125] Luek, J.L., *et al.*, Halogenated organic compounds identified in hydraulic fracturing wastewaters using ultrahigh resolution mass spectrometry, *Environmental Science & Technology*, 51(10):(2017) pp. 5377–5385, doi:10.1021/acs.est.6b06213
- [126] Maizel, A.C., Remucal, C.K., The effect of advanced secondary municipal wastewater treatment on the molecular composition of dissolved organic matter, *Water Research*, 122:(2017) pp. 42–52, doi:<https://doi.org/10.1016/j.watres.2017.05.055>
- [127] Wang, X., *et al.*, New insights into trihalomethane and haloacetic acid formation potentials: correlation with the molecular composition of natural organic matter in source water, *Environmental science & technology*, 51(4):(2017) pp. 2015–2021
- [128] Wang, X., *et al.*, Molecular characterization of effluent organic matter in secondary effluent and reclaimed water: Comparison to natural organic matter in source water, *Journal of Environmental Sciences*, 63:(2018) pp. 140–146, doi:<https://doi.org/10.1016/j.jes.2017.03.020>
- [129] Bell, N.G.A., *et al.*, Molecular level study of hot water extracted green tea buried in soils - a proxy for labile soil organic matter, *Sci Rep*, 10(1):(2020) p. 1484, doi:10.1038/s41598-020-58325-8
- [130] Avneri-Katz, S., *et al.*, Adsorptive fractionation of dissolved organic matter (dom) by mineral soil: Macroscale approach and molecular insight, *Organic Geochemistry*, 103:(2017) pp. 113–124, doi:<https://doi.org/10.1016/j.orggeochem.2016.11.004>
-

-
- [131] Choi, J.H., *et al.*, Chemical characterization of dissolved organic matter in moist acidic tussock tundra soil using ultra-high resolution 15t ft-icr mass spectrometry, *Biotechnology and Bioprocess Engineering*, 22(5):(2017) pp. 637–646, doi:10.1007/s12257-017-0121-4
- [132] D’Andrilli, J., *et al.*, Characterization of dissolved organic matter in northern peatland soil porewaters by ultra high resolution mass spectrometry, *Organic Geochemistry*, 41(8):(2010) pp. 791–799, doi:https://doi.org/10.1016/j.orggeochem.2010.05.009
- [133] Guigue, J., *et al.*, Ultrahigh-resolution ft-icr mass spectrometry for molecular characterisation of pressurised hot water-extractable organic matter in soils, *Biogeochemistry*, 128(3):(2016) pp. 307–326, doi:10.1007/s10533-016-0209-5
- [134] Ji, M., *et al.*, Molecular and microbial insights towards understanding the effects of hydrochar on methane emission from paddy soil, *Science of The Total Environment*, 714:(2020) p. 136769, doi:https://doi.org/10.1016/j.scitotenv.2020.136769
- [135] Lu, M., *et al.*, Remediation of petroleum-contaminated soil after composting by sequential treatment with fenton-like oxidation and biodegradation, *Bioresource Technology*, 101(7):(2010) pp. 2106–2113, doi:https://doi.org/10.1016/j.biortech.2009.11.002
- [136] Mangal, V., *et al.*, Linking molecular and optical properties of dissolved organic matter across a soil-water interface on akimiski island (nunavut, canada), *Science of The Total Environment*, 704:(2020) p. 135415, doi:https://doi.org/10.1016/j.scitotenv.2019.135415
- [137] Roth, V.N., *et al.*, The molecular composition of dissolved organic matter in forest soils as a function of ph and temperature, *PLoS one*, 10(3):(2015) pp. e0119188–e0119188, doi:10.1371/journal.pone.0119188
- [138] Zhang, P., *et al.*, Spectroscopic and molecular characterization of biochar-derived dissolved organic matter and the associations with soil microbial responses, *Science of The Total Environment*, 708:(2020) p. 134619, doi:https://doi.org/10.1016/j.scitotenv.2019.134619
- [139] Vuitton, V., *et al.*, Very high resolution mass spectrometry of hcn polymers and tholins, *Faraday Discussions*, 147(0):(2010) pp. 495–508, doi:10.1039/C003758C
- [140] Danger, G., *et al.*, Insight into the molecular composition of laboratory organic residues produced from interstellar/pre-cometary ice analogues using very high resolution mass spectrometry, *Geochimica et Cosmochimica Acta*, 189:(2016) pp. 184–196, doi:https://doi.org/10.1016/j.gca.2016.06.014
- [141] Schmitt-Kopplin, P., *et al.*, High molecular diversity of extraterrestrial organic matter in Murchison meteorite revealed 40 years after its fall, *Proc Natl Acad Sci U S A*, 107(7):(2010) pp. 2763–8, doi:10.1073/pnas.0912157107
- [142] HAACK, H., *et al.*, Maribo—a new cm fall from Denmark, *Meteoritics & Planetary Science*, 47(1):(2012) pp. 30–50, doi:10.1111/j.1945-5100.2011.01311.x
- [143] Orthous-Daunay, F.R., *et al.*, Polymeric series of large nonpolar molecules found in Murchison by Orbitrap mass spectrometry, *Meteoritics and Planetary Science Supplement*, 76:(2013) p. 5247
-

-
- [144] Popova, O.P., *et al.*, Chelyabinsk airburst, damage assessment, meteorite recovery, and characterization, *Science*, 342(6162):(2013) pp. 1069–1073, doi:10.1126/science.1242642
- [145] Keil, K., *et al.*, The vicência meteorite fall: A new unshocked (s1) weakly metamorphosed (3.2) il chondrite, *Meteoritics & Planetary Science*, 50(6):(2015) pp. 1089–1111, doi:10.1111/maps.12456
- [146] Naraoka, H., *et al.*, Molecular evolution of n-containing cyclic compounds in the parent body of the murchison meteorite, *ACS Earth and Space Chemistry*, 1(9):(2017) pp. 540–550, doi:10.1021/acsearthspacechem.7b00058
- [147] Hertzog, J., *et al.*, Profiling murchison soluble organic matter for new organic compounds with appi- and esi-ft-icr ms, *Life (Basel)*, 9(2), doi:10.3390/life9020048
- [148] Hertkorn, N., *et al.*, Nontarget analysis of murchison soluble organic matter by high-field nmr spectroscopy and fticr mass spectrometry, *Magn Reson Chem*, 53(9):(2015) pp. 754–68, doi:10.1002/mrc.4249
- [149] Langbroek, M., *et al.*, The cm carbonaceous chondrite regolith diepenveen, *Meteoritics & Planetary Science*, 54(7):(2019) pp. 1431–1461, doi:10.1111/maps.13297
- [150] Cody, G.D., *et al.*, Solid-state (1h and 13c) nuclear magnetic resonance spectroscopy of insoluble organic residue in the murchison meteorite: a self-consistent quantitative analysis, *Geochimica et Cosmochimica Acta*, 66(10):(2002) pp. 1851–1865, doi:https://doi.org/10.1016/S0016-7037(01)00888-2
- [151] Hewins, R.H., *et al.*, The paris meteorite, the least altered cm chondrite so far, *Geochimica et Cosmochimica Acta*, 124:(2014) pp. 190–222, doi:https://doi.org/10.1016/j.gca.2013.09.014
- [152] Jenniskens, P., *et al.*, Radar-enabled recovery of the sutter’s mill meteorite, a carbonaceous chondrite regolith breccia, *Science*, 338(6114):(2012) pp. 1583–1587, doi:10.1126/science.1227163
- [153] Jenniskens, P., *et al.*, Fall, recovery, and characterization of the novato l6 chondrite breccia, *Meteoritics & Planetary Science*, 49(8):(2014) pp. 1388–1425, doi:10.1111/maps.12323
- [154] Purcell, E.M., *et al.*, Resonance absorption by nuclear magnetic moments in a solid, *Physical review*, 69(1-2):(1946) p. 37
- [155] Mao, J., *et al.*, Advanced solid-state nmr spectroscopy of natural organic matter, *Progress in Nuclear Magnetic Resonance Spectroscopy*, 100:(2017) pp. 17–51, doi:https://doi.org/10.1016/j.pnmrs.2016.11.003
- [156] Hertkorn, N., *et al.*, High-field nmr spectroscopy and fticr mass spectrometry: powerful discovery tools for the molecular level characterization of marine dissolved organic matter, *Biogeosciences*, 10(3):(2013) pp. 1583–1624, doi:10.5194/bg-10-1583-2013
- [157] Lankes, U., *et al.*, Search for basic relationships between “molecular size” and “chemical structure” of aquatic natural organic matter—answers from 13c and 15n cpmas nmr spectroscopy, *Water Research*, 42(4):(2008) pp. 1051–1060, doi:https://doi.org/10.1016/j.watres.2007.09.028

-
- [158] Drewes, J.E., Fox, P., Fate of natural organic matter (nom) during groundwater recharge using reclaimed water, *Water Science and Technology*, 40(9):(1999) pp. 241–248, doi:[https://doi.org/10.1016/S0273-1223\(99\)00662-9](https://doi.org/10.1016/S0273-1223(99)00662-9)
- [159] Koegel-Knabner, I., ^{13}C and ^{15}N nmr spectroscopy as a tool in soil organic matter studies, *Geoderma*, 80(3):(1997) pp. 243–270, doi:[https://doi.org/10.1016/S0016-7061\(97\)00055-4](https://doi.org/10.1016/S0016-7061(97)00055-4)
- [160] Keeler, C., Maciel, G.E., Quantitation in the solid-state ^{13}C nmr analysis of soil and organic soil fractions, *Analytical Chemistry*, 75(10):(2003) pp. 2421–2432, doi:10.1021/ac020679k
- [161] Preston, C.M., Applications of nmr to soil organic matter analysis: history and prospects, *Soil Science*, 161(3):(1996) pp. 144–166
- [162] Mahieu, N., *et al.*, Statistical analysis of published carbon-13 cpmas nmr spectra of soil organic matter, *Soil Science Society of America Journal*, 63(2):(1999) pp. 307–319, doi:10.2136/sssaj1999.03615995006300020008x
- [163] Mathers, N., *et al.*, Recent advances in the application of ^{13}C and ^{15}N nmr spectroscopy to soil organic matter studies, *Soil Research*, 38(4):(2000) pp. 769–787
- [164] Peuravuori, J., *et al.*, Critical comments on accuracy of quantitative determination of natural humic matter by solid state ^{13}C nmr spectroscopy, *Talanta*, 59(1):(2003) pp. 177–189, doi:[https://doi.org/10.1016/S0039-9140\(02\)00476-9](https://doi.org/10.1016/S0039-9140(02)00476-9)
- [165] Cody, G.D., Alexander, C.M.D., Nmr studies of chemical structural variation of insoluble organic matter from different carbonaceous chondrite groups, *Geochimica et Cosmochimica Acta*, 69(4):(2005) pp. 1085–1097, doi:<https://doi.org/10.1016/j.gca.2004.08.031>
- [166] Cronin, J.R., Pizzarello, S., Aliphatic hydrocarbons of the murchison meteorite, *Geochimica et Cosmochimica Acta*, 54(10):(1990) pp. 2859–2868, doi:[https://doi.org/10.1016/0016-7037\(90\)90020-L](https://doi.org/10.1016/0016-7037(90)90020-L)
- [167] Pizzarello, S., *et al.*, The organic content of the tagish lake meteorite, *Science*, 293(5538):(2001) p. 2236, doi:10.1126/science.1062614
- [168] Fundamentals and General Terminology*, pp. 9–48, doi:10.1002/9783527816347.ch2
- [169] Richardson, S.D., The role of gc-ms and lc-ms in the discovery of drinking water disinfection by-products, *Journal of Environmental Monitoring*, 4(1):(2002) pp. 1–9
- [170] Cimetiere, N., *et al.*, Standard addition method for the determination of pharmaceutical residues in drinking water by spe-lc-ms/ms, *Environmental technology*, 34(22):(2013) pp. 3031–3041
- [171] Wang, L., *et al.*, Photochemical fate of beta-blockers in nom enriched waters, *Science of the total environment*, 426:(2012) pp. 289–295
- [172] Halling-Sørensen, B., *et al.*, Characterisation of the abiotic degradation pathways of oxytetracyclines in soil interstitial water using lc-ms-ms, *Chemosphere*, 50(10):(2003) pp. 1331–1342
- [173] Bugsel, B., Zwiener, C., Lc-ms screening of poly- and perfluoroalkyl substances in contaminated soil by Kendrick mass analysis, *Analytical and Bioanalytical Chemistry*, pp. 1–9
-

-
- [174] Glavin, D.P., *et al.*, Amino acid analyses of antarctic cm2 meteorites using liquid chromatography-time of flight-mass spectrometry, *Meteoritics & Planetary Science*, 41(6):(2006) pp. 889–902
- [175] Martins, Z., *et al.*, Indigenous amino acids in primitive cr meteorites, *Meteoritics & Planetary Science*, 42(12):(2007) pp. 2125–2136
- [176] Rios, A., Cooper, G., Finding evidence of a prebiotic pyruvate reaction network in meteorites
- [177] Lawrence, E.O., Livingston, M.S., The production of high speed light ions without the use of high voltages, *Physical Review*, 40(1):(1932) p. 19
- [178] Hipple, J., *et al.*, A precise method of determining the faraday by magnetic resonance, *Physical Review*, 76(12):(1949) p. 1877
- [179] Wobschall, D., *et al.*, Ion cyclotron resonance and the determination of collision cross sections, *Physical Review*, 131(4):(1963) p. 1565
- [180] Wobschall, D., Ion cyclotron resonance spectrometer, *Review of Scientific Instruments*, 36(4):(1965) pp. 466–475
- [181] Easterling, M.L., Agar, J.N., Fundamentals, strengths, and future directions for Fourier transform ion cyclotron resonance mass spectrometry, pp. 63–88, (Elsevier2019)
- [182] Cooley, J., *et al.*, The application of the fast fourier transform algorithm to the estimation of spectra and cross-spectra, *Journal of sound and vibration*, 12(3):(1970) pp. 339–352
- [183] Cooley, J.W., *et al.*, The fast fourier transform and its applications, *IEEE Transactions on Education*, 12(1):(1969) pp. 27–34
- [184] Cooley, J.W., Tukey, J.W., An algorithm for the machine calculation of complex fourier series, *Mathematics of computation*, 19(90):(1965) pp. 297–301
- [185] Smith, D.F., *et al.*, 21 tesla ft-icr mass spectrometer for ultrahigh-resolution analysis of complex organic mixtures, *Analytical chemistry*, 90(3):(2018) pp. 2041–2047
- [186] Nikolaev, E.N., *et al.*, Fourier transform ion cyclotron resonance (ft icr) mass spectrometry: Theory and simulations, *Mass Spectrometry Reviews*, 35(2):(2016) pp. 219–258, doi:10.1002/mas.21422
- [187] Nikolaev, E.N., *et al.*, Initial experimental characterization of a new ultra-high resolution fticr cell with dynamic harmonization, *Journal of the American Society for Mass Spectrometry*, 22(7):(2011) pp. 1125–1133, doi:10.1021/jasms.8b04059
- [188] Gross, J.H., Basem kanawati and philippe schmitt-kopplin (eds.): Fundamentals and applications of fourier transform mass spectrometry, *Analytical and Bioanalytical Chemistry*, 412(2):(2020) pp. 257–258
- [189] Tsybin, Y.O., *et al.*, Advanced fundamentals in Fourier transform mass spectrometry, pp. 113–132, (Elsevier2019)
- [190] G Marshall, A., *et al.*, Mass resolution and mass accuracy: how much is enough?, *Mass spectrometry (Tokyo, Japan)*, 2(Spec Iss):(2013) pp. S0009–S0009, doi:10.5702/massspectrometry.S0009

-
- [191] Kanawati, B., *et al.*, Chapter 6 - Data processing and automation in Fourier transform mass spectrometry, pp. 133–185, (Elsevier2019), doi:<https://doi.org/10.1016/B978-0-12-814013-0.00006-5>
- [192] Munson, M.S., Field, F.H., Chemical ionization mass spectrometry. i. general introduction, *Journal of the American Chemical Society*, 88(12):(1966) pp. 2621–2630
- [193] Kreutzer, L., *et al.*, In situ metabolomics in cancer tissue by high-resolution mass spectrometry imaging, pp. 253–279, (Elsevier2019)
- [194] Wang, Y., *et al.*, Current state of the art of mass spectrometry-based metabolomics studies—a review focusing on wide coverage, high throughput and easy identification, *Rsc Advances*, 5(96):(2015) pp. 78728–78737
- [195] Li, D.X., *et al.*, Gas chromatography coupled to atmospheric pressure ionization mass spectrometry (gc-api-ms), *Analytica chimica acta*, 891:(2015) pp. 43–61
- [196] Gu, C., *et al.*, Mass spectrometry in small molecule drug development, *Am Pharm Rev*
- [197] Bruins, A.P., Mechanistic aspects of electrospray ionization, *Journal of Chromatography A*, 794(1):(1998) pp. 345–357, doi:[https://doi.org/10.1016/S0021-9673\(97\)01110-2](https://doi.org/10.1016/S0021-9673(97)01110-2)
- [198] Ho, C.S., *et al.*, Electrospray ionisation mass spectrometry: principles and clinical applications, *The Clinical biochemist Reviews*, 24(1):(2003) pp. 3–12
- [199] Fenn, J.B., *et al.*, Electrospray ionization for mass spectrometry of large biomolecules, *Science*, 246(4926):(1989) pp. 64–71
- [200] Leito, I., *et al.*, Towards the electrospray ionization mass spectrometry ionization efficiency scale of organic compounds, *Rapid Communications in Mass Spectrometry: An International Journal Devoted to the Rapid Dissemination of Up-to-the-Minute Research in Mass Spectrometry*, 22(3):(2008) pp. 379–384
- [201] Kauppila, T.J., *et al.*, Atmospheric pressure photoionization mass spectrometry. ionization mechanism and the effect of solvent on the ionization of naphthalenes, *Analytical chemistry*, 74(21):(2002) pp. 5470–5479
- [202] Ghislain, T., *et al.*, Detection and monitoring of pah and oxy-pahs by high resolution mass spectrometry: Comparison of esi, apci and appi source detection, *Journal of the American Society for Mass Spectrometry*, 23(3):(2012) pp. 530–536, doi: [10.1021/jasms.8b04234](https://doi.org/10.1021/jasms.8b04234)
- [203] Kuhn, W., Nmr microscopy—fundamentals, limits and possible applications, *Ange wandte Chemie International Edition in English*, 29(1):(1990) pp. 1–19, doi: [10.1002/anie.199000013](https://doi.org/10.1002/anie.199000013)
- [204] Bloch, F., Nuclear induction, *Physical review*, 70(7-8):(1946) p. 460
- [205] Nakanishi, K., One-dimensional and two-dimensional NMR spectra by modern pulse techniques, (University Science Books1990)
- [206] Martin, G.E., Zektzer, A.S., Two-dimensional NMR methods for establishing molecular connectivity: a chemist’s guide to experiment selection, performance, and interpretation, (VCH New York1988)

-
- [207] Aue, W., *et al.*, Two-dimensional spectroscopy. application to nuclear magnetic resonance, *The Journal of Chemical Physics*, 64(5):(1976) pp. 2229–2246
- [208] Pohmann, R., *Physical basics of NMR*, pp. 3–21, (Springer2011)
- [209] Legchenko, A., *The basics of nmr, Magnetic Resonance Imaging for Groundwater*, pp. 15–44
- [210] Hornak, J.P., *The basics of nmr*, 1997, Cited on, p. 9
- [211] Hiroaki, H., *Magnetic resonance spectroscopy. 1. basics of nmr*, *Bunko Kenkyu*, 55(1):(2006) pp. 54–66
- [212] Friebolin, H., *Ein-und zweidimensionale NMR-Spektroskopie: eine Einfuehrung*, (John Wiley & Sons2013)
- [213] Burnell, E.E., De Lange, C.A., *NMR of ordered liquids*, (Springer Science & Business Media2013)
- [214] Runge, F.F., *Der Bildungstrieb der Stoffe: veranschaulicht in selbstständig gewachsenen Bildern; Fortsetzung der Musterbilder*, (Selbstverl.1855)
- [215] Martin, A.J., Synge, R.L., A new form of chromatogram employing two liquid phases: A theory of chromatography. 2. application to the micro-determination of the higher monoamino-acids in proteins, *Biochemical Journal*, 35(12):(1941) p. 1358
- [216] Halasz, I., Horvath, C., Open tube columns with impregnated thin layer support for gas chromatography, *Analytical Chemistry*, 35(4):(1963) pp. 499–505
- [217] Huber, J., Hulsman, J., A study of liquid chromatography in columns, the time of separation, *Analytica chimica acta*, 38:(1967) pp. 305–313
- [218] Kirkland, J.J., High-performance ultraviolet photometric detector for use with efficient liquid chromatographic columns, *Analytical Chemistry*, 40(2):(1968) pp. 391–396
- [219] Touchstone, J.C., History of chromatography, *Journal of Liquid Chromatography & Related Technologies*, 16(8):(1993) pp. 1647–1665
- [220] Seidel-Morgenstern, A., *Fundamentals and general terminology*, *Preparative Chromatography*, pp. 9–48
- [221] Nagy, K., VÉKey, K., Chapter 5 - Separation methods, pp. 61–92, (Elsevier, Amsterdam2008), doi:<https://doi.org/10.1016/B978-044451980-1.50007-0>
- [222] Kind, T., Fiehn, O., Seven golden rules for heuristic filtering of molecular formulas obtained by accurate mass spectrometry, *BMC bioinformatics*, 8(1):(2007) p. 105
- [223] Tziotis, D., *et al.*, Kendrick-analogous network visualisation of ion cyclotron resonance fourier transform mass spectra: improved options for the assignment of elemental compositions and the classification of organic molecular complexity, *Eur J Mass Spectrom (Chichester)*, 17(4):(2011) pp. 415–21, doi:10.1255/ejms.1135
- [224] Forcisi, S., *et al.*, Solutions for low and high accuracy mass spectrometric data matching: A data-driven annotation strategy in nontargeted metabolomics, *Analytical Chemistry*, 87(17):(2015) pp. 8917–8924, doi:10.1021/acs.analchem.5b02049

-
- [225] Moritz, F., *et al.*, Characterization of poplar metabotypes via mass difference enrichment analysis, *Plant, Cell & Environment*, 40(7):(2017) pp. 1057–1073, doi: 10.1111/pce.12878
- [226] Van Krevelen, D.W., Graphical-statistical method for the study of structure and reaction processes of coal, *Fuel*, 29:(1950) pp. 269–284
- [227] Hertkorn, N., *et al.*, Natural organic matter and the event horizon of mass spectrometry, *Analytical chemistry*, 80(23):(2008) pp. 8908–8919
- [228] Bae, E., *et al.*, Study of double bond equivalents and the numbers of carbon and oxygen atom distribution of dissolved organic matter with negative-mode ft-icr ms, *Analytical chemistry*, 83(11):(2011) pp. 4193–4199
- [229] Koch, B., Dittmar, T., From mass to structure: An aromaticity index for high-resolution mass data of natural organic matter, *Rapid communications in mass spectrometry*, 20(5):(2006) pp. 926–932
- [230] Yassine, M.M., *et al.*, Structural characterization of organic aerosol using fourier transform ion cyclotron resonance mass spectrometry: aromaticity equivalent approach, *Rapid Commun Mass Spectrom*, 28(22):(2014) pp. 2445–54, doi:10.1002/rcm.7038
- [231] Kroll, J.H., *et al.*, Carbon oxidation state as a metric for describing the chemistry of atmospheric organic aerosol, *Nature chemistry*, 3(2):(2011) p. 133
- [232] Liger-Belair, G., *et al.*, Unraveling different chemical fingerprints between a champagne wine and its aerosols, *Proceedings of the National Academy of Sciences of the United States of America*, 106(39):(2009) pp. 16545–16549, doi: 10.1073/pnas.0906483106
- [233] Rosselló-Mora, R., *et al.*, Metabolic evidence for biogeographic isolation of the extremophilic bacterium *salinibacter ruber*, *The ISME Journal*, 2(3):(2008) pp. 242–253, doi:10.1038/ismej.2007.93
- [234] Pizzarello, S., *et al.*, The nature and distribution of the organic material in carbonaceous chondrites and interplanetary dust particles, *Meteorites and the early solar system II*, 1:(2006) pp. 625–651
- [235] Freund, F., *et al.*, Carboxylic and dicarboxylic acids extracted from crushed magnesium oxide single crystals, *Orig Life Evol Biosph*, 29(5):(1999) pp. 489–509, doi: 10.1023/a:1006698710710
- [236] Unsalan, O., *et al.*, The sariçiçek howardite fall in turkey: Source crater of hed meteorites on vesta and impact risk of vestoids, *Meteoritics & Planetary Science*, 54(5):(2019) pp. 953–1008
- [237] Cronin, J., Pizzarello, S., Amino acids in meteorites, *Advances in Space Research*, 3(9):(1983) pp. 5–18
- [238] Callahan, M.P., *et al.*, Carbonaceous meteorites contain a wide range of extraterrestrial nucleobases, *Proceedings of the National Academy of Sciences*, 108(34):(2011) pp. 13995–13998
- [239] Furukawa, Y., *et al.*, Extraterrestrial ribose and other sugars in primitive meteorites, *Proceedings of the National Academy of Sciences*, 116(49):(2019) pp. 24440–24445

-
- [240] Srinivasan, B., Anders, E., Noble gases in the murchison meteorite: Possible relics of s-process nucleosynthesis, *Science*, 201(4350):(1978) pp. 51–56
- [241] Lauretta, D.S., McSween, H.Y., *Meteorites and the early solar system II*, (University of Arizona Press 2006)
- [242] Hashiguchi, M., Naraoka, H., High-mass resolution molecular imaging of organic compounds on the surface of murchison meteorite, *Meteoritics & Planetary Science*, 54(2):(2019) pp. 452–468
- [243] Kaplan, I.R., Hulston, J.R., The isotopic abundance and content of sulfur in meteorites, *Geochimica et Cosmochimica Acta*, 30(5):(1966) pp. 479–496, doi:[https://doi.org/10.1016/0016-7037\(66\)90059-7](https://doi.org/10.1016/0016-7037(66)90059-7)
- [244] Tenailleau, C., *et al.*, A neutron powder diffraction study of Fe and Ni distributions in synthetic pentlandite and violarite using ⁶⁰Ni isotope, *American Mineralogist*, 91(8-9):(2006) pp. 1442–1447
- [245] Orthous-Daunay, F.R., *et al.*, Speciation of sulfur in the insoluble organic matter from carbonaceous chondrites by Xanes spectroscopy, *Earth and Planetary Science Letters*, 300(3-4):(2010) pp. 321–328
- [246] Van Schmus, W.R., Wood, J.A., A chemical-petrologic classification for the chondritic meteorites, *Geochimica et Cosmochimica Acta*, 31(5):(1967) pp. 747–765, doi:[https://doi.org/10.1016/S0016-7037\(67\)80030-9](https://doi.org/10.1016/S0016-7037(67)80030-9)
- [247] Wakil, S.J., Fatty acid synthase, a proficient multifunctional enzyme, *Biochemistry*, 28(11):(1989) pp. 4523–4530
- [248] Summons, R.E., *et al.*, Molecular biosignatures, *Space Science Reviews*, 135(1-4):(2008) pp. 133–159
- [249] Sears, D., Temperature gradients in meteorites produced by heating during atmospheric passage, *Modern Geology*, 5:(1975) pp. 155–164
- [250] Toppani, A., *et al.*, Experimental simulation of atmospheric entry of micrometeorites, *Meteoritics & Planetary Science*, 36(10):(2001) pp. 1377–1396
- [251] Gattacceca, J., *et al.*, The meteoritical bulletin, no. 107, *Meteoritics & Planetary Science*, 55(2):(2020) pp. 460–462, doi:10.1111/maps.13440
- [252] Bonal, L., *et al.*, Thermal history of type 3 chondrites from the antarctic meteorite collection determined by Raman spectroscopy of their polyaromatic carbonaceous matter, *Geochimica et Cosmochimica Acta*, 189:(2016) pp. 312–337, doi:<https://doi.org/10.1016/j.gca.2016.06.017>
- [253] Matzka, M., *et al.*, Thermal history of asteroid parent bodies is reflected in their metalorganic chemistry, *The Astrophysical Journal Letters*, 915(1):(2021) p. L7, doi:10.3847/2041-8213/ac0727
- [254] Aoudjehane, H.C., *et al.*, Tissint martian meteorite: A fresh look at the interior, surface, and atmosphere of Mars, *Science*, 338(6108):(2012) pp. 785–788
- [255] Baziotis, I.P., *et al.*, The Tissint martian meteorite as evidence for the largest impact excavation, *Nature Communications*, 4(1):(2013) pp. 1–7
- [256] Heberle, H., *et al.*, InteractiVenn: a web-based tool for the analysis of sets through Venn diagrams, *BMC Bioinformatics*, 16(1):(2015) pp. 1–7
-

-
- [257] Cordero, M.M., Wesdemiotis, C., Characterization of the neutral products formed upon charge-remote fragmentation of fatty acid ions, *Analytical chemistry*, 66(6):(1994) pp. 861–866
- [258] Wesdemiotis, C., *et al.*, Fragmentation pathways of polymer ions, *Mass Spectrometry Reviews*, 30(4):(2011) pp. 523–559, doi:<https://doi.org/10.1002/mas.20282>
- [259] Kingston, D.G., *et al.*, Intramolecular hydrogen transfer in mass spectra. ii. mclafferty rearrangement and related reactions, *Chemical Reviews*, 74(2):(1974) pp. 215–242
- [260] Aponte, J.C., *et al.*, Extraterrestrial organic compounds and cyanide in the cm2 carbonaceous chondrites aguas zarcas and murchison, *Meteoritics & Planetary Science*, n/a(n/a), doi:10.1111/maps.13531
- [261] Demarque, D.P., *et al.*, Fragmentation reactions using electrospray ionization mass spectrometry: an important tool for the structural elucidation and characterization of synthetic and natural products, *Natural Product Reports*, 33(3):(2016) pp. 432–455
- [262] Schuiling, R.D., de Boer, P.L., Rolling stones; fast weathering of olivine in shallow seas for cost-effective CO₂ capture and mitigation of global warming and ocean acidification, *Earth Syst Dynam Discuss*, 2011:(2011) pp. 551–568, doi:10.5194/esdd-2-551-2011
- [263] Li, S., Xia, M., Review of high-content screening applications in toxicology, *Archives of toxicology*, 93(12):(2019) pp. 3387–3396
- [264] Krot, A.N., *et al.*, Evidence for oxygen-isotope exchange in refractory inclusions from kaba (cv3. 1) carbonaceous chondrite during fluid-rock interaction on the cv parent asteroid, *Geochimica et Cosmochimica Acta*, 246:(2019) pp. 419–435
- [265] Suttle, M., *et al.*, The alteration history of the cy chondrites, investigated through analysis of a new member: Dhofar 1988, *Geochimica et Cosmochimica Acta*, 295:(2021) pp. 286–309
- [266] Walker, A., *et al.*, Sulfonolipids as novel metabolite markers of alistipes and odoribacter affected by high-fat diets, *Scientific reports*, 7(1):(2017) pp. 1–10
- [267] Witting, M., *et al.*, Optimizing a ultrahigh pressure liquid chromatography-time of flight-mass spectrometry approach using a novel sub-2µm core-shell particle for in depth lipidomic profiling of caenorhabditis elegans, *Journal of Chromatography A*, 1359:(2014) pp. 91 – 99, doi:<https://doi.org/10.1016/j.chroma.2014.07.021>

List of tables

1	Paper 2 Table 1	71
2	Paper 2 Table 2	89
3	Paper 2 Table 3	107
4	Erosion of Olivine	114
A.1	Paper 1 Table 1	126

List of Figures

1	Schematic classification of meteorite	6
2	Scheme of theorized IOM of meteorites	8
3	Evolution of molecules to life	9
4	Shape of Olivine	12
5	Olivine scheme	21
6	Exemplary FT-ICR-MS spectrum	30
7	Comparison of ionization techniques	31
8	¹ H NMR shifts	34
9	Van Krevelen Diagram	40
10	Paper 1 Figure 1	54
11	Paper 1 Figure 2	56
12	Paper 1 Figure 3	57
13	Paper 1 Figure 4	59
14	Paper 1 Figure 5	62
15	Paper 2 Figure 1	68
16	Paper 2 Figure 2	70
17	Paper 2 Figure 3	72
18	Paper 2 Figure 4	75
19	Paper 2 Figure 5	77
20	Paper 2 Figure 6	79
21	Paper 2 Figure 7	80
22	Paper 2 Figure 8	83
23	Paper 2 Figure 9	84
24	Paper 2 Figure 10	86
25	Paper 2 Figure 11	87
26	Paper 2 Figure 12	88
27	Paper 2 Figure 13	91

28	Paper 2 Figure 14	94
29	Paper 2 Figure 15	96
30	Paper 2 Figure 16	98
31	Paper 2 Figure 17	100
32	Paper 2 Figure 18	104
33	Paper 2 Figure 19	106
34	Paper 2 Figure 20	108
35	Water Erosion Experiment	115
36	CHOMgBr isotopic pattern	117
37	HCS Results from Kilauea 2018	119
A.1	Paper 1 Figure A1	127
A.2	Paper 1 Figure A2	128
A.3	Paper 1 Figure A3	129
A.4	Paper 1 Figure A4	130
A.5	Paper 1 Figure A5	131
A.6	Paper 1 Figure A6	131
A.7	Paper 1 Figure A7	132
A.8	Paper 1 Figure A8	133
A.9	Paper 1 Figure A9	134
A.10	Paper 1 Figure A10	135
A.11	Paper 1 Figure A11	136

List of Listings

1	Function to assign chemical spaces	41
2	Function to assign chemical composition	43
3	Calculation of descriptive values	44
4	Van Krevelen Diagram	45
5	Mass-edited H/C Diagram	45

List of scientific communications

Published Papers

- Matzka, M.; M.Lucio.; B. Kanawati.; E. Quirico; L. Bonal; S. Loehle; P. Schmitt-Kopplin
Profiling of magnesium organosulfur chemistry in meteorites
Published Paper - The Astrophysical Journal Letters
- Kunzke T, Prade VM, Buck A, Sun N, Feuchtinger A, Matzka, M., Fernandez IE, Wuyts W, Ackermann M, Jonigk D, Aichler M, Schmid RA, Eickelberg O, Berezowska S, Walch A.
Patterns of Carbon-Bound Exogenous Compounds in Patients with Lung Cancer and Association with Disease Pathophysiology
Published Paper - Cancer Research
- G. Danger; V. Vinogradoff; M. Matzka; J-C. Vienne; L. Remusat; S. Bernard; A. Ruf; L. Le Sergeant d'Hendecourt; P. Schmitt-Kopplin
Exploring the link between molecular cloud ices and chondritic organic matter in laboratory
Published Paper - Nature Communications
- Brau, J.; Matzka, M.; Scheu, B.; Hertkorn, N.; Schmitt-Kopplin, P.; Dingwell, D.B.
Experimental determination of thermal stability of metal-organic compounds in volcanic olivines
Conference Paper - Goldschmidt 2020 Conference
- Schmitt-Kopplin, Ph.; Hertzog, J.; Matzka, M.; Hertkorn, N.; Harir, M.
(Ultra)high-Resolution Organic Spectroscopy Analysis of Soluble Organic Matter in Meteorites
Conference Paper - 82nd Annual Meeting of The Meteoritical Society

Scientific Conferences

- CRC - Emergence of Life Winter Retreat 2019
18-21 February 2019
Talk and poster presentation
- CRC - Emergence of Life Winter Retreat 2020
17-20 February 2020
Talk and poster presentation
- Molecular Origins of Life, Munich 2020
08-10 July 2020 (Virtual Conference)
Poster presentation
- Goldschmidt Virtual 2020
21-26 June 2020 (Virtual Conference)
Poster presentation
- Goldschmidt Virtual 2021
04-09 July 2021 (Virtual Conference)
Poster presentation plus three minute flash talk